Coordinated memory processing between the dorsal and ventral hippocampus and the nucleus accumbens

by
Marielena Sosa

DISSERTATION
Submitted in partial satisfaction of the requirements for degree of
DOCTOR OF PHILOSOPHY
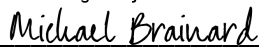
in

Neuroscience

in the

GRADUATE DIVISION
of the
UNIVERSITY OF CALIFORNIA, SAN FRANCISCO

Approved:

Michael Brainard
_____
Chair

Loren Frank, PhD
_____

Anatol Kreitzer, PhD
_____

Mazen Kheirbek
_____

_____
Committee Members

DEDICATION

To the Sosa and Scharlat families

for generations of sacrifice and resilience that made my life and opportunities possible

And to my parents, John and Tobi Sosa

for limitless love, support, and guidance

ACKNOWLEDGEMENTS

First and foremost, I am honored and extremely grateful to have been trained by Dr. Loren Frank. Loren has been an incredible mentor in many ways, but I'd like to highlight several of his qualities that I most appreciate: (1) his technical expertise, such as his guidance in how to adjust tetrodes and ability to debug/write software key to the experiment; (2) his optimism and infectious belief in making the impossible possible – he has inspired me to exceed what I think I'm capable of scientifically and personally; (3) his integrity and high standard of scientific rigor, which has trained me to be a careful and principled scientist; (4) his insights into the data that rapidly expand into big-picture hypotheses; and (5) his compassion and trust in me as a trainee. Thank you, Loren, for teaching me how to be more resilient and confident in myself, and how to do science with both practicality and a healthy dose of pathological optimism.

Another of Loren's strengths is choosing an outstanding team of people. I thank my colleagues in the Frank lab for the years of insightful discussions, support, and generous assistance: Kenneth Kay, Jason Chung, Shantanu Jadhav, Gideon Rothschild, Mattias Karlsson, Daniel Liu, Jai Yu, Anna Gillespie, Hannah Joo, David Kastner, Michael Coulter, Abhilasha Joshi, Alison Comrie, Tom Davidson, Demetris Roumis, Kevin Fan, Irene Grossrubatcsher, Charlotte Geaghan-Breiner, Daniela Astudillo Maya, Jen Guidera, Emily Jones, Hexin Liang, Jojo Yang, and Clay Smyth. I have learned an indescribable amount from all of them. I thank our lab managers past and present: Sheri Harris, Gomathi Ramakrishnan, and Anya Kiseleva, for fostering a healthy lab environment and being instrumental in our ability to do science. I thank Irene Grossrubatcsher, Eric Miller, and Viktor Kharazia for technical and histological assistance. I thank Daniel Liu, Jason Chung, Demetris Roumis, and Tom Davidson for their selfless technical development work that has benefited the whole lab.

CONTRIBUTIONS

Chapter 1 is reproduced with permission, excluding the overview, from:

> Sosa, M.*, Gillespie, A.K.*, and Frank, L.M. (2016) Neural Activity Patterns Underlying Spatial Coding in the Hippocampus. In: Clark R.E., Martin S. (eds) Behavioral Neuroscience of Learning and Memory. *Current Topics in Behavioral Neurosciences*, vol 37. Springer, Cham.

M.S. and A.K.G. contributed equally to the published book chapter. We are grateful to Kenneth Kay for

providing the neural data shown in Chapter 1, Fig. 2, and to members of the Frank laboratory for their

insightful feedback.

Chapter 2 is currently in revision. The preprint version of this paper appears at:

> Sosa, M., Joo, H.R., and Frank, L.M. (2019) Dorsal and ventral hippocampus engage opposing networks in the nucleus accumbens. *bioRxiv*: 604116.

M.S. and L.M.F. designed the study. M.S. led experiments and M.S. and H.R.J. conducted experiments.

M.S. analyzed the data. M.S. and L.M.F. wrote the manuscript with contributions from H.R.J.

Chapter 3 was written by Marielena Sosa.

Coordinated memory processing between the dorsal and ventral hippocampus and the nucleus accumbens

Marielena Sosa

ABSTRACT

The brain's ability to associate experiences with subsequent rewards is fundamental to learning and memory and critical for animal survival. The neural substrates of this process are only partially understood, but are thought to rely on interactions between the hippocampus and nucleus accumbens (NAc). In particular, hippocampal input to the NAc is thought to be crucial for learning and remembering links between spatial information and reward. Hippocampal projections to the NAc arise from both the ventral hippocampus (vH) and the dorsal hippocampus (dH), and studies using optogenetic interventions have demonstrated that either vH or dH input to the NAc can support behaviors dependent on spatial-reward associations. It remains unclear, however, whether dH, vH, or both coordinate memory processing of spatial-reward information in the hippocampal-NAc circuit under normal conditions. Moreover, as dH and vH are thought to encode different aspects of an experience, whether the hippocampus can compartmentalize different types of information to circuits in the NAc is unknown.

Times of memory reactivation within and outside the hippocampus are marked by hippocampal sharp-wave ripples (SWRs), discrete events which facilitate investigation of inter-regional information processing. It is unknown whether dH and vH SWRs act in concert or separately to engage NAc neuronal networks, and whether either dH or vH SWRs are preferentially linked to spatial-reward representations. To address these questions, we performed simultaneous extracellular recordings using multi-tetrode arrays in the dH, vH, and NAc of rats learning and performing an appetitive spatial task and during sleep. We report that dH and vH SWRs occur asynchronously, and that individual NAc neurons activated during SWRs from one subdivision of the hippocampus are typically suppressed or unmodulated during SWRs

from the other. Furthermore, NAc neurons activated during dH versus vH SWRs show markedly different task-related firing patterns, with NAc representations related to space and reward selectively activated during dH SWRs and not vH SWRs.

Our findings reveal that dorsal and ventral hippocampal interactions with the NAc are temporally and anatomically separable at times of memory processing. This work suggests that the dH-NAc and vH-NAc networks provide distinct information channels, with the dH-NAc channel dedicated to linking spatial paths with reward and reward-seeking actions. More broadly, these circuit dynamics could provide a potential neural substrate for the brain's ability to compartmentalize aspects of experience in memory.

TABLE OF CONTENTS

LIST OF FIGURES

CHAPTER 1

Introduction to neural activity patterns in the hippocampus

1.1 Overview of dissertation

A given episodic experience is comprised of many different elements, including location, context, actions, events, and emotions. In order for the memory of this experience to optimally guide future behavior, the stored relationship between these features must be both precise and generalizable to similar experiences. For instance, suppose an animal encounters a novel food source. Several aspects of this experience could be remembered to help the animal find food in the future: the particular route the animal took to find the food, the actions it took at locations along that route, and whether those actions led to reward. Other information may or may not be relevant to the specific task of finding food: the context of this particular experience (the weather, for example), the animal's emotional state, and so on. All of these aspects could be stored simultaneously to create a complete memory of the experience. Alternatively, each aspect could be stored either at different moments in time or in distinct neural circuits, to facilitate the flexible retrieval of each piece of information in the future. How the brain stores and retrieves these different elements of an experience remains incompletely understood.

The rodent spatial navigation system provides a unique model to elucidate this process. In Chapter 1, we introduce in depth the neural activity patterns in the hippocampal circuit that are thought to give rise to spatial navigation and memory processing (systems that share crucial features, and thus rely on the same underlying circuits). In particular, attention is given to two main brain states: (1) the sharp-wave ripple (SWR) state, which occurs during pauses in movement and during sleep; and (2) the locomotor state, when the hippocampal theta rhythm is prominent. In Chapter 2, we use times of locomotion to understand how individual neurons represent features of experience, and SWRs to understand times of memory-related communication between brain areas.

During SWRs, hippocampal cells reactivate in a manner that recapitulates prior experience. These reactivations engage neural activity patterns across the brain, including in the nucleus accumbens (NAc), a striatal area specialized in reward and value representations. Our overarching hypothesis is that hippocampal SWRs bind spatial and reward-related representations between hippocampus and NAc, facilitating memory storage and retrieval during a rewarding experience. However, at the beginning of this

dissertation project, our understanding of SWRs (and spatial memory in general) came primarily from studies in dorsal hippocampus, while ventral hippocampal SWRs during behavior remained unexplored. This made the nature of hippocampal-NAc interactions even more elusive, as it was thought until recently that only the ventral hippocampus sent strong and direct anatomical projections to the NAc. Years of anatomical tracing studies indicated that projections from dorsal hippocampus were mostly routed indirectly through regions like the subiculum and entorhinal cortex (e.g. Groenewegen et al., 1987). As such, a longstanding hypothesis in the field was that the ventral hippocampus would be primarily involved in associations of space and valence, likely via its connections with the NAc. While we now know that dorsal hippocampus directly innervates the NAc as well (albeit more sparsely; Trouche et al., 2019), an investigation of how all three brain areas (dorsal hippocampus, ventral hippocampus, and NAc) communicate with each other was lacking. This gap in knowledge was largely due to the technical challenges of recording from ventral hippocampus in rodents. Yet knowing how the other half of the hippocampus communicates with downstream brain regions is critical to our understanding of learning and memory.

We addressed these gaps in knowledge by performing simultaneous extracellular recordings from the dorsal hippocampus, ventral hippocampus, and NAc of rats in the context of a spatial memory task. In Chapter 2, we investigated the interactions between dorsal and ventral hippocampal SWRs and neurons in the NAc. Specifically, we found that largely distinct subpopulations of NAc neurons are engaged during dorsal versus ventral hippocampal SWRs in opposing ways. Furthermore, only NAc neurons activated during dorsal hippocampal SWRs represent spatially organized actions that lead to reward across multiple spatial paths.

Finally, in Chapter 3, I discuss the significance, implications, and caveats of these findings for learning and memory more broadly. As dorsal and ventral hippocampus have been implicated in encoding different aspects of experience (e.g. Strange et al., 2014), their opposing interaction with the NAc provides a candidate circuit for the separate memory storage and retrieval of different aspects of experience.

1.2 Introduction to the hippocampus

Decades of study have established the hippocampus as a critical center for memory processing in the brain. The hippocampus, along with several associated brain regions, processes the events of daily life and facilitates the long-term storage of these experiences. The link between the medial temporal lobes and memory was indicated first by Scoville and Milner in 1957 as a result of their evaluation of patient now known as H.M. At the age of 27, H.M. underwent bilateral medial temporal lobectomy in a medical effort to alleviate his intractable epilepsy. While the surgical procedure reduced his seizures, H.M. was also rendered unable to form new episodic memories (Scoville and Milner, 1957). Subsequent studies of additional patients with more restricted medial temporal lobe lesions, as well as studies in non-human primates, identified the hippocampus and parahippocampal gyrus as the most critical regions for memory function (for review, see Squire and Wixted, 2011).

While the hippocampus was becoming established as a memory formation center in primates, a seminal series of studies in rodents revealed that hippocampal neurons were remarkably well tuned to spatial location, suggesting a critical role in encoding space. The first evidence for this view of hippocampal function emerged in 1971, when O'Keefe and Dostrovsky reported that a subset of hippocampal neurons fired when rats occupied a specific location in an environment (O'Keefe and Dostrovsky, 1971). These neurons became known as place cells, and were shown to be ubiquitous throughout the hippocampus (Jung and McNaughton, 1993; Muller et al., 1987; O'Keefe, 1976). Moreover, lesion studies of the rat hippocampus revealed a specific deficit in navigation-based memory tasks, further corroborating a role for the hippocampus in spatial processing (Mishkin, 1978; Morris et al., 1982; Olton and Papas, 1979). Based on these findings, O'Keefe and Nadel proposed that hippocampal neural activity constituted a cognitive map of space, in which individual place cells function to map out the animal's location in reference to its spatial environment (O'Keefe and Nadel, 1978).

Since this proposal, many studies have demonstrated that hippocampal neural activity can represent far more than simply spatial location, including aspects of contextual information, object recognition, and time (Eichenbaum et al., 1987; Hok et al., 2007; Komorowski et al., 2009; Manns and Eichenbaum, 2009;

Moita et al., 2003; Pastalkova et al., 2008; Young et al., 1994). For example, beyond providing a framework for linking locations together to form spatial trajectories, the hippocampus can associate multiple objects with a context (Komorowski et al., 2009), and further link a series of events in a temporally specific order to represent a complex experience (Allen et al., 2016). These observations have led to a proposed expansion of the original spatial cognitive map theory, describing the hippocampal network as a more general relational processing system which enables the rapid association of spatial, temporal, and conceptual aspects of experience (Eichenbaum and Cohen, 2001; Eichenbaum et al., 2012). This perspective serves to unify the general memory function of the hippocampus from human and primate studies with the extensive demonstration of a spatial processing function in rodent research.

While these conceptual advances have been important, a complete understanding of the role of the hippocampus will require knowledge of how hippocampal neurons cooperate at a network level to encode, store, and retrieve as memories the complex relationships and experiences that characterize daily life. The original discovery of place cells marked a critical step toward this understanding, as it pointed to a neural mechanism for encoding discrete experiences in the hippocampus. Since then, spatial encoding has been used as a model for the formation of representations that could underlie memory (Eichenbaum and Cohen, 2014; Schiller et al., 2015). In this chapter, we will therefore focus on spatial learning and memory as a means to understand mnemonic processing more broadly. In particular, we will explore how coordinated patterns of network activity both within and across the subregions of the hippocampus contribute to spatial memory processing.

1.3 Measuring neural activity

Recording neural activity during behavior allows us to understand how information is processed during an experience and stored as memories. We will discuss two primary types of data collected during this process: single unit activity and local field potential (LFP).

Single unit activity refers to the action potentials, or spikes, fired by individual neurons. Although spikes can now be recorded in vivo using whole cell patch clamp techniques (Tao et al., 2015) or calcium

imaging (Ziv et al., 2013), the predominant method for recording unit activity *in vivo* is extracellular recording. An action potential alters the ionic charge in the extracellular space, as positive sodium ions flow into the cell and away from the recording electrode. The cell's depolarization is therefore reflected as a sharp negative deflection on the extracellular electrode, the inverse of an intracellular recording. The amplitude of this deflection, or waveform, is a function of the electrode's proximity to the cell, as an electrode closer to the cell will measure a larger voltage change. However, because the cell layers of the hippocampus are so densely populated, it can be challenging to distinguish the activity of a single neuron from the surrounding neurons. To address this, hippocampal electrophysiologists typically use recording probes with several closely spaced electrode sites, such as tetrodes, which consist of four insulated electrode wires twisted together (for review, see Buzsaki, 2004). Each wire picks up a cell's spike at a slightly different amplitude due to the different proximity of each wire to the cell. This allows the spikes of the cell to be "clustered" by comparing the recorded amplitudes between pairs of electrode wires (Gray et al., 1995; Jog et al., 2002), thus isolating the cluster from clusters of neighboring cells in amplitude space. In contrast, single-site electrodes can be sufficient to isolate cells in less densely packed brain regions such as the cortex. Once spikes have been clustered to link them to a particular neuron, parameters such as the neuron's firing rate, inter-spike interval, and spike waveform can be analyzed to better understand its activity. In the hippocampus, pyramidal cells and fast-spiking interneurons can be putatively identified by their different waveform shapes and firing rates (Fox and Ranck, 1981). Not all neuronal populations have clearly differentiable waveforms, however, so it is difficult to definitively identify cell types using extracellular recording alone. Further analysis often describes how the timing of spikes is modulated by behavioral events or by local network activity, as reflected by local field potentials.

Local field potentials (LFP) are defined as the extracellular voltage at lower frequencies relative to spiking, which reflect neural network oscillations (hippocampal spiking is typically filtered between ~600-6000 Hz, LFP between ~1-400 Hz) (for review see Buzsaki et al., 2012). The LFP signal is dominated by synaptic and dendritic activity near the recording electrode, for two main reasons. First, high frequency action potentials are largely removed by the low pass filter. Second, and more importantly, dendritic post-

synaptic currents occur at slower timescales than action potentials, increasing the chance of events coinciding in time. The ionic flux of many coincident small synaptic events accumulates, resulting in relatively large fluctuations in the LFP. In laminar structures in which the dendrites and cell bodies of principal neurons are segregated, such as the hippocampus, synaptic input often aligns spatially and temporally, resulting in characteristic layer-specific LFP activity. The amplitude of the LFP signal is influenced by the scale, anatomical organization, and synchrony of inputs to a particular layer (Kajikawa and Schroeder, 2011), as well as the proximity of the electrode to the site of maximal current flow, which can be measured using current source density analysis (CSD) (Mitzdorf, 1985). CSD utilizes the change in LFP signal across closely spaced recording sites to help identify the location of inward or outward current flows. A CSD sink is a negative deflection that represents predominantly positive ions moving into a cell (i.e. an input generating local action potentials), and a source is a positive deflection that is typically interpreted as reflecting the compensatory exit of those positive ions from another part of the cell.

There are many methods for analyzing LFP signals to gain an understanding of how network-level activity is organized within and across brain regions. To isolate particular rhythms, LFPs are often decomposed into their time and frequency components. Measuring the relative intensity of different frequency components can be done using spectral analysis, and the interaction between different frequencies of oscillation can be described by cross frequency coupling parameters (Tort et al., 2010). LFP can also be compared across multiple brain areas using a measure called coherence, which describes the coordinated modulation of the phase or amplitude of the LFP signals, and may reflect common driving inputs or information flow between the regions (Fries, 2005). Finally, as mentioned above, the phase-preference of single-unit spiking can be determined to understand how LFP signals modulate the firing of local neuronal ensembles. Together, action potentials from individual cells (single unit activity) combined with coordinated network signals (LFP) enable detailed description of neural activity within and across brain regions.

1.4 Anatomical organization of the hippocampal network

To fully understand how hippocampal network activity contributes to learning and memory, it is important to have a sense for the underlying anatomy that supports this activity. Others have written excellent and detailed reviews, (see van Strien et al., 2009; Witter and Amaral, 2004), so our goal here is to highlight the fundamental connections in the hippocampal network that facilitate information processing.

The rodent hippocampal formation is a cashew-shaped structure (**Fig. 1.1 [A]**) which includes the dentate gyrus (DG), the subiculum, and the hippocampus proper: CA1, CA2 and CA3 (as defined in Witter, 1986; Witter et al., 2000).   The key axes often used to describe the hippocampus are dorsoventral (often used synonymously with septotemporal, which describes the long axis from the septal, dorsomedial pole of the hippocampus to its temporal pole; **Fig. 1.1 [B]**), transverse, and proximodistal (in which proximity is measured relative to DG, **Fig. 1.1 [C]**). These axes can delineate anatomical as well as functional gradients, especially along the dorsoventral axis, as we will discuss later. Each hippocampal subregion is organized into layers, formed by the alignment of the principal neurons (Amaral and Witter, 1989; Ishizuka et al., 1995). In the hippocampus proper, principal pyramidal neurons are oriented with their basal dendrites in stratum oriens (SO), pyramidal cell bodies in stratum pyramidale (SP), and the apical dendrites in stratum radiatum (SR) and stratum lacunosum moleculare (SLM; **Fig. 1.1 [C]**). Various types of interneurons with distinct morphological and functional properties are interspersed throughout each layer (Klausberger and Somogyi, 2008). In the DG, the principal granule cell layer is bordered by a molecular layer separating it from the hippocampal fissure. The two "blades" of the granule cell layer surround the hilus, or polymorphic layer, which is composed of interneurons and hilar mossy cells (Freund and Buzsaki, 1996; van Strien et al., 2009). The diverse collection of neuronal populations in each hippocampal subregion strongly influences the activity patterns expressed across the hippocampal network.

The hippocampal circuit has canonically been described as a trisynaptic pathway, which involves the perforant path inputs of the entorhinal cortex (EC) to the DG, the mossy fiber projection from the DG to CA3, and the Schaffer collateral projection from CA3 to CA1 (Lorente de Nó, 1933, 1934; Ramón y Cajal, 1893). However, many local, recurrent, and extrahippocampal connections add complexity to the

flow of information through the hippocampus, as we will summarize below.

Hippocampal inputs.   Inputs to the hippocampal formation originate from both cortical and subcortical structures. The hippocampus receives its primary cortical innervation from the entorhinal cortex (Steward and Scoville, 1976), via a projection called the perforant pathway (**Fig. 1.1 [C]**). EC layer II projects to the apical dendrites of DG granule cells as well as CA3 and CA2 pyramidal cells. While there is some evidence of additional EC input directly onto granule cell bodies (Deller et al., 1996), most EC inputs target the DG molecular layer and SLM of CA2/CA3, with axons from the medial EC (MEC) terminating superficially and axons from the lateral EC (LEC) terminating in the deep part of the layer, closer to principal cell bodies (Witter et al., 1989). The stratification of inputs here may be important for dendritic summation and contribute in specific ways to local LFP (Bragin et al., 1995b; McNaughton and Barnes, 1977). In contrast, EC layer III projects to CA1 and the subiculum. In these regions, the subdivision of the MEC and LEC occurs along the proximodistal axis, with the LEC targeting distal CA1 and proximal subiculum, and the MEC targeting proximal CA1 and distal subiculum (van Strien et al., 2009). Direct inputs from sensory and associational cortices primarily target the subiculum, although CA1 has been recently described to receive input directly from the anterior cingulate cortex (Rajasethupathy et al., 2015).

Subcortical inputs to the EC and the hippocampus arise from a variety of structures. The medial septum and diagonal band of Broca (MSDB) send long-range GABAergic and cholinergic afferents to the DG as well as to CA1, CA2 and CA3 (Amaral and Kurz, 1985; Freund and Antal, 1988; Frotscher and Leranth, 1985; Petsche and Stumpf, 1962). Additional modulatory inputs come from regions such as the locus coeruleus, the raphe nucleus, and others (Beckstead, 1978; Loughlin et al., 1986). CA1 additionally communicates bidirectionally with the amygdala (Pikkarainen et al., 1999; Pitkanen et al., 2000), which has been long been implicated in emotional forms of learning and conditioned fear memory (Duvarci and Pare, 2014; Gallagher and Chiba, 1996; Janak and Tye, 2015; Paz and Pare, 2013). Specifically, the inputs from amygdala to ventral hippocampus have been causally to anxiety-like behaviors (Felix-Ortiz et al., 2013; Felix-Ortiz and Tye, 2014). CA1 also receives direct input from the nucleus reuniens of the thalamus
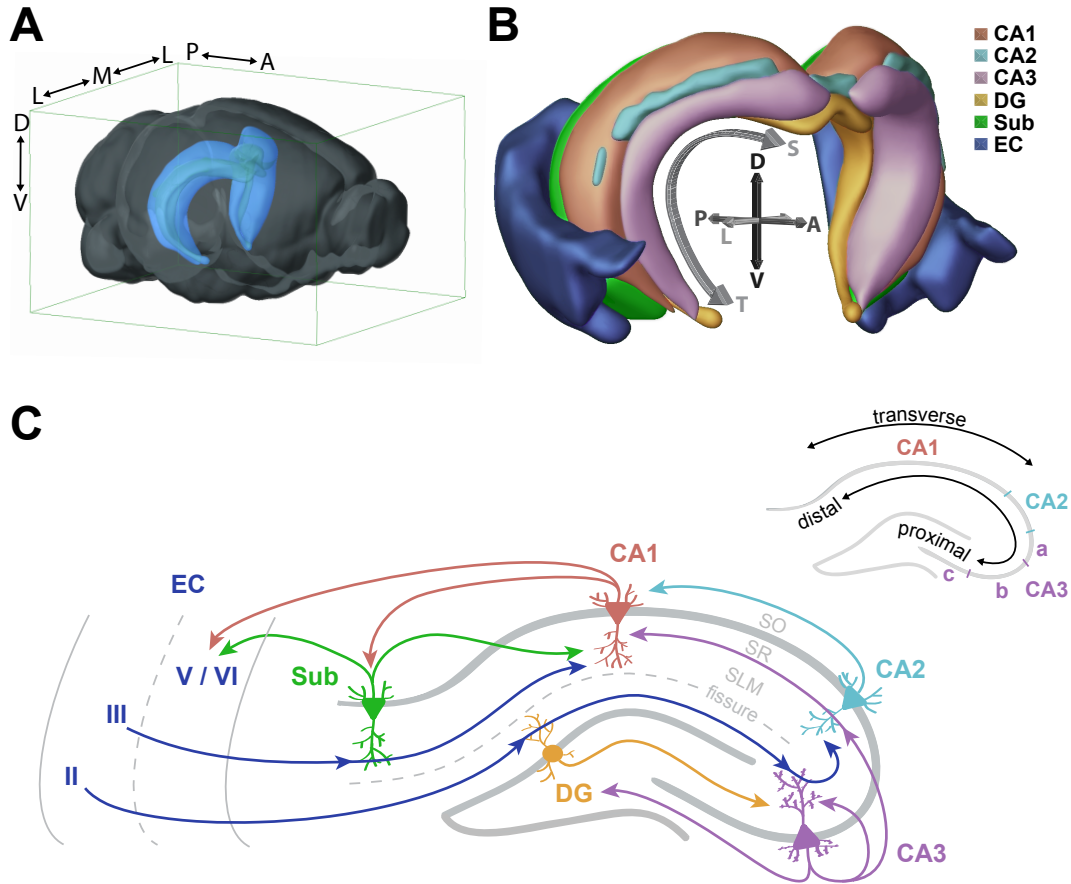
Figure 1.1 | Anatomical organization of the hippocampal network.
(A) Relative location of the hippocampi within the mouse brain. Blue structures highlight the hippocampus proper (CA1, CA2, CA3, and DG) in each hemisphere. The geometry of the hippocampus is very similar in the rat brain. D: dorsal, V: ventral, A: anterior, P: posterior, M: medial, L: lateral.
(B) Three-dimensional organization of the hippocampal formation and entorhinal cortex. The hippocampal subregions in each hemisphere are nested such that the DG resides most medially, and the EC wraps around the ventroposterior extent of the hippocampal formation, next to the subiculum (Sub). The curved arrow delineates the septotemporal axis (S: septal, T: temporal). Note that in this representation, the transverse axis lies perpendicular to the septotemporal axis, and thus is similar but not exactly analogous to the coronal plane. (A) and (B) are adapted from Brain Explorer 2, © 2015 Allen Institute for Brain Science. Allen Mouse Brain Atlas [Internet]. Available from: http://mouse.brain-map.org. **(C)** The hippocampal circuit. Major projections into and within the hippocampal circuit are depicted here, following as closely as possibly the true trajectory of axons through the hippocampal layers (SO: stratum oriens, SR: stratum radiatum, SLM: stratum lacunosum moleculare). For example, EC projections target distal apical dendrites of CA1, CA2, and CA3 neurons in SLM, while CA3 targets the proximal apical dendrites of CA2 and CA1 neurons in SR. Minor projections, as well as interneurons and mossy cells, have been omitted for clarity; however, note that these cells are the targets of the depicted CA3 backprojection to the DG hilus. Arrows represent synapses, but are not weighted by strength. Dotted grey lines represent a subset of layer boundaries, including the hippocampal fissure and the boundary between EC layers II/III and V/VI. The depiction of the EC immediately next to the subiculum is a simplification; note that this exact geometry is only preserved in the horizontal plane of the ventral hippocampus (see panel B). Inset: the transverse and proximodistal axes of the hippocampus. Also shown are approximate subdivisions of CA3a, b, and c.

(Dolleman-Van der Weel and Witter, 1996; Herkenham, 1978; Vertes et al., 2007) which is critical for the modulation of hippocampal firing by past and future trajectories (Ito et al., 2015). For a complete review of hippocampal inputs, see (Witter et al., 1989).

DG to CA3. Dentate granule cells receive their primary input from the EC and then project to CA3 pyramidal neurons as well as to the other neuronal populations located in the dentate hilus. The DG projection to CA3 is known as the mossy fiber pathway, because of the extensive arborization of granule cell axons and the high density of elaborate postsynaptic spines known as thorny excrescences, which give a "mossy" appearance (Gonzales et al., 2001). In addition to its complex spine structure, CA3 is characterized by heavily recurrent connectivity, meaning that CA3 cells often project onto other CA3 cells (Ishizuka et al., 1990). While recurrence also exists in other hippocampal subregions, it is substantially more prominent in CA3. Specifically, CA3c (**Fig. 1.1 [C]**) projects recurrently to the same septotemporal levels of CA3c, while CA3b and CA3a project more extensively within CA3, both across the transverse axis and throughout the septotemporal axis. CA3 is therefore hypothesized to help coordinate activity across the septotemporal extent of the hippocampus (Ishizuka et al., 1990; Li et al., 1994). Furthermore, CA3 projects back to the DG hilus, most strongly from dorsal CA3c and ventral CA3. This backprojection primarily targets excitatory mossy cells and inhibitory interneurons in the hilus, and is therefore hypothesized to indirectly provide both excitation and inhibition of granule cells (Scharfman, 2007).

CA3 to CA1. By far the most intensively studied hippocampal projections are the Schaffer collateral projections from CA3 pyramidal cells to CA1, both ipsilaterally and contralaterally through the hippocampal commissure. The Schaffer collaterals synapse primarily onto the apical dendrites of CA1 pyramidal cells in SR (**Fig. 1.1 [C]**), and are stratified by origin: CA3c projects to superficial SR, CA3b to deep SR, and CA3a to SO. Distal CA3 projects to proximal CA1, and proximal CA3 projects to distal CA1 (Ishizuka et al., 1990; Laurberg, 1979). Single CA1 pyramidal cells and interneurons receive convergent inputs from both EC layer III and CA3 (Kajiwara et al., 2008; Megias et al., 2001). Although modulated by neural state, the CA3 drive of CA1 is generally thought to be stronger than that of the EC (Spruston, 2008).

CA2. CA2 has received relatively little attention until recently, leaving the functional role of its connections in the hippocampal circuit unclear. CA2 receives input from EC layer II and CA3, as well as strong innervation from the supramammillary nucleus of the hypothalamus (Chevaleyre and Siegelbaum, 2010; Hitti and Siegelbaum, 2014; Ishizuka et al., 1990; Zhao et al., 2007). Furthermore, neurons in CA2 are extensively recurrently connected and send a strong projection from CA2 to CA1, synapsing primarily in SO and to a lesser degree in SR, and a backprojection from CA2 to CA3 (Cui et al., 2013; Hitti and Siegelbaum, 2014; Ishizuka et al., 1990; Tamamaki et al., 1988). Other connections have been more controversial. Notably, individual studies have reported a CA2 to EC layer II projection (Rowland et al., 2013) and a DG to CA2 projection (Kohara et al., 2014), while others do not observe such projections (e.g. Cui et al., 2013).

CA1. CA1 sends its strongest outputs to the subiculum and to the deep layers of the EC (layers V and VI). The projection to the subiculum is segregated such that proximal CA1 projects most strongly to distal subiculum while distal CA1 projects to proximal subiculum (Amaral et al., 1991). In addition, both CA1 and CA3 project directly to the MSDB (Gulyas et al., 2003; Meibach and Siegel, 1977; Toth et al., 1993; Toth and Freund, 1992), while other direct projections predominantly from ventral CA1 disperse hippocampal output widely across the brain (Cenquizca and Swanson, 2007). Within CA1, local connectivity may have an influence on network patterns and on information processing before signals are sent outward. Specifically, CA1 pyramidal cells synapse laterally onto CA1 interneurons (Amaral et al., 1991; Takacs et al., 2012), which in turn can even project back to CA3 SR and SO as well as to the DG hilus (Sik et al., 1995; Sik et al., 1994). Furthermore, CA1 axons projecting forward to the subiculum extend collaterals that loop back into CA1 SO (Amaral et al., 1991), providing a small amount of recurrent connectivity within CA1.

Subiculum. The inputs and outputs of the subiculum differ substantially along the dorsal-ventral axis as well as the proximal-distal axis. Dorsal subiculum mostly innervates neocortical regions and receives most inputs from CA1 as well as perirhinal cortex, prefrontal cortex, visual cortex, and MSDB. The ventral subiculum receives the majority of its non-CA1 input from subcortical structures, including

hypothalamic nuclei, MSDB, and the amygdala, and returns projections to these regions as well as to the nucleus reuniens of the thalamus and the nucleus accumbens (Ishizuka, 2001; Witter, 2006; Witter and Amaral, 2004). Recently, the early demonstration of a subicular backprojection to CA1 (Finch et al., 1983; Kohler, 1985) was confirmed elegantly using Cre-dependent rabies tracing (Sun et al., 2014). Interestingly, both glutamatergic and GABAergic subicular pyramidal neurons innervate all layers of CA1, and the subicular neurons that backproject are the same neurons that receive direct input from CA1. These same cells also receive input from entorhinal cortex, visual cortex, and the medial septum, and both CA1 pyramidal cells and interneurons are targets of this backprojection (Sun et al., 2014). This newly elaborated circuit may provide an important substrate for feedback and fine tuning of hippocampal processing.

1.5 Electrophysiological signatures of the hippocampus

To understand how neural activity in the hippocampal circuit enables the encoding, consolidation, and retrieval of memories, rodent studies of the hippocampus often use place cells as a model for how information can be represented on the single cell and cell ensemble levels. For each subregion of the hippocampal network, we will describe how space is represented at the level of individual neurons, and then how these spatial representations are structured within rhythmic network activity. We will focus on two network patterns that have been implicated in the encoding and retrieval of mnemonic information: theta oscillations and sharp-wave ripples. By understanding how network patterns organize the firing of place cells, we may begin to understand how neural networks may organize information into memories useful for guiding subsequent behavior.

Place cells. The most striking characteristic of hippocampal neurons are their spatial firing fields, also known as place fields (O'Keefe and Dostrovsky, 1971). These stable, location-based receptive fields are now known to be characteristic of the majority of excitatory hippocampal neurons in all subregions (Jung and McNaughton, 1993; Muller and Kubie, 1987; O'Keefe and Dostrovsky, 1971; Thompson and Best, 1990). It is important to note that the characterization of place cells is generally done during locomotion, including much of the information we will discuss in the following sections. However, a wealth

of evidence suggests that neural activity maintains its place representations across behavioral states (e.g. de Lavilleon et al., 2015; Kay et al., 2016; Pavlides and Winson, 1989). Place fields develop over the first few minutes of exploration in a new environment and become more refined with experience (Frank et al., 2004; Hill, 1978; Wilson and McNaughton, 1994). Although exact definitions vary, a cell's place field is generally defined as the region in which its firing exceeds 1 Hz or a certain proportion of the cell's peak firing rate in the environment, such that the place cell fires maximally when the animal is centered in its place field and sparsely or not at all in distant regions of the environment (Muller et al., 1987; O'Keefe, 1976). Some place cells have multiple fields, especially in large environments (Fenton et al., 2008; Park et al., 2011). In different environments, different subsets of neurons will become active; this shift in ensemble place activity is called global remapping (Lever et al., 2002; Markus et al., 1995; Muller et al., 1987). A local alteration in an environment (e.g. elimination or addition of a visual cue) might induce rate remapping, in which the active place cell ensemble remains the same, but the firing rates of the ensemble change (Allen et al., 2012; Anderson and Jeffery, 2003; Leutgeb et al., 2005b). Rate remapping is thus hypothesized to contribute to the representation of new information within a pre-established spatial framework, while global remapping reflects the creation of an independent spatial representation. Overall, these encoding mechanisms show how neural ensemble activity relates to a representation of the animal's experience, providing a means to investigate how experience is processed within the hippocampal circuit.

Theta Oscillations. During movement, place cells fire at specific times relative to a network rhythm known as theta. Theta is a low frequency oscillation (~8 Hz, or more broadly 5-12 Hz) which dominates the local field potential (LFP) during locomotion (**Fig. 1.2**) and during periods of overtly active engagement in the environment, such as rearing, exploring objects, and preparation for movement (Foster et al., 1989; Grastyan et al., 1959; Green and Arduini, 1954; Vanderwolf, 1969). An extensive body of literature has thus described theta as the critical marker of active, location-encoding behavioral state in rodents. Moreover, as theta is known to coordinate place cell firing in this state, it has long been thought to be an important contributor to hippocampal processing (for review see Buzsaki, 2002).
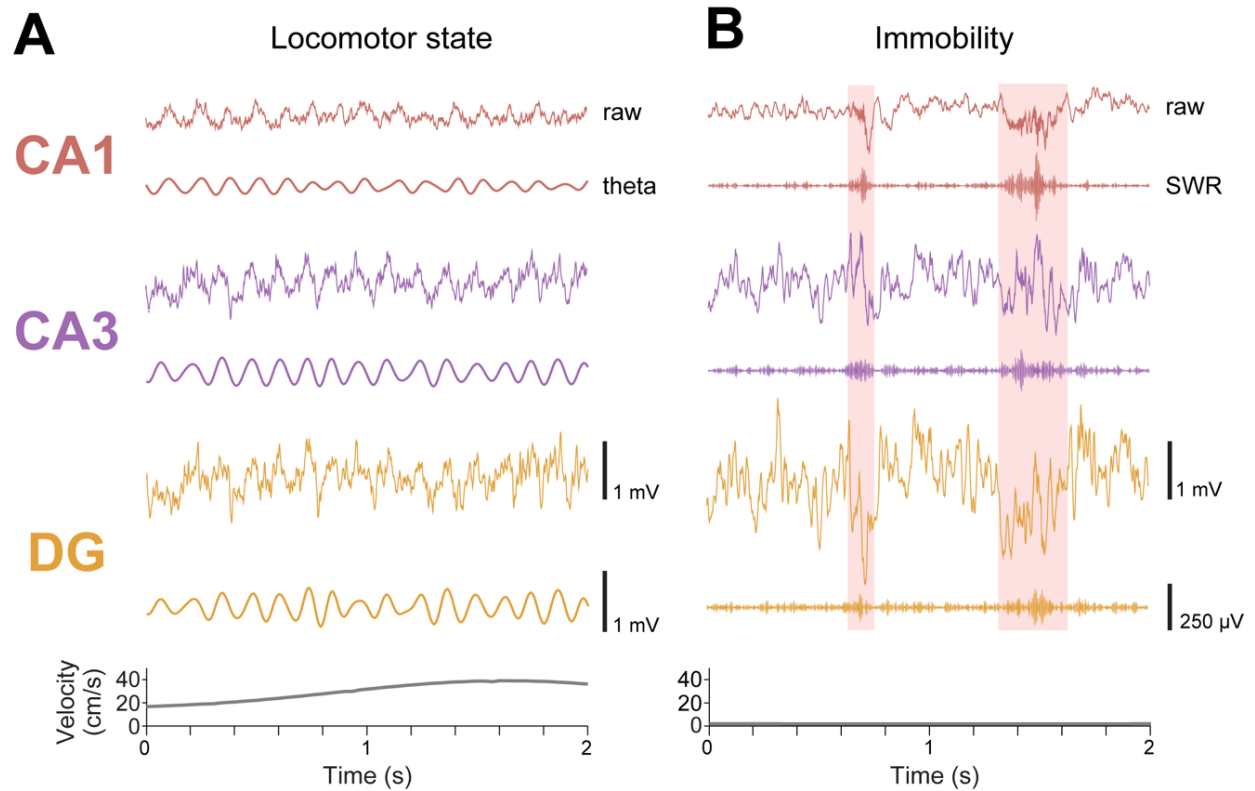
Figure 1.2 | LFP signatures of the hippocampal network.
To illustrate the distinct features of hippocampal LFP, we show raw and filtered LFP detected simultaneously in a single rat from tetrodes located in the principal layer of each major subregion of the hippocampus. During the locomotor state (left), persistent theta oscillation dominates the raw LFP signal in all three subregions. As seen in both the raw and theta filtered (5-11 Hz) traces, theta amplitude is smallest in CA1, larger in CA3, and largest in the DG. Graph of the rat's velocity (bottom) shows that during this period, the animal is constantly in motion. In contrast, traces on the right show LFP data acquired during awake immobility. Instead of the highly regular rhythmic activity during locomotion, the LFP signal is far more varied, but also increases in amplitude from CA1 to the DG. SWRs detected in CA1 are highlighted in pink, and are easily distinguishable as periods of increased power in the ripple filtered trace (150-250 Hz). The high frequency component of the SWRs are most dominant in CA1, while the sharp wave component is more visible in CA3 and the DG. Note that a substantial amount of time during immobility does not contain SWRs, during which the rat presumably still maintains spatial representations but perhaps through alternate coding mechanisms. During this period, the velocity plot (bottom) shows that the rat is motionless.

15

It is worth noting that while theta has been observed in mammals other than rodents (Arnolds et al., 1980; Winson, 1972), theta is substantially less prominent in bats, cats, monkeys, and humans during analogous periods of locomotion and decision-making (Jutras et al., 2013; Kemp and Kaada, 1975; Ulanovsky and Moss, 2007; Watrous et al., 2013). For this reason, the specific significance of theta defined as a 5-12 Hz rhythm is not clear. It is possible that an alternative low frequency signal, or irregular but time-locked activity, may perform similar roles in other species (Ulanovsky and Moss, 2007; Watrous et al., 2013; Yartsev et al., 2011). To encompass the general behavioral state marked by movement and active sensory engagement across species, we will refer to such periods of activity as the **locomotor state.** However, as most studies of hippocampal activity to date were conducted in rodents, we will discuss theta in the locomotor state as one potential mechanism for binding spatial and mnemonic representations.

Hippocampal theta is dependent on activity in the MSDB. Lesions of the MSDB abolish theta activity throughout the entire neocortex (Mitchell et al., 1982; Petsche and Stumpf, 1962; Stewart and Fox, 1990), and theta suppression from MSDB inactivation has been directly linked to spatial working memory (Givens and Olton, 1990; Mitchell et al., 1982; Mizumori et al., 1989; Winson and Abzug, 1978). However, other regions such as the supramammillary nuclei may also contribute to the pacing of theta (Kocsis and Vertes, 1997; Pan and McNaughton, 2002). In addition, lesions of the EC drastically reduce theta power in the hippocampus, suggesting that entorhinal input may be critical for supporting a strong hippocampal theta signal (Buzsaki et al., 1983). Interestingly, while MS inactivation abolishes theta entirely, place coding in the hippocampus is somewhat abnormal but not absent (Brandon et al., 2014; Mizumori et al., 1989). The functional role of theta in establishing hippocampal representations thus remains somewhat unclear.

In the rodent hippocampus, theta phase and amplitude are variable across layers (Bullock et al., 1990; Buzsaki et al., 1986) and change along the dorsoventral axis within the same layer (Patel et al., 2012). Theta phase is most consistent just above SP, in SO or corpus callosum, where phase changes within the layer are minimal along the dorsoventral axis (Lubenov and Siapas, 2009). The phases of theta represent varying levels of excitation and inhibition. At the trough, for example, inhibition from local inhibitory interneurons is thought to be least, permitting strong firing in local pyramidal cells (Csicsvari et al., 1999b).

During the locomotor state, the phase of theta at which a neuron fires is also governed by the animal's proximity to the center of the place field, a phenomenon known as phase precession (O'Keefe and Recce, 1993; Skaggs et al., 1996). As an animal enters a place field, that neuron will begin to fire in the later phases of theta, toward the peak of the oscillation. As the animal runs through the neuron's place field, each spike of the neuron will align to a progressively earlier phase of the theta cycle, firing near the trough of theta in the place field center and on the descending phases as the rat moves past the place field center (O'Keefe and Recce, 1993; Skaggs et al., 1996). This results in each cycle of theta containing a range of place cell activity ordered by location. During most theta cycles, the place cells that fire are those with fields spanning from just ahead to just behind the current position of the animal, such that this sequence of locations is compressed into one theta cycle (Itskov et al., 2008). This has been suggested as a strategy for compressing experience from the timescale of behavior down to the millisecond time scale of spike-timing-dependent plasticity (Skaggs et al., 1996), potentially enabling the rapid encoding of experience in novel environments (Cheng and Frank, 2008) and the efficient transmission of spatial information to downstream brain regions (Ego-Stengel and Wilson, 2007; Olypher et al., 2003; Skaggs et al., 1996). However, some theta cycles contain a range of place cells representing locations more distant from the animal, and these have been proposed to play a role in planning future trajectories (Gupta et al., 2012; Wikenheiser and Redish, 2015). In general, place cell activity coupled to theta is thought to provide an ongoing representation of location and potentially represent immediate upcoming plans during active behavior.

Sharp-wave ripples (SWRs). In contrast to the overt rhythmicity of theta during the locomotor state, the hippocampal LFP signal is far more irregular during times of awake immobility (**Fig. 1.2**) and slow wave sleep. These periods are punctuated by hippocampal sharp-wave ripples (SWRs) (for review see Buzsaki, 2015). SWRs are perhaps the most synchronous events in the healthy brain, with an estimated 50,000-100,000 neurons discharging over ~50-150 milliseconds in the hippocampus and EC (Chrobak and Buzsaki, 1996; Csicsvari et al., 1999a). SWRs have been seen in mammals ranging from mice to humans (Axmacher et al., 2008; Buzsaki et al., 2003; Skaggs et al., 2007; Ulanovsky and Moss, 2007), suggesting

that their function is likely to be conserved across species. In the rodent, SWRs are characterized by a high frequency ripple oscillation (150-250 Hz) predominantly in the CA1 subregion (Buzsaki et al., 1992) as well as a sharp wave: a simultaneous large negative deflection of the LFP signal detectable throughout most of the hippocampus (Buzsaki, 1986). During SWRs, ensembles of place cells become sequentially active in a time-compressed manner, often recapitulating prior experience at high speed (Buzsaki, 1989; Lee and Wilson, 2002; Pavlides and Winson, 1989; Skaggs and McNaughton, 1996; Wilson and McNaughton, 1994). These sequential reactivations are known as replay events, and are hypothesized to be a key mechanism of hippocampal memory. Complementary to the rapid encoding enabled by compressed place cell sequences within theta cycles, replay during SWRs has been linked to memory consolidation and retrieval. Multiple studies have demonstrated that disrupting SWRs, either during awake immobility or sleep, is sufficient to impair performance on memory-dependent tasks (Ego-Stengel and Wilson, 2010; Girardeau et al., 2009; Jadhav et al., 2012; Nokia et al., 2012). Furthermore, SWRs may contribute directly to forming new associations, potentially linking outcomes, such as reward, with the route that leads to them and thus guiding future behavior (Foster and Wilson, 2006; Lansink et al., 2008; Lansink et al., 2009; Singer and Frank, 2009). Distinct patterns of activity concurrent with SWRs have been detected in numerous distant brain areas, suggesting that these events coordinate memory processes across the entire brain (Logothetis et al., 2012).

Network activity outside of theta and SWRs. While theta and SWRs have been extensively studied as network patterns that facilitate spatial encoding, consolidation, and retrieval, relatively little is known about how information in encoded outside of these patterns. During immobility and periods of slow movement, such as when an animal is consuming reward or simply sitting quietly awake, SWRs only comprise a small fraction (<10%; Buzsaki, 1989, 2015; Kay et al., 2016; Suzuki and Smith, 1987) of the ongoing network activity. Recently, a subpopulation of principal neurons in CA2 has been shown to encode location in the absence of locomotion, firing specifically outside of SWRs. Along with neurons in CA1 and CA3, these neurons fire during a transient ~200 ms network pattern with opposite polarity to that of sharp-waves. These findings indicate a distinct hippocampal sub-network dedicated to coding the animal's

current location during immobility and even sleep (Kay et al., 2016). In particular, spatial coding during sleep occurred during periods marked by small-amplitude LFP activity distinct from the more commonly studied slow-wave sleep and REM sleep states (Grosmark et al., 2012; Jarosiewicz et al., 2002; Louie and Wilson, 2001; Montgomery et al., 2008; Vanderwolf, 1969). Overall, these observations illustrate that that our understanding of the breadth of brain states relevant to hippocampal processing remains incomplete.

Gamma oscillations. During both the locomotor state and quiescent brain states, an additional rhythm can be seen in the 20-110 Hz range, known as gamma. In the cortex, gamma oscillations have been proposed to play a role in binding neural ensembles, contributing to information transfer and spike-timing dependent plasticity (Fell and Axmacher, 2011; Gerstner et al., 1996; Markram et al., 1997), and it is likely that they play similar roles in the hippocampus. However, unlike cortical gamma, hippocampal gamma has been subdivided into several frequency bands, each of which associates with specific states and subregions and is driven by distinct inputs and mechanisms (Belluscio et al., 2012; Buzsaki and Wang, 2012). Slow (or low) gamma (20-50 Hz) is thought to be driven predominantly by CA3 (Bragin et al., 1995a; Colgin et al., 2009), while fast gamma (50-90Hz) is thought to be driven by the MEC (Colgin et al., 2009). An even higher gamma band (90-150 Hz), sometimes called the epsilon band, has also been suggested (Csicsvari et al., 1999a; Freeman, 2007; Sullivan et al., 2011). During the locomotor state, all three gamma bands can be observed nested within theta cycles, generally with a single gamma band predominating in each cycle. Thus individual theta cycles tend to exhibit either slow or fast gamma in an interleaved fashion, likely dependent on the cognitive demands experienced by the animal. The frequency of gamma coupled to theta may influence the function and content of theta sequences (Colgin et al., 2009; Zheng et al., 2016). During SWRs, slow gamma in particular is transiently increased in power and coherence throughout the hippocampal circuit, and has been proposed as a clocking mechanism to coordinate accurate replay (Carr et al., 2012; Pfeiffer and Foster, 2015).

In the remainder of this chapter, we will focus on the unique contributions of each hippocampal subregion to the patterns of cellular and network activity associated with spatial mnemonic processing in the locomotor state and during SWRs.

1.6 Entorhinal cortex

The EC is the main conduit of information to the hippocampus, sending projections to every subregion. The EC receives and integrates sensory information from the primary sensory cortices and head direction information from the thalamic nuclei via the pre- and para-subiculum. In turn, the EC receives direct feedback from the hippocampus. In rodents, the EC is comprised of medial and lateral subregions with distinct functional roles and anatomical connectivity, which are likely preserved in primates although the anatomical delineation between regions is less clear (Kerr et al., 2007; Witter, 1993). The MEC conveys mostly spatial information, while encoding in the LEC tends to correspond more to objects, object-context associations, cues, and odors (Deshmukh and Knierim, 2013).

Cell characteristics of the EC

Within the MEC, distinct subpopulations of cells have been shown to represent major features of any environment. Grid cells are the most common, comprising 30% of MEC cells, and are found in layers II and III (Zhang et al., 2013). The firing field of a grid cell forms a triangular lattice spanning the entire environment (Hafting et al., 2005). Grid cells are organized into modules that share similar grid scale and orientation; those located in dorsal MEC have smaller grid spacing than those in ventral MEC (Stensola et al., 2012). The other two major MEC populations are border cells, which exhibit firing fields specific to the edge of an environment (Lever et al., 2009; Savelli et al., 2008; Solstad et al., 2008), and head direction cells, which show preference for the animal facing a certain direction independent of location (Sargolini et al., 2006; Taube, 2007). These populations can overlap, as some neurons, especially in layers III and V of the MEC, show both grid and head direction tuning (Sargolini et al., 2006). While grid, head direction, and border cells have been the most extensively characterized populations, they comprise only 50% of the neurons in the MEC, and it is unclear what the contribution of the remaining neural population may be (Sasaki et al., 2015; Zhang et al., 2013). Recently discovered speed cells may comprise part of this population (Kropff et al., 2015), and may be important for the constant updating of an animal's location on the grid cell map, a process known as path integration (for review see McNaughton et al., 2006). Together,

MEC cells likely provide the animal with a spatial map of the environment and a continuous representation of self-location and transmit that information to the hippocampus.

In contrast to the thoroughly studied MEC, the role of the LEC is much less clear. Current evidence suggests that the LEC may be responsible for encoding the objects, odors, and local cues that occur within an environment rather than mapping space on a global scale (Neunuebel et al., 2013). While objects and local cues can also influence the development of place fields in the MEC, LEC neurons generally lack the spatial tuning frequently seen in MEC neurons (Deshmukh and Knierim, 2011; Yoganarasimha et al., 2011). Furthermore, lesions of the LEC have been shown to impair the association of objects with environmental contexts, despite sparing normal object recognition and context recognition (Wilson et al., 2013). This finding, along with others, suggests that the LEC plays a role in linking items and cues with the environment in which they were experienced (Neunuebel et al., 2013). Together, the MEC and LEC are thought to provide the "where" and "what" of an experience to the hippocampus, where it can then be compared to previous experience, integrated with existing frameworks, and stored. In particular, the EC may establish location-based representations of stimuli that could be the basis for the spatial encoding seen in hippocampal cells.

EC network activity

During the locomotor state, theta is prominent in the MEC and strongly entrains neuronal spiking (Deshmukh et al., 2010). Grid cells show theta phase precession (Hafting et al., 2008), and the integrity of grid cell firing is dependent on theta oscillations (Koenig et al., 2011). Surprisingly, although the MEC was initially suspected to be the primary driver of place cell activity, lesions of the MEC do not abolish hippocampal place fields (Hales et al., 2014; Van Cauter et al., 2008). However, MEC lesions do disrupt hippocampal theta phase precession and reduce the spatial specificity and stability of place fields (Hales et al., 2014; Schlesiger et al., 2015; Van Cauter et al., 2008), concomitantly impairing spatial navigation-dependent behavior (Hales et al., 2014). This evidence suggests that the MEC provides critical spatial and temporal cues to refine hippocampal representations of location. Conversely, grid cell integrity is heavily

dependent on hippocampal feedback, as inactivation of the hippocampus abolishes grid cell periodicity (Hafting et al., 2008) (Bonnevie et al., 2013). In parallel to the reduced spatial encoding observed in the LEC compared to the MEC, the power of the theta rhythm is lower in the LEC than in the MEC or hippocampus, and entrainment of LEC neurons by theta is less prominent. This suggests that theta may be particularly important for coordinating spatial processing across the MEC and hippocampus, and less so for non-spatial object information in the LEC (Deshmukh et al., 2010).

Cells in the layers of the EC that project to the hippocampus are thought to be relatively inactive during SWRs themselves (Chrobak and Buzsaki, 1994). However, several studies indicate that the EC, together with the rest of the neocortex, experiences periods of higher firing (up states) and periods of relative inactivity (down states) governed by the neocortical slow oscillation which may be tied to SWR activity in the hippocampus (Battaglia et al., 2004a; Isomura et al., 2006; Sirota et al., 2003; Steriade et al., 1993). SWRs are more likely to occur during up states (Battaglia et al., 2004a; Sullivan et al., 2011), suggesting that the overall cortical state may influence the ability of the hippocampus to generate SWRs, and this modulation may be conveyed by EC inputs.

1.7 Dentate gyrus

Despite its prominent place in the hippocampal circuit, the DG has been one of the least studied of the hippocampal subregions with respect to patterns of network activity. However, it has garnered attention due to several unique characteristics. Most notably, the DG is one of the only regions in the brain that supports persistent neurogenesis throughout life. The regular addition of new neurons to DG circuitry has major implications for network activity in the region (Ge et al., 2008; Schmidt-Hieber et al., 2004) and for behavior dependent on the DG (Dupret et al., 2008; Garthe et al., 2009; Jessberger et al., 2009; Shors et al., 2001; Wojtowicz et al., 2008). A second key feature of the DG is the highly sparse firing of its principal cells, which have very low spontaneous firing rates (Amaral et al., 1990; Jung and McNaughton, 1993) and of which only a very small fraction are active in any given environment (Guzowski et al., 1999). It has been proposed that the sparse firing of distributed ensembles and the addition of newborn neurons into those

ensembles make the DG uniquely suited to perform pattern separation, a process by which similar experiences are disambiguated and encoded by orthogonal representations (Clelland et al., 2009; Marr, 1971).

Cell characteristics of the DG

The principal cell type in the DG is the granule cell (GC). These small, tightly packed cells make up the cell layer 'blades' of the DG. Neurogenesis in the subgranular zone lining the border between the GC layer and hilus consistently adds newborn GCs to the GC layer. These newborn cells migrate and integrate into existing GC layer circuitry over a 4-8 week period, during which they show increased excitability compared to mature GCs (Danielson et al., 2016; Esposito et al., 2005; Ge et al., 2008; Gu et al., 2012; Li et al., 2012; Marin-Burgin et al., 2012; Schmidt-Hieber et al., 2004). GCs tend to fire very sparsely (generally less than 0.5 Hz in awake recordings), and have narrow, asymmetric waveforms (Jung and McNaughton, 1993). Recordings from putative GCs suggest that they have spatially and directionally specific place fields that are highly stable, although smaller than those found in CA3 and CA1 (Jung and McNaughton, 1993; Leutgeb et al., 2007). Moreover, these putative GCs may have more discontiguous sub-place fields than CA3 and CA1 pyramidal cells, although due to dense cellular packing of the DG, this conclusion is confounded by the challenge of identifying the cell type being recorded. It is possible that the cells with multiple sub-place fields may be the hyperexcitable newborn GCs or mossy cells, another excitatory neuronal population in the DG (Danielson et al., 2016; Neunuebel and Knierim, 2012).

Small, subtle changes in an environment are sufficient to prompt global remapping of DG ensembles and thus change DG input to CA3, in contrast to CA3 ensembles which adjust slightly but do not remap (Danielson et al., 2016; Leutgeb et al., 2007; Neunuebel and Knierim, 2014). This falls in line with the idea of pattern separation, showing that the DG can amplify differences between similar experiences. However, it remains challenging to differentiate the contribution of young and mature GCs to ensemble representations. New GCs seem to be important for pattern separation, as blocking neurogenesis impairs pattern separation while stimulating neurogenesis enhances it (Clelland et al., 2009; Creer et al.,

2010; Nakashiba et al., 2012; Sahay et al., 2011; Tronel et al., 2012). This finding is somewhat contradicted, however, by the hyperactive nature of young GCs, which would seem to undermine the activation of orthogonal ensembles capable of distinguishing similar experiences (Danielson et al., 2016; Johnston et al., 2016). However, young GCs have also been shown to more effectively promote feedback inhibition than mature GCs (Temprana et al., 2015), which may offset their hyperactivity (McAvoy et al., 2015).

The sparse firing of granule cells is enforced by high levels of GABAergic inhibition from local inhibitory interneurons. Various interneuron subtypes provide both feedback and feedforward inhibition onto GCs by targeting GC bodies or dendrites, respectively (Savanthrapadian et al., 2014). In addition to interneurons, the hilus also contains excitatory mossy cells (Henze and Buzsaki, 2007; Scharfman and Myers, 2012). As mossy cells are relatively rare (1:100 ratio of mossy cells to granule cells; (Henze and Buzsaki, 2007), and because it is unclear how best to distinguish them from GCs, they have not been well characterized electrophysiologically (Neunuebel and Knierim, 2012). Mossy cells receive inputs either directly from the EC or indirectly through GCs, and synapse onto hilar interneurons and remote GCs (Buckmaster et al., 1996; Larimer and Strowbridge, 2008).   This may allow them to integrate activity across the septotemporal axis of the DG by transferring excitation between GCs, or by suppressing the activity of distant GC populations via feed-forward inhibition (Henze and Buzsaki, 2007; Larimer and Strowbridge, 2008). Together, the interactions between sparsely firing mature GCs, excitable newborn GCs, mossy cells, and interneurons may underlie the DG's ability to integrate entorhinal inputs into distinct representations of mnemonic experience.

DG network activity during the locomotor state

Large, clear theta oscillations can be observed in the DG during the locomotor state (Bragin et al., 1995b) (**Fig. 1.2**). Theta entrains the spiking of both GCs and interneurons (Skaggs et al., 1996), although newborn GCs may be more weakly modulated (Rangel et al., 2013). Spatially modulated GCs also exhibit theta phase precession (Skaggs et al., 1996). Theta phase, as well as the coherence of DG theta with the rest of hippocampus, varies by layer, which may be due to the stratification of inputs from different EC layers

(Montgomery et al., 2009). Theta power and coherence measures also fluctuate based on the activity being performed, although the significance of these observations remains unclear.

During the locomotor state, gamma oscillations nested within the theta rhythm are larger in the hilus than anywhere else in the hippocampus (Bragin et al., 1995a; Buzsaki, 2002; Montgomery and Buzsaki, 2007). Like theta, the power and coherence of DG gamma with the rest of the circuit fluctuates with the cognitive demands of activity performed (Montgomery and Buzsaki, 2007), but the exact role of DG gamma is not known. A study using current source density analysis (see Box) showed the largest gamma current sink in the middle third of the DG molecular layer, where axons from the MEC terminate. This current sink disappeared upon lesion of the EC, further suggesting that DG gamma activity is primarily driven by the EC during locomotor state (Bragin et al., 1995a). This study did not differentiate slow gamma from fast gamma; however, as the EC is thought to promote fast rather than slow gamma in the hippocampus (Colgin et al., 2009), the CSD finding may predominantly reflect fast gamma in the DG.

DG network activity during SWRs

Since SWRs are thought to originate in CA3 and proceed to CA1, as described later in this chapter, most studies have focused on the SWR-related activity that occurs in those subregions. However, several pieces of evidence suggest that the DG also participates in SWR-associated activity. First, granule cell activity has been observed during SWRs (Penttonen et al., 1997) including reactivation during sleep (Shen et al., 1998), potentially driven by the CA3 backprojection (Scharfman, 1994, 2007). Second, state-dependent activity in the DG may affect SWR generation. During slow wave sleep, DG activity can be categorized into "up" and "down" states which correlate with those seen in neocortex (Isomura et al., 2006; Sullivan et al., 2011). As mentioned above, SWRs are more likely to occur during up states than down states (Battaglia et al., 2004a; Isomura et al., 2006; Sullivan et al., 2011). This suggests state-dependent modulation of SWR generation, however, it is unclear whether the DG contributes to this modulation directly, or whether both the DG and CA3 are influenced by EC up/down states in parallel. Finally, a recent study has shown that slow gamma activity in the DG increases during SWRs (Gillespie et al., in press).

This is similar to an SWR-associated transient slow gamma increase observed in CA3 (Carr et al., 2012), which may serve as a critical timing mechanism to organize replay activity during SWRs (Pfeiffer Foster 2015), as we will further discuss below. In the DG, the power of slow gamma transiently increases during SWRs, as does coherence in this frequency band between DG-CA3 and DG-CA1. These results suggest that slow gamma activity engages all subregions of the hippocampus proper during SWRs, potentially coordinating information flow through the circuit. Disruption of DG circuitry, caused by the loss of hilar interneuron populations, results in impaired SWR-associated slow gamma activity throughout the hippocampal circuit, further indicating that the DG may be actively engaged during SWRs (Gillespie et al., in press).

Interestingly, there is another pattern of activity called dentate spikes (DSs) that also occurs in the DG during awake immobility and slow wave sleep (Bragin et al., 1995b; Penttonen et al., 1997). DSs are brief, large-amplitude LFP deflections seen in the hilus and granule cell layer. Two types have been described, one (DS1) which has a broad waveform, shows a phase reversal in the outer molecular layer, and contains some fast gamma activity, and another (DS2) which shows a single narrow LFP peak with a phase reversal in the inner molecular layer (Bragin et al., 1995b). Lesions of the EC eliminate both DS types, and CSD analysis of these events as well as the location of their phase reversals suggests LEC and MEC drive of DS1 and DS2, respectively (Bragin et al., 1995b). Although DSs and SWRs appear during the same behavioral state, they do not coincide. Instead, DSs seem to have the opposite effect on the hippocampus from SWRs; rather than inducing ensemble activity downstream, DSs seem to transiently suppress CA3 and CA1 activity (Bragin et al., 1995b; Buzsaki et al., 2003; Penttonen et al., 1997). Although behavioral correlates of DSs are not well understood, this observation suggests that they may enable a transient blockade of hippocampal output via CA1.

1.8 CA3 and CA1

CA3 and CA1 are by far the most well-studied subregions of the hippocampus. As activity patterns are highly coordinated across CA3 and CA1, we will discuss their network activity in parallel, while highlighting the distinctions that embody each region's unique role in hippocampal processing.

Functional roles of CA3

CA3 has been functionally implicated in rapid task acquisition (Cravens et al., 2006; Kesner, 2007; Lee and Kesner, 2003, 2004; Nakashiba et al., 2008; Nakazawa et al., 2003), as well as task recall (Kesner, 2007; Lee et al., 2005; Nakazawa et al., 2002; Schlesiger et al., 2013), the latter of which is likely facilitated by the retrieval of previously learned patterns. For example, lesions of CA3 impair the ability of animals to use partial cues to trigger memory-based performance of a task acquired in the presence of full cues (Gold and Kesner, 2005). This ability to recall a whole memory based on a partial cue is known as pattern completion, and may be a critical neural process for comparing current events to past memories and generalizing across similar experiences (for review see Knierim and Neunuebel, 2016; Leutgeb and Leutgeb, 2007; Rolls, 2007). Pattern completion may be supported by the trait that most often distinguishes CA3 in the current literature: its relatively high level of recurrent connectivity compared to other hippocampal subregions (Ishizuka et al., 1990; Li et al., 1994; Witter, 2007). This recurrence has been presented as anatomical evidence that CA3 acts as an autoassociative network (Gilbert and Brushfield, 2009; Guzowski et al., 2004; Marr, 1971; McClelland and Goddard, 1996; Papp et al., 2007; Rolls, 2007; Treves and Rolls, 1991; Treves and Rolls, 1992, 1994). Autoassociation implies that the activation of a subset of neurons within an ensemble can drive sustained activation of the entire ensemble by propagating excitation through reciprocal connections between cells (Lisman, 2003). Such an autoassociative network might also exhibit attractor dynamics (Kali and Dayan, 2000; Lengyel et al., 2005; Leutgeb et al., 2005c; Marr, 1971; Mcnaughton and Morris, 1987; Rolls, 2007). In CA3, an ensemble of neurons representing a stored memory could act as the attractor basin; when an input is similar enough to the stored memory, the activity in the network settles on that ensemble. When an external input is sufficiently distinct from the

27

stored pattern, it would outweigh the ongoing activity to transition the pattern of activity to a new group of cells, and thus form a distinct memory (Colgin et al., 2010; Leutgeb and Leutgeb, 2007; Renno-Costa et al., 2014). While there is not yet definitive evidence that CA3 functions as a true attractor network, the importance of its recurrent collaterals to pattern completion have been supported by recent findings. Results showing that distal CA3 (where the level of recurrence is highest) shows stronger autoassociation than proximal CA3 (where recurrence is lowest) suggest that the contribution of CA3 subregions to pattern completion depends on the local recurrent connectivity (Lee et al., 2015). The autoassociative nature of CA3 is further supported by the stability of CA3 population representations in response to small changes in environmental cues (Neunuebel and Knierim, 2014), indicating that weak sensory inputs are insufficient to substantially alter the representation.

Functional roles of CA1

The CA1 network represents the final stage of hippocampal processing before information is sent to the subiculum and to the rest of the brain. CA1 continually integrates input received from CA3 and the EC during ongoing experience (Bittner et al., 2015; Kali and Freund, 2005; Milstein et al., 2015; Piskorowski and Chevaleyre, 2012; Spruston, 2008) and permits incremental spatial learning and retrieval even in the absence of CA3 input (Nakashiba et al., 2008). One possible function of CA1 is to compare past experiences stored in and retrieved by CA3 with new information from ongoing experiences transmitted by the EC. CA1 would then create a new representation when there is no past experience that directly corresponds to current input (Duncan et al., 2012; Hasselmo and Schnell, 1994; Lee et al., 2004a; Lisman, 1999; Lisman and Grace, 2005; Meeter et al., 2004; Vinogradova, 2001). CA1 may therefore compile memories by layering newly learned spatial information onto past and current representations of the global environment.

The possibility that CA1 somehow compares stored and new information is consistent with observations that CA1 responds to novelty (Kumaran and Maguire, 2007; Li et al., 2003; Lisman and Otmakhova, 2001), specifically by signaling the presence of a novel experience and potentially enhancing

the incorporation of novel information into existing memories (Larkin et al., 2014). In particular, CA1 place cells change their firing rates in response to novel or changing objects (Deshmukh and Knierim, 2013; Fyhn et al., 2002; Larkin et al., 2014; Lenck-Santini et al., 2005) and novel spatial environments (Karlsson and Frank, 2008; Nitz and McNaughton, 2004; VanElzakker et al., 2008). CA1 network patterns, including SWRs and gamma, are also modulated by novelty both during the novel experience and during sleep afterward (Cheng and Frank, 2008; Dupret et al., 2010; Eschenko et al., 2008; Karlsson and Frank, 2009; Kemere et al., 2013; O'Neill et al., 2008; Ramadan et al., 2009; Singer and Frank, 2009). Importantly, novelty-induced increases in firing rate and SWR reactivation appear to be specific to CA1, and not CA3 (Karlsson and Frank, 2008), suggesting that the recognition of novelty is a function that emerges uniquely in CA1 or in conjunction with the EC, rather than through input to CA1 from CA3 (Larkin et al., 2014).

Cell characteristics of CA3 and CA1

In support of their complementary functional roles, CA3 and CA1 exhibit small but important differences in how their principal cells represent space and other variables. Place cells in the two regions have similar spatial coverage and firing rates (Best and Ranck, 1982; O'Keefe and Dostrovsky, 1971; Olton et al., 1978) but CA3 is thought to be more strictly responsive to spatial location than CA1 (Barnes et al., 1990; Knierim et al., 2006; Lee et al., 2004b; Leutgeb et al., 2005a; Leutgeb et al., 2005b; Leutgeb et al., 2004; Vazdarjanova and Guzowski, 2004). Once CA3 places fields are established in a given environment, firing rates and spatial coverage remain stable over time (Mankin et al., 2015; Mankin et al., 2012). CA3 ensembles also show higher sensitivity to absolute location than CA1 ensembles, as distinct populations of CA3 cells can represent distinct spatial locations, even if the local environments in those locations are visually identical (Leutgeb et al., 2004). In contrast, the fields of CA1 cells show prolonged susceptibility to modulation by sensory cues and changes in the environment (e.g. Leutgeb et al., 2004; Vazdarjanova and Guzowski, 2004), and thus are more likely to globally remap their firing fields within the same environment than CA3 cells. In addition to encoding spatial information, CA1 place cells can integrate nonspatial information into their firing patterns, usually via rate remapping, to odors, objects, goals, and

conditioned stimuli (Dupret et al., 2010; Eichenbaum et al., 1987; Hok et al., 2007; Kennedy and Shapiro, 2009; Kobayashi et al., 1997; Komorowski et al., 2009; Manns and Eichenbaum, 2009; McKenzie et al., 2014; Moita et al., 2003). The sensitivity of CA1 ensembles is further reflected in novel environments, in which CA1 firing rates start high and then decline along with the proportion of active CA1 cells as an environment becomes familiar. This tunes the population representation to a subset of CA1 neurons (Karlsson and Frank, 2008).

During early exposure to an environment, place cells in both CA3 and CA1 may fire in any direction of movement through their place field (Muller et al., 1987). However, over the course of experience on a stereotyped path, such as a linear track, cells tend to develop a directionality preference (Battaglia et al., 2004b; Frank et al., 2004; McNaughton et al., 1983). This directional bias is informative, as the ordered firing of unidirectional place cells enables the decoding of not only the spatial trajectory of an animal, but also the animal's direction of movement. In addition, cells in both CA3 and CA1 are capable of developing path equivalence through experience, in which cells fire similarly in geometrically or behaviorally similar areas of a spatial maze. This path equivalence reflects an ability of CA3/CA1 neurons to generalize across related locations and episodes, rather than an inability to distinguish locations (Singer et al., 2010).

Interestingly, despite the flow of information in the canonical trisynaptic loop, the DG is not required for the spatial specificity of place fields in CA3 (McNaughton et al., 1989). Likewise, neither inactivation of CA3 nor the EC is sufficient to abolish place fields in CA1, yet both result in more diffuse, less spatially tuned place fields in CA1 (Brun et al., 2008a; Brun et al., 2002; Mizumori et al., 1989; Nakashiba et al., 2008; Van Cauter et al., 2008). Together, these results suggest that although CA1 place fields can be derived from either EC or CA3 input, both projections are required for robust spatial specificity. These findings also support a role for CA3 in providing a stable spatial framework onto which other types of information can be layered via the more malleable encoding seen in CA1.

CA3 and CA1 network activity during the locomotor state

During locomotion, CA3 and CA1 cell activity is tightly coupled to the theta rhythm, with both regions exhibiting temporally compressed place cell sequences via theta phase precession that emerge rapidly during novel experience (Feng et al., 2015). As mentioned previously, theta phase precession is thought to be a mechanism by which on-line spatial encoding is compressed onto a time scale conducive to neural plasticity (Skaggs et al., 1996). Theta phase precession has likewise been proposed to promote synaptic plasticity between CA3 and CA1 cells, such that synapses are strengthened between cells with overlapping place fields via the repeated coincident firing of those cells during experience (Isaac et al., 2009; Mehta et al., 2002; Mehta et al., 2000; O'Neill et al., 2008). Moreover, the theta phase at which a place cell fires indicates how far into the firing field the animal is, providing a temporal code for location. This temporal code, consisting of the precise timing of spikes relative to theta, exists independently from the rate code of the local network. The rate code is defined as the collective firing rates of the local ensemble, which represent both location as well as other nonspatial features due to rate remapping (Huxter et al., 2003; Jensen and Lisman, 2000; Mehta et al., 2002). The addition of a temporal code to this framework thus allows for precise spatial coding despite firing rates that may be highly variable (Ahmed and Mehta, 2009; Hopfield, 1995; Mehta et al., 2002).

The phases of theta have functional implications in terms of inputs to the circuit, possibly segregating encoding and retrieval (Hasselmo, 2005; Hasselmo et al., 2002; Mizuseki et al., 2009). At the trough of theta, Schaffer collateral synapses are highly susceptible to long-term potentiation (Hyman et al., 2003; Kwag and Paulsen, 2009) and receive maximal excitation from the EC, potentially facilitating the encoding of new information (Brankack et al., 1993; Colgin et al., 2009; Kamondi et al., 1998; Mizuseki et al., 2009). At the peak of theta, EC input to CA1 decreases and gives way to maximal CA3 input, but CA3 synapses onto CA1 neurons are more likely to be depressed than potentiated (Hyman et al., 2003; Kwag and Paulsen, 2009). This may allow for retrieval via CA3 without corrupting or re-storing the retrieved information (Hasselmo, 2005; Hasselmo et al., 2002; Mizuseki et al., 2009). Importantly, the theta referred to here was recorded from the hippocampal fissure, which is ~180 degrees out of phase with the theta

recorded in the CA1 pyramidal cell layer (Hasselmo, 2005). Recent behavioral evidence supports this hypothesis of input segregation, as inhibition of CA1 at the peak of theta enhanced spatial working memory performance when delivered during the encoding phase of the task, while inhibition during the trough improved performance during the retrieval phase of the task (Siegle and Wilson, 2014). This balance of encoding and retrieval within single theta cycles could be due to the dendritic integration of CA3 and EC inputs on CA1 neurons, regulated by waxing and waning inhibition at theta frequencies (Milstein et al., 2015).

Another critical function of theta in CA3 and CA1 may be the exploration of future trajectories and goals. Early in learning, an animal will often pause at decision points on a maze and visually survey possible routes before choosing a trajectory (termed vicarious trial and error, or VTE) (Muenzinger, 1938; Tolman, 1938). During periods of VTE behavior, the neural representation of location sweeps ahead of the animal as distant place cells activate (Johnson and Redish, 2007). These sweeps of activity within a theta cycle, called theta sequences, are distinct from the majority of theta content because they activate representations outside the animal's current position. Similarly, nonlocal theta sequences can be predictive, reflecting the upcoming behavior of the animal. When deciding between possible reward locations, place cells representing the chosen goal location become active during theta cycles ahead of their place fields, despite often substantial distances from the animal's current location (Wikenheiser and Redish, 2015).

During ongoing locomotion, place cells may also fire at different rates in the same location depending on the animal's future destination (prospective coding) as well as previous positions (retrospective coding) (Ainge et al., 2007; Ferbinteanu and Shapiro, 2003; Frank et al., 2000; Ito et al., 2015; Wood et al., 2000). These types of coding suggest that place field activity can encode not only absolute location, but also the animal's position relative to an ongoing trajectory (Frank et al., 2000) and thus reflects both upcoming and past experience. Interestingly, the prospective coding phenomenon has also been observed in cells which are modulated by time rather than location (for review see Eichenbaum, 2014). These "time cells" were first observed to fire at temporally specific intervals while an animal ran on a treadmill in a singular location, forming sequences which predicted the animal's upcoming trajectory

(Pastalkova et al., 2008). Time cells exhibit theta phase precession and can also have place properties, suggesting that time and place encoding coexist within theta sequences (Kraus et al., 2013; MacDonald et al., 2011). Time cell coupling to the theta rhythm has also been described in the context of odor memory in head-fixed animals, indicating that temporal encoding also exists in the absence of movement (MacDonald et al., 2013). Together the current evidence points to a role for theta in exploring future possibilities and temporally organizing spatial experience.

As mentioned earlier, gamma band activity can be found nested within theta oscillations during the locomotor state (Belluscio et al., 2012; Bragin et al., 1995a; Colgin et al., 2009; Csicsvari et al., 2003). The frequency of both slow and fast gamma bands increases with increasing speed of locomotion, as do theta frequencies, indicating locomotor-driven coupling (Ahmed and Mehta, 2012). In both CA1 and CA3, slow gamma shows a subtle increase in frequency at higher velocities, while the frequency of fast gamma is strongly modulated by speed (Ahmed and Mehta, 2012; Zheng et al., 2015). In addition to modulating oscillation frequency, movement speed differentially alters the power of slow and fast gamma in rats. With increasing speed, slow gamma power decreases while fast gamma power increases, suggesting continuous modulation of the circuit as the behavioral state of the animal changes (Kemere et al., 2013). However, both slow and fast gamma power were positively modulated by speed in mice, suggesting that gamma power modulation varies across species (Chen et al., 2011). The shift to higher frequencies and power of fast gamma is mirrored by an increase in MEC firing rates at faster speeds (Zheng et al., 2015), suggesting predominant engagement of CA1 by the EC at high speeds and by CA3 at low speeds (Kemere et al., 2013; Zheng et al., 2015).

The coupling of theta with either slow or fast gamma has been proposed to underlie dynamic switching between different sources of information in the hippocampus, modulated by behavioral and cognitive demands. Fast gamma, driven by the MEC, is thought to convey information about current location and state, and coincides with spiking activity enriched for cells with place fields near the animal's current position. In contrast, slow gamma, driven by CA3 (Belluscio et al., 2012; Colgin et al., 2009; Scheffer-Teixeira et al., 2012), may be more likely to coincide with place field spiking that represents

trajectories extending beyond the current location (Zheng et al., 2016). The theta cycles containing slow gamma are likely to correspond with the nonlocal representations during VTE or trajectory planning, as mentioned above (Johnson and Redish, 2007; Wikenheiser and Redish, 2015). As further evidence for a role in active information processing, the phase coupling between theta and both slow and fast gamma is increased during awake locomotion as compared to REM sleep (Montgomery et al., 2008). Together, the evidence suggests that dynamic coupling between network oscillations may reflect changing cognitive demand on the hippocampal circuit during active learning and navigation (Axmacher et al., 2010; Bott et al., 2015; Colgin, 2015; Colgin et al., 2009; Igarashi et al., 2014; Montgomery and Buzsaki, 2007; Tort et al., 2009; Zheng et al., 2016).

CA3 and CA1 network activity during SWRs

CA1 and CA3 are the main contributors to the network activity involved in SWRs and play distinct but highly intertwined roles in supporting these events. SWRs are an intrinsic hippocampal pattern, frequently occurring in hippocampal slice preparations in which major hippocampal afferents, such as those from the EC, are generally disrupted (e.g. Maier et al., 2003). Since the discovery of replay during SWRs, hundreds of studies have investigated their origins and functional contributions to memory processes like consolidation and retrieval.

During SWRs, ensembles of neurons are reactivated in a precise, time-compressed sequence that recapitulates experience. Place cell reactivation was originally demonstrated during sleep after the animal had traversed the reactivated cell's place field (Pavlides and Winson, 1989). Ensemble reactivation during sleep was then demonstrated by the finding that pairs of cells with overlapping place fields in a previously explored environment reactivated together more frequently than pairs of cells with distant place fields (Wilson and McNaughton, 1994). With improvements in large scale recording technology, it became possible to observe the reactivation of longer neuronal sequences during sleep that recapitulated awake experience (Kudrimoti et al., 1999; Lee and Wilson, 2002; Nadasdy et al., 1999; Skaggs and McNaughton, 1996). These replay events were shown to occur specifically during SWRs (Kudrimoti et al., 1999; Lee

and Wilson, 2002). Replay was also suggested to occur during periods of awake immobility (Kudrimoti et al., 1999; Pavlides and Winson, 1989) and then confirmed during pauses in awake behavior (Diba and Buzsaki, 2007; Foster and Wilson, 2006; Jackson et al., 2006; O'Neill et al., 2006). Some studies have reported that SWRs can even occur during movement (Cheng and Frank, 2008; O'Neill et al., 2006). The time-compressed representation of prior experience during SWRs made these network events compelling candidates for neural mechanisms of memory processes.

In support of this theory, several studies have provided causal evidence for the essential role of SWRs in learning and memory. During rest immediately following training sessions on a spatial memory task, disruption of SWRs impaired subsequent task performance and delayed task acquisition (Ego-Stengel and Wilson, 2010; Girardeau et al., 2009). These results suggest a critical role for SWRs during sleep in memory consolidation. Disruption of SWRs during awake immobility also had a detrimental effect on spatial task acquisition, impairing the component of the task that most relied on linking experiences across time and making choices based on immediate past experience (Jadhav et al., 2012). This result implicates SWRs in retrieval during ongoing decision-making. Conversely, successful performance of working memory tasks can be correlated with enhanced content or increased incidence of SWRs (Dupret et al., 2010; Eschenko et al., 2006; Eschenko et al., 2008; Molle et al., 2009; Ramadan et al., 2009) or even predicted by high place cell reactivation during SWRs (Singer et al., 2013). In addition, experiences such as the exploration of novel environments or receipt of reward increase SWR incidence both in the awake state and during sleep afterwards (Cheng and Frank, 2008; Eschenko et al., 2008; Karlsson and Frank, 2009; Kudrimoti et al., 1999; Singer and Frank, 2009; Wu and Foster, 2014), suggesting that particularly salient experiences increase SWR activity. The increase in awake SWRs may facilitate the association of novel spatial trajectories with their outcomes, while the increase in sleep SWRs may support the consolidation of those experiences through persistent reactivation and communication with the neocortex (Carr et al., 2011; O'Neill et al., 2010). Interestingly, SWRs during wakefulness tend to be more accurate in replicating past experience, while SWRs during sleep show lower fidelity (Karlsson and Frank, 2009). This may relate to their proposed functional differences: awake SWRs may be critical for the rapid, accurate retrieval of stored

experiences to evaluate a current decision, while sleep SWRs may rely on less accurate replay to more flexibly integrate new experiences with existing memory frameworks (Roumis and Frank, 2015).

The content of SWR replay is directly dependent on prior experience (Silva et al., 2015), but can also be influenced by many factors with implications for replay function. During sleep SWRs, replay content can be biased by current odor or sound cues, despite the animal not attending to the stimulus (Bendor and Wilson, 2012). During awake SWRs, replay often begins at the animal's current location (Csicsvari et al., 2007; Davidson et al., 2009; Karlsson and Frank, 2009). The length of a SWR event has been shown to correlate with the length of the trajectory replayed, and multiple SWRs can chain together with replay spanning across the chain (Davidson et al., 2009). Replay events can be either forward or reverse; meaning exactly as the event was initially experienced, or "rewinding" through the steps of a trajectory. The distinction between these two options, especially on mazes in which the animal can traverse each section in both directions, relies on the directionality of the cells involved (Diba and Buzsaki, 2007; Foster and Wilson, 2006). Because place field activity on a linear track becomes more unidirectional with experience (Battaglia et al., 2004b; Frank et al., 2004; McNaughton et al., 1983), unique ensembles distinguish trajectories in the two directions, differentiating forward and reverse replay (Csicsvari et al., 2007; Diba and Buzsaki, 2007; Foster and Wilson, 2006; Gupta et al., 2010). Forward replay is more common before an animal embarks on a trajectory, suggesting a potential role for planning or evaluating choices. In contrast, reverse replay is observed more after trajectories are completed, which may be important for associating the location of a reward with the steps taken to reach it (Diba and Buzsaki, 2007). While functional and correlative studies have pointed to a role for SWRs in planning and reward associations (Pfeiffer and Foster, 2013; Singer et al., 2013; Singer and Frank, 2009), none have been able to address directional specificity, so the potential implications of forward and reverse replay remain speculative. In addition to the replay of previous and upcoming trajectories, replay of remote environments and distant locations has also been observed during the awake state (Davidson et al., 2009; Karlsson and Frank, 2009). The diversity of SWR content likely enables the flexible consolidation and possibly retrieval functions of hippocampal replay.

Several lines of evidence indicate that SWRs are generated in CA3. During SWRs, synchronous neuronal discharge is seen first in the CA3a and b subregions, and later in CA3c and CA1, suggesting a flow of activity (Csicsvari et al., 2000). More than 10% of the CA3 population must burst synchronously in order to significantly increase firing rates in CA1 (Csicsvari et al., 2000). This burst in CA3 activity results in the sharp wave of the SWR, a large deflection lasting ~200 ms (Buzsaki, 1986) in the LFP signal thought to be caused by the massive depolarization of CA1 pyramidal cells from the influx of CA3 excitation. The sharp wave lasts the duration of the SWR (~100 ms or more)(Buzsaki et al., 1992). Once discharged by CA3, the spiking of CA1 pyramidal cells then drives firing of basket and chandelier interneurons in CA1(Csicsvari et al., 1999b). The fast feedback between excitation and inhibition in the local network results in the characteristic high frequency ripple oscillation detected in CA1, with principal cells firing at the trough of the oscillation and interneurons firing at the peaks (Buzsaki et al., 1992; Csicsvari et al., 1999b; Cutsuridis and Taxidis, 2013; Ylinen et al., 1995). Pharmacological blockade of GABAergic signaling eliminates SWRs, demonstrating a dependence on local inhibition to pace and sustain the high frequency oscillation (Stark et al., 2014). Recently, the sharp wave depolarization of CA1 dendrites was shown to be critical for the long term potentiation of CA3-to-CA1 synapses between cell pairs involved in SWR replay events (Sadowski et al., 2016), although the role of local inhibition in this plasticity remains unknown.

Strikingly, CA1 can generate and maintain brief, high frequency events even when CA3 inputs are removed (Nakashiba et al., 2009). However, these SWR-like events oscillate at a lower frequency than normal SWRs and do not show the ordered reactivation of ensembles indicative of replay (Nakashiba et al., 2009; Stark et al., 2014). This further suggests that CA3 provides important excitatory drive to CA1 that activates the pyramidal cell ensembles underlying meaningful replay events.

Surprisingly, although ensembles active during SWRs often include neurons from the CA3 and CA1 regions of both hemispheres, ripple oscillations themselves are not always coherent across subregions or hemispheres (Csicsvari et al., 1999a; Sullivan et al., 2011; Ylinen et al., 1995). This suggests that a separate network oscillation is necessary for coordinating place cell spiking activity across regions.

Recently, a transient increase in slow gamma (20-50 Hz) power during SWRs was observed in CA1 and CA3, which may be an important organizational signal for replay. Specifically, slow gamma coherence between CA3 and CA1 increases during awake SWRs and is positively correlated with higher fidelity of replay, suggesting that slow gamma may coordinate replay activity between the two regions (Carr et al., 2012). As mentioned previously, slow gamma is thought to originate in CA3 (Colgin et al., 2009) and shows highest power in the CA1 SR, where input from CA3 reaches CA1. Evidence of slow gamma in the DG also coherent with CA3 and CA1 during SWRs (Gillespie et al., in press), suggests that slow gamma activity might coordinate SWR activity throughout the entire hippocampus. With an established role in binding ensembles at a time scale optimal for plasticity (Axmacher et al., 2006; Bibbig et al., 2001; Isaac et al., 2009; Kopell et al., 2000; Wespatat et al., 2004), slow gamma may provide the temporal organization critical for replay during SWRs (Carr et al., 2012; Colgin, 2012). Furthermore, recent evidence shows that spatial trajectories during replay events do not proceed at a constant rate, but instead alternate between virtual movement and stillness in a manner time-locked to the slow gamma rhythm (Pfeiffer and Foster, 2015). Together, these findings suggest that slow gamma activity in CA1 and CA3 plays an important organizational role during SWRs.

1.9 CA2

Relative to CA3 and CA1, CA2 has received relatively little attention in the hippocampal literature. CA2 was first characterized as a distinct hippocampal subregion due to the absence of both thorny excrescences on dendrites and afferent mossy fibers from the DG, thus distinguishing it from CA3, while its enlarged somata distinguished it from CA1 (Ishizuka et al., 1995; Lorente de Nó, 1934). More recently, CA2 has been distinguished by a variety of molecular markers (Lee et al., 2010; Lein et al., 2005; Lein et al., 2004; San Antonio et al., 2014; Vellano et al., 2011; Zhao et al., 2001), distinct reciprocal connections with the supramammillary nucleus of the hypothalamus (Cui et al., 2013), and the expression of receptors for the neuromodulators vasopressin and adenosine (Ochiishi et al., 1999; Young et al., 2006). Partially because of these markers, there have been some recent advances in our understanding of CA2's physiology

and function. However, molecularly defined CA2 neurons are intermingled with overlapping cells from proximal CA1 and CA3a (Dudek et al., 2016; Hitti and Siegelbaum, 2014; Lein et al., 2005), making it a challenge to study CA2 neurons specifically.

Electrophysiological properties of CA2 remained almost completely unexplored until recently, but it is now clear that CA2 is more than simply a relay center between CA3 and CA1 (Bartesaghi and Gessi, 2004; Jones and McHugh, 2011; Mercer et al., 2007; Sekino et al., 1997). Plasticity at the CA3-CA2 synapse is surprisingly hard to induce, and CA2 cells do not show changes in synaptic strength with conventional protocols of long term potentiation and depression used in CA3 and CA1 (Simons et al., 2009; Zhao et al., 2007) This is partially because CA2 cells have more negative resting membrane potentials than CA3/CA1 neurons, thus requiring greater input current to fire spikes necessary for activity-dependent synaptic plasticity (Zhao et al., 2007). In addition, CA2 interneurons provide feedback and feedforward inhibition to CA3 and CA1, which may be important for circuit function (Mercer et al., 2012; Mercer et al., 2007; Valero et al., 2015). CA2 pyramidal neurons are also unique in their dendritic integration. Unlike CA1 neurons, CA2 neurons are more strongly excited by EC layer II synapses onto their distal dendrites than by CA3 synapses onto their proximal dendrites (Chevaleyre and Siegelbaum, 2010). CA2 could thus act as a strong relay from EC to CA1, which may account for the persistence of spatial encoding in CA1 in the absence of CA3 input (Chevaleyre and Siegelbaum, 2010; Nakashiba et al., 2008). This idea is supported by slice physiology demonstrating strong excitation of CA1 pyramidal cells at synapses from CA2 (Chevaleyre and Siegelbaum, 2010; Kohara et al., 2014).

One of the most intriguing functional roles for CA2 is its contribution to social recognition memory (Hitti and Siegelbaum, 2014; Stevenson and Caldwell, 2014). This was originally proposed based on strong vasopressinergic afferents to CA2 from the paraventricular nucleus of the hypothalamus (Cui et al., 2013) and the potentiation of CA2 responses to vasopressin (Pagani et al., 2015), given vasopressin's known role in social behavior (DeVito et al., 2009; Wersinger et al., 2002; Wersinger et al., 2004). This role was specifically tested in mice with inhibited CA2 synaptic output. These mice were significantly impaired in their ability to recognize and distinguish familiar companion mice from novel mice. However, spatial

working memory and general sociability was left intact (Hitti and Siegelbaum, 2014). The relevance of social experience to CA2 is further supported by recent findings showing that social experience prompts CA2 to globally remap in the absence of any environmental change (Alexander et al., 2016). These studies are the first to link CA2 neural activity with behavioral consequences.

Cell characteristics of CA2

CA2 place cells were previously thought to be functionally indistinguishable from CA1 place cells (Martig and Mizumori, 2011). Recent studies, however, have suggested unique encoding properties of CA2 cells. Compared to CA1 and CA3 place cells, cells recorded in CA2 tend to have higher mean firing rates, larger spatial coverage of the environment and more spatial firing fields per cell (Lu et al., 2015; Mankin et al., 2015). In addition, they exhibit lower preference for spatial context, such that putative CA2 cells distinguish different environments much more weakly than do CA1 and CA3 cells. Notably, a recent study reports that the CA2 population representation of similar environments decorrelates over extended periods of time, indicating that CA2 cells may facilitate the encoding of similar memory episodes occurring at different time points (Mankin et al., 2015).

Recent evidence suggests that the CA2 neurons described by Mankin and colleagues may comprise a subpopulation of the neurons found at the CA2 anatomical locus. In addition to these neurons, there also exists a subpopulation of cells with spatially specific fields that are predominantly active during periods of low velocity and immobility. These neurons located in CA2 encode the animal's location in the absence of movement, and continue to encode for location during periods of sleep characterized by desynchronized activity (Kay et al., 2016).

CA2 network activity

Very little is known about network activity in CA2. The frequency of theta detected in CA2 is similar to CA1, and CA2 neurons exhibit comparable levels of theta modulation to CA1 neurons (Kay et al., 2016; Mankin et al., 2015), with slightly slower theta phase precession in cells with enlarged place

fields (Mankin et al., 2015). During SWRs, recent findings have highlighted a potentially unique activity pattern in CA2. In a study of a small population of cells, Valero and colleagues demonstrated that CA2 neurons hyperpolarize during SWRs *in vivo* while CA1 and CA3 neurons are depolarized and excited (Valero et al., 2015). In line with this evidence, it has been hypothesized that CA2 would be largely suppressed during strong activation of CA3 as is thought to occur during SWRs (Jones and McHugh, 2011). Notably, the subpopulation of neurons located in CA2 that were uniquely active during immobility were found to be either unmodulated or negatively modulated by SWRs, raising the possibility that lack of participation in SWRs is a defining property of CA2 neurons (Kay et al., 2016).

1.10 Subiculum

The subiculum is a major site of hippocampal output and is responsible for distributing information received from CA1 pyramidal cells to the neocortex and subcortical structures, as its projections are generally much more numerous than those directly from CA1 (Meibach and Siegel, 1977; O'Mara, 2006; Rosene and Van Hoesen, 1977; Swanson and Cowan, 1977). Lesions of the subiculum result in comparable impairment of learning and memory performance to lesions of the hippocampus proper (Morris et al., 1990). Lesions of both hippocampus and subiculum cause a more severe impairment, suggesting that the subiculum adds a layer of functionality rather than simply relaying hippocampal output (Morris et al., 1990; Potvin et al., 2006; Potvin et al., 2007). The dorsal subiculum is thought to be particularly important for spatial memory, and evidence exists to suggest that subicular neurons integrate many layers of information from CA1 and project rich representations to downstream areas. In addition, the ventral subiculum, with substantial inputs from and outputs to subcortical areas, plays a key role in the inhibition of the hypothalamic-pituitary-adrenal axis, thus serving as the interface between hippocampal mnemonic activity and the limbic stress response (O'Mara, 2006).

Cell characteristics of the subiculum

Historically, subicular principal cells have often been categorized into two populations: bursting cells and regular-firing cells (Witter, 2006). It has been suggested that bursting cells are more likely to target more spatial areas, like the MEC, while regular spiking cells may send more projections to the amygdala and LEC (Kim and Spruston, 2012). While some evidence suggests that subicular neurons lie on a spectrum of "burstiness" regardless of their location in the subiculum (Kim et al., 2012), other findings indicate that burstiness, as well as firing rates and spatial tuning, depends on the cell's position within the subiculum relative to CA1 (Jarsky et al., 2008; Sharp, 2006; Sharp and Green, 1994; Staff et al., 2000). Indeed, firing patterns of subicular neurons differ substantially along the proximal-distal axis (Sharp, 1996), with pyramidal cells in the proximal subiculum (nearest CA1) exhibiting lower firing rates and relatively smaller firing fields, similar to CA1 place cells, than neurons in the distal subiculum (Kim et al., 2012). The dispersed but rate-modulated firing fields of distal subicular neurons allow them to encode more spatial information than CA1 place cells, and may enable the efficient transfer of this information to the neocortex (Kim et al., 2012). Further in support of this idea, many CA1 neurons are thought to converge onto single subicular neurons, potentially explaining their complex rather than simply location-modulated firing fields. This may allow the subiculum to integrate dispersed CA1 information into a more compressed, rich representation for broad dispersal throughout the brain (O'Mara, 2005) (Deadwyler and Hampson, 2004).

Subiculum network activity

Although generally understudied, several findings inform our understanding of network activity in the subiculum during various behavioral states. During the locomotor state, subicular neurons show robust phase precession similar to CA1 (Kim et al., 2012). During awake immobility and rest, SWRs can be detected in subiculum at the same time as in CA1 (Bohm et al., 2015; Chrobak and Buzsaki, 1994, 1996). SWRs differentially modulate populations of subicular neurons; bursting cells tend to be activated during SWRs, while regular-firing cells are suppressed by SWRs (Bohm et al., 2015; Eller et al., 2015). The isolated subiculum has been shown to generate both slow and fast gamma oscillations *in vitro* (Jackson et

al., 2011), suggesting that the subiculum may participate in gamma activity during the locomotor state and SWRs. Beyond this, little is understood of how the subiculum engages in and contributes to network activity in order to facilitate widespread distribution of hippocampal output.

1.11 Hippocampal function along the dorsoventral axis

The vast majority of our knowledge about hippocampal activity comes from studies of the dorsal hippocampus (dH). This is primarily because it is easily accessible for electrophysiological recording, whereas recording from a deep brain structure such as ventral hippocampus (vH) is more technically challenging. Thus far, the hypothesized functional distinction between dH and vH (which describes roles in spatial and emotional processing, respectively) comes mostly from anatomical connectivity, lesion studies, differences in the spatial specificity of each region's place fields, and differential genetic expression (Dong et al., 2009; Fanselow and Dong, 2010; Moser and Moser, 1998; Strange et al., 2014). In particular, genetic markers are expressed in a gradient along the dorsoventral axis and highly differentiate ventral pyramidal neurons from dorsal pyramidal neurons (Cembrowski et al., 2016). Dorsal hippocampus receives more visual cortical inputs via the EC, while vH receives more olfactory and gustatory inputs. In terms of outputs, dH projects directly to the deep layers of the EC and mostly indirectly, via the subiculum, to other cortical areas such as the retrosplenial cortex and prefrontal cortices. In contrast, vH projects not only to the deep layers of the EC but also heavily and directly to the medial prefrontal cortex, orbitofrontal cortex, olfactory and auditory cortices, amygdala (Cenquizca and Swanson, 2007), nucleus accumbens (Brog et al., 1993; Groenewegen et al., 1987), and hypothalamus (Cenquizca and Swanson, 2006). These distinct anatomical outputs suggest that vH dominates the hippocampal innervation of areas associated with processing emotional information, such as anxiety and reward. Lesion studies further implicate the dH in spatial learning to a greater extent than vH (Bannerman et al., 1999; Ferbinteanu and McDonald, 2001; Moser et al., 1993; Moser et al., 1995; Pothuizen et al., 2004; Richmond et al., 1999), which is implicated in anxiety (Bannerman et al., 2004; Henke, 1990; Kjelstrup et al., 2002; Wang et al., 2013; Weeden et al., 2015; Zhang et al., 2001). However, the results of these studies may depend on the animal's training

protocol, such that the vH is sufficient for spatial learning over longer time periods while dH may be required for rapid acquisition of spatial tasks (Bast, 2007; Bast et al., 2009; de Hoz et al., 2003; Loureiro et al., 2012). Ventral hippocampus may also be important for developing representations of environmental context over time (Komorowski et al., 2013) and transferring spatial knowledge across contexts to facilitate learning in new environments based on prior experience (de Hoz and Martin, 2014).

Cell characteristics across the dorsoventral axis

The landmark electrophysiological finding that distinguished dorsal and ventral hippocampus is that place fields increase gradually in size along the dorsoventral axis, tightly defined in dH and reaching vast spatial coverage at the ventral pole (Ciocchi et al., 2015; Jung et al., 1994; Kjelstrup et al., 2008; Komorowski et al., 2013; Poucet et al., 1994; Royer et al., 2010). This is consistent with an increase in the spacing of grid cell fields along the dorsoventral axis of entorhinal cortex (Brun et al., 2008b; Stensola et al., 2012). From these findings it was hypothesized that vH could not accurately encode for spatial information using cells with such little spatial specificity. Recently, however, a study of ventral CA1 in mice suggested that the distributed representations of space in vH may actually be ideal for transmitting spatial information to downstream regions (Keinath et al., 2014). While single-cell spatial selectivity is lower in vCA1 due to large place field sizes, the population of vCA1 cells encodes an animal's location just as accurately as the dorsal CA1 population. This is possible via population coding: with some overlap in cells' place fields, each spatial location will be represented by a specific subset of cells firing at specific rates (Keinath et al., 2014; Kim et al., 2012; Olypher et al., 2003; Osborne et al., 2008). In addition to spatial information, non-spatial correlates seem to increase in strength in vH, in contrast to dH where representation of variables other than place is limited. For example, some ventral CA3 cells are active in motivationally related, but spatially distinct, areas of an environment such as reward sites (Ciocchi et al., 2015; Royer et al., 2010). Cells in vH also tend to represent contextual similarity between locations (Komorowski et al., 2013; Royer et al., 2010) in a manner that develops with experience (Komorowski et al., 2013). In addition, place cells in vH have been shown to track changes in olfactory stimuli (Keinath et

al., 2014; Petrulis et al., 2005) and may represent locations associated with elevated anxiety (Ciocchi et al., 2015; Royer et al., 2010). While the functional implications of these representations remain largely unexplored, optogenetic manipulation studies point to a role in anxiety behaviors for the vH (Kheirbek et al., 2013) and its projections to the medial prefrontal cortex (Padilla-Coreano et al., 2016), and a role for vH projections to the nucleus accumbens in promoting reward associations (Britt et al., 2012).

Network activity across the dorsoventral axis

Although few studies have recorded simultaneous network activity in dH and vH, several differences have been observed which may have functional relevance. Notably, the theta rhythm is weaker in power in vH and less modulated by run speed than in dH (Patel et al., 2012; Royer et al., 2010; Schmidt et al., 2013). However, vH place cells still exhibit theta phase precession even though they are large, with smaller incremental phase changes such that phase precession persists across the extent of the place field (Kjelstrup et al., 2008). vH theta is also shifted 180 degrees relative to dH theta, suggesting that theta appears to be a wave that propagates along the dorsoventral axis (Lubenov and Siapas, 2009; Patel et al., 2012). How this "traveling wave" might coordinate activity across the axis in the context of learning and memory remains an open question.

SWRs in vH are largely similar in their fundamental characteristics to SWRs in dH, with the exception that ripples in vH are typically smaller in amplitude and slightly lower in oscillation frequency (Patel et al., 2013). This is likely due to the more diffuse pyramidal cell layers and lower burstiness of vH cells (Fanselow and Dong, 2010; Royer et al., 2010). vH SWRs tend to occur independently of dH SWRs in sleep, although they can also propagate along the entire dorsoventral axis in either direction. The degree of propagation, or synchrony, between dH and vH may depend on the amplitude of the SWR (Patel et al., 2013), indicating that larger SWRs engage a greater portion of the hippocampus and therefore may reflect cognitive demand during behavior. Interestingly, cells of ventral CA1 with tri-directional projections to the medial prefrontal cortex, amygdala, and nucleus accumbens are activated during SWRs in sleep to a greater degree than cells that project to only one or two of those regions (Ciocchi et al., 2015). This suggests

that SWRs in vH are indeed important for integrating information and synchronizing transfer to distant hippocampal targets. The characteristics and function of vH SWRs in the awake state have yet to be explored.

1.12 Hippocampal output

Neural activity time-locked to both hippocampal theta and SWRs has been observed in the downstream targets of the hippocampus, suggesting that these network patterns facilitate the integration of spatial information with other modalities. Theta has been posited as a coordinator of brain regions particularly during periods of attention and working memory. Theta power is positively correlated not only with velocity (Montgomery et al., 2009) but also with working memory demands (Belchior et al., 2014; Richard et al., 2013; Schmidt et al., 2013; Tesche and Karhu, 2000). Moreover, theta coherence increases between hippocampus and its projection targets (such as mPFC) during coding phases of working memory tasks (Backus et al., 2016; Benchenane et al., 2010; Harris and Gordon, 2015). In addition, phase precession relative to hippocampal theta has been observed in the prefrontal cortex (Jones and Wilson, 2005; Siapas et al., 2005) as well as in spatially-modulated, reward-predictive cells of the nucleus accumbens (Malhotra et al., 2012; van der Meer and Redish, 2011). These results point to theta as a mechanism for broadcasting spatial information to downstream regions and coordinating spatial and non-spatial representations across distant brain areas.

In addition, there is substantial evidence that SWRs engage not only the hippocampus but also its projection targets. SWRs can be detected in the deep layers of the EC following the occurrence of CA1 SWRs (Chrobak and Buzsaki, 1994, 1996). Strikingly, SWRs also modulate cell ensembles in distant brain regions, including prefrontal cortex (Jadhav et al., 2016; Siapas and Wilson, 1998; Wierzynski et al., 2009), visual cortex (Ji and Wilson, 2007), nucleus accumbens (Lansink et al., 2008; Lansink et al., 2009), and the ventral tegmental area (Gomperts et al., 2015). Activity time-locked to SWRs recorded elsewhere in the brain suggests that the information contained in SWRs is being communicated or integrated with other memory-related modalities (Chrobak and Buzsaki, 1996; Siapas and Wilson, 1998; Sirota et al., 2003;

Wierzynski et al., 2009). SWR-triggered whole-brain MRI in monkeys shows widespread activation of cortical areas and coincident suppression of subcortical areas (Logothetis et al., 2012), and the modulation of cohesive functional networks that have been associated with memory processes (Kaplan et al., 2016). These findings point to a pivotal role for SWRs in coordinating memory processes across the entire brain.

1.13 Conclusion

Since the identification of the hippocampus as a critical neural center for spatial mnemonic processing, our understanding of memory has expanded in stride with developments in neural recording techniques and subsequent discoveries of hippocampal network activity. In particular, by identifying the spatial aspect of memory as a key to decoding hippocampal activity, and beginning to tease apart the unique contributions of each hippocampal subregion to spatial representations, we can begin to understand the patterns of coordinated neural activity that underlie memory function. In this chapter, we have highlighted two key patterns of activity, theta and sharp-wave ripples, which are largely distinct during exploratory activity and quiescence and specialized within each subregion, but that both coordinate the activation and reactivation of neuronal ensembles with high temporal precision. Although our understanding of these patterns focuses largely on spatial memory, we are gradually appreciating the ability of the hippocampus to build relational maps between diverse types of information. Dense, large scale single unit and LFP recordings, optical recording methods, optogenetics, and many other developing techniques will continue to expand our ability to characterize and manipulate hippocampal network activity in order to further our grasp on hippocampal mnemonic processing.

1.14 References

Ahmed, O.J., and Mehta, M.R. (2009). The hippocampal rate code: anatomy, physiology and theory. Trends Neurosci 32, 329-338.

Ahmed, O.J., and Mehta, M.R. (2012). Running speed alters the frequency of hippocampal gamma oscillations. J Neurosci 32, 7373-7383.

Ainge, J.A., Tamosiunaite, M., Woergoetter, F., and Dudchenko, P.A. (2007). Hippocampal CA1 place cells encode intended destination on a maze with multiple choice points. J Neurosci 27, 9769-9779.

Alexander, G.M., Farris, S., Pirone, J.R., Zheng, C., Colgin, L.L., and Dudek, S.M. (2016). Social and novel contexts modify hippocampal CA2 representations of space. Nat Commun 7, 10300.

Allen, K., Rawlins, J.N., Bannerman, D.M., and Csicsvari, J. (2012). Hippocampal place cells can encode multiple trial-dependent features through rate remapping. J Neurosci 32, 14752-14766.

Allen, T.A., Salz, D.M., McKenzie, S., and Fortin, N.J. (2016). Nonspatial Sequence Coding in CA1 Neurons. J Neurosci 36, 1547-1563.

Amaral, D.G., Dolorfo, C., and Alvarez-Royo, P. (1991). Organization of CA1 projections to the subiculum: a PHA-L analysis in the rat. Hippocampus 1, 415-435.

Amaral, D.G., Ishizuka, N., and Claiborne, B. (1990). Neurons, numbers and the hippocampal network. Prog Brain Res 83, 1-11.

Amaral, D.G., and Kurz, J. (1985). An analysis of the origins of the cholinergic and noncholinergic septal projections to the hippocampal formation of the rat. J Comp Neurol 240, 37-59.

Amaral, D.G., and Witter, M.P. (1989). The three-dimensional organization of the hippocampal formation: a review of anatomical data. Neuroscience 31, 571-591.

Anderson, M.I., and Jeffery, K.J. (2003). Heterogeneous modulation of place cell firing by changes in context. J Neurosci 23, 8827-8835.

Arnolds, D.E., Lopes da Silva, F.H., Aitink, J.W., Kamp, A., and Boeijinga, P. (1980). The spectral properties of hippocampal EEG related to behaviour in man. Electroencephalogr Clin Neurophysiol 50, 324-328.

Axmacher, N., Elger, C.E., and Fell, J. (2008). Ripples in the medial temporal lobe are relevant for human memory consolidation. Brain 131, 1806-1817.

Axmacher, N., Henseler, M.M., Jensen, O., Weinreich, I., Elger, C.E., and Fell, J. (2010). Cross-frequency coupling supports multi-item working memory in the human hippocampus. Proc Natl Acad Sci USA 107, 3228-3233.

Axmacher, N., Mormann, F., Fernandez, G., Elger, C.E., and Fell, J. (2006). Memory formation by neuronal synchronization. Brain Res Rev 52, 170-182.

Backus, A.R., Schoffelen, J.M., Szebenyi, S., Hanslmayr, S., and Doeller, C.F. (2016). Hippocampal-Prefrontal Theta Oscillations Support Memory Integration. Curr Biol 26, 450-457.

Bannerman, D.M., Rawlins, J.N., McHugh, S.B., Deacon, R.M., Yee, B.K., Bast, T., Zhang, W.N., Pothuizen, H.H., and Feldon, J. (2004). Regional dissociations within the hippocampus--memory and anxiety. Neurosci Biobehav Rev 28, 273-283.

Bannerman, D.M., Yee, B.K., Good, M.A., Heupel, M.J., Iversen, S.D., and Rawlins, J.N. (1999). Double dissociation of function within the hippocampus: a comparison of dorsal, ventral, and complete hippocampal cytotoxic lesions. Behav Neurosci 113, 1170-1188.

Barnes, C.A., McNaughton, B.L., Mizumori, S.J., Leonard, B.W., and Lin, L.H. (1990). Comparison of spatial and temporal characteristics of neuronal activity in sequential stages of hippocampal processing. Prog Brain Res 83, 287-300.

Bartesaghi, R., and Gessi, T. (2004). Parallel activation of field CA2 and dentate gyrus by synaptically elicited perforant path volleys. Hippocampus 14, 948-963.

Bast, T. (2007). Toward an integrative perspective on hippocampal function: from the rapid encoding of experience to adaptive behavior. Rev Neurosci 18, 253-281.

Bast, T., Wilson, I.A., Witter, M.P., and Morris, R.G. (2009). From rapid place learning to behavioral performance: a key role for the intermediate hippocampus. PLoS Biol 7, e1000089.

Battaglia, F.P., Sutherland, G.R., and McNaughton, B.L. (2004a). Hippocampal sharp wave bursts coincide with neocortical "up-state" transitions. Learn Mem 11, 697-704.

Battaglia, F.P., Sutherland, G.R., and McNaughton, B.L. (2004b). Local sensory cues and place cell directionality: additional evidence of prospective coding in the hippocampus. J Neurosci 24, 4541-4550.

Beckstead, R.M. (1978). Afferent connections of the entorhinal area in the rat as demonstrated by retrograde cell-labeling with horseradish peroxidase. Brain Res 152, 249-264.

Belchior, H., Lopes-Dos-Santos, V., Tort, A.B., and Ribeiro, S. (2014). Increase in hippocampal theta oscillations during spatial decision making. Hippocampus 24, 693-702.

Belluscio, M.A., Mizuseki, K., Schmidt, R., Kempter, R., and Buzsaki, G. (2012). Cross-frequency phase-phase coupling between theta and gamma oscillations in the hippocampus. J Neurosci 32, 423-435.

Benchenane, K., Peyrache, A., Khamassi, M., Tierney, P.L., Gioanni, Y., Battaglia, F.P., and Wiener, S.I. (2010). Coherent theta oscillations and reorganization of spike timing in the hippocampal- prefrontal network upon learning. Neuron 66, 921-936.

Bendor, D., and Wilson, M.A. (2012). Biasing the content of hippocampal replay during sleep. Nat Neurosci 15, 1439-1444.

Best, P.J., and Ranck, J.B., Jr. (1982). Reliability of the relationship between hippocampal unit activity and sensory-behavioral events in the rat. Exp Neurol 75, 652-664.

Bibbig, A., Faulkner, H.J., Whittington, M.A., and Traub, R.D. (2001). Self-organized synaptic plasticity contributes to the shaping of gamma and beta oscillations in vitro. J Neurosci 21, 9053-9067.

Bittner, K.C., Grienberger, C., Vaidya, S.P., Milstein, A.D., Macklin, J.J., Suh, J., Tonegawa, S., and Magee, J.C. (2015). Conjunctive input processing drives feature selectivity in hippocampal CA1 neurons. Nat Neurosci 18, 1133-1142.

Bohm, C., Peng, Y., Maier, N., Winterer, J., Poulet, J.F., Geiger, J.R., and Schmitz, D. (2015). Functional Diversity of Subicular Principal Cells during Hippocampal Ripples. J Neurosci 35, 13608-13618.

Bonnevie, T., Dunn, B., Fyhn, M., Hafting, T., Derdikman, D., Kubie, J.L., Roudi, Y., Moser, E.I., and Moser, M.B. (2013). Grid cells require excitatory drive from the hippocampus. Nat Neurosci 16, 309-317.

Bott, J.B., Muller, M.A., Jackson, J., Aubert, J., Cassel, J.C., Mathis, C., and Goutagny, R. (2015). Spatial Reference Memory is Associated with Modulation of Theta-Gamma Coupling in the Dentate Gyrus. Cereb Cortex.

Bragin, A., Jando, G., Nadasdy, Z., Hetke, J., Wise, K., and Buzsaki, G. (1995a). Gamma (40-100 Hz) oscillation in the hippocampus of the behaving rat. J Neurosci 15, 47-60.

Bragin, A., Jando, G., Nadasdy, Z., van Landeghem, M., and Buzsaki, G. (1995b). Dentate EEG spikes and associated interneuronal population bursts in the hippocampal hilar region of the rat. J Neurophysiol 73, 1691-1705.

Brandon, M.P., Koenig, J., Leutgeb, J.K., and Leutgeb, S. (2014). New and distinct hippocampal place codes are generated in a new environment during septal inactivation. Neuron 82, 789-796.

Brankack, J., Stewart, M., and Fox, S.E. (1993). Current source density analysis of the hippocampal theta rhythm: associated sustained potentials and candidate synaptic generators. Brain Res 615, 310-327.

Britt, J.P., Benaliouad, F., McDevitt, R.A., Stuber, G.D., Wise, R.A., and Bonci, A. (2012). Synaptic and behavioral profile of multiple glutamatergic inputs to the nucleus accumbens. Neuron 76, 790-803.

Brog, J.S., Salyapongse, A., Deutch, A.Y., and Zahm, D.S. (1993). The patterns of afferent innervation of the core and shell in the "accumbens" part of the rat ventral striatum: immunohistochemical detection of retrogradely transported fluoro-gold. J Comp Neurol 338, 255-278.

Brun, V.H., Leutgeb, S., Wu, H.Q., Schwarcz, R., Witter, M.P., Moser, E.I., and Moser, M.B. (2008a). Impaired spatial representation in CA1 after lesion of direct input from entorhinal cortex. Neuron 57, 290-302.

Brun, V.H., Otnass, M.K., Molden, S., Steffenach, H.A., Witter, M.P., Moser, M.B., and Moser, E.I. (2002). Place cells and place recognition maintained by direct entorhinal-hippocampal circuitry. Science 296, 2243-2246.

Brun, V.H., Solstad, T., Kjelstrup, K.B., Fyhn, M., Witter, M.P., Moser, E.I., and Moser, M.B. (2008b). Progressive increase in grid scale from dorsal to ventral medial entorhinal cortex. Hippocampus 18, 1200-1212.

Buckmaster, P.S., Wenzel, H.J., Kunkel, D.D., and Schwartzkroin, P.A. (1996). Axon arbors and synaptic connections of hippocampal mossy cells in the rat in vivo. J Comp Neurol 366, 271-292.

Bullock, T.H., Buzsaki, G., and McClune, M.C. (1990). Coherence of compound field potentials reveals discontinuities in the CA1-subiculum of the hippocampus in freely-moving rats. Neuroscience 38, 609-619.

Buzsaki, G. (1986). Hippocampal sharp waves: their origin and significance. Brain Res 398, 242-252.

Buzsaki, G. (1989). Two-stage model of memory trace formation: a role for "noisy" brain states. Neuroscience 31, 551-570.

Buzsaki, G. (2002). Theta oscillations in the hippocampus. Neuron 33, 325-340.

Buzsaki, G. (2004). Large-scale recording of neuronal ensembles. Nat Neurosci 7, 446-451.

Buzsaki, G. (2015). Hippocampal sharp wave-ripple: A cognitive biomarker for episodic memory and planning. Hippocampus.

Buzsaki, G., Anastassiou, C.A., and Koch, C. (2012). The origin of extracellular fields and currents--EEG, ECoG, LFP and spikes. Nat Rev Neurosci 13, 407-420.

Buzsaki, G., Buhl, D.L., Harris, K.D., Csicsvari, J., Czeh, B., and Morozov, A. (2003). Hippocampal network patterns of activity in the mouse. Neuroscience 116, 201-211.

Buzsaki, G., Czopf, J., Kondakor, I., and Kellenyi, L. (1986). Laminar distribution of hippocampal rhythmic slow activity (RSA) in the behaving rat: current-source density analysis, effects of urethane and atropine. Brain Res 365, 125-137.

Buzsaki, G., Horvath, Z., Urioste, R., Hetke, J., and Wise, K. (1992). High-frequency network oscillation in the hippocampus. Science 256, 1025-1027.

Buzsaki, G., Leung, L.W., and Vanderwolf, C.H. (1983). Cellular bases of hippocampal EEG in the behaving rat. Brain Res 287, 139-171.

Buzsaki, G., and Wang, X.J. (2012). Mechanisms of gamma oscillations. Annu Rev Neurosci 35, 203-225.

Carr, M.F., Jadhav, S.P., and Frank, L.M. (2011). Hippocampal replay in the awake state: a potential substrate for memory consolidation and retrieval. Nat Neurosci 14, 147-153.

Carr, M.F., Karlsson, M.P., and Frank, L.M. (2012). Transient slow gamma synchrony underlies hippocampal memory replay. Neuron 75, 700-713.

Cembrowski, M.S., Bachman, J.L., Wang, L., Sugino, K., Shields, B.C., and Spruston, N. (2016). Spatial Gene-Expression Gradients Underlie Prominent Heterogeneity of CA1 Pyramidal Neurons. Neuron.

Cenquizca, L.A., and Swanson, L.W. (2006). Analysis of direct hippocampal cortical field CA1 axonal projections to diencephalon in the rat. J Comp Neurol 497, 101-114.

Cenquizca, L.A., and Swanson, L.W. (2007). Spatial organization of direct hippocampal field CA1 axonal projections to the rest of the cerebral cortex. Brain Res Rev 56, 1-26.

Chen, Z., Resnik, E., McFarland, J.M., Sakmann, B., and Mehta, M.R. (2011). Speed controls the amplitude and timing of the hippocampal gamma rhythm. PLoS One 6, e21408.

Cheng, S., and Frank, L.M. (2008). New experiences enhance coordinated neural activity in the hippocampus. Neuron 57, 303-313.

Chevaleyre, V., and Siegelbaum, S.A. (2010). Strong CA2 pyramidal neuron synapses define a powerful disynaptic cortico-hippocampal loop. Neuron 66, 560-572.

Chrobak, J.J., and Buzsaki, G. (1994). Selective activation of deep layer (V-VI) retrohippocampal cortical neurons during hippocampal sharp waves in the behaving rat. J Neurosci 14, 6160-6170.

Chrobak, J.J., and Buzsaki, G. (1996). High-frequency oscillations in the output networks of the hippocampal-entorhinal axis of the freely behaving rat. J Neurosci 16, 3056-3066.

Ciocchi, S., Passecker, J., Malagon-Vina, H., Mikus, N., and Klausberger, T. (2015). Brain computation. Selective information routing by ventral hippocampal CA1 projection neurons. Science 348, 560-563.

Clelland, C.D., Choi, M., Romberg, C., Clemenson, G.D., Jr., Fragniere, A., Tyers, P., Jessberger, S., Saksida, L.M., Barker, R.A., Gage, F.H., et al. (2009). A functional role for adult hippocampal neurogenesis in spatial pattern separation. Science 325, 210-213.

Colgin, L.L. (2012). Slow gamma takes the reins in replay. Neuron 75, 549-550.

Colgin, L.L. (2015). Theta-gamma coupling in the entorhinal-hippocampal system. Curr Opin Neurobiol 31, 45-50.

Colgin, L.L., Denninger, T., Fyhn, M., Hafting, T., Bonnevie, T., Jensen, O., Moser, M.B., and Moser, E.I. (2009). Frequency of gamma oscillations routes flow of information in the hippocampus. Nature 19;462, 353-357.

Colgin, L.L., Leutgeb, S., Jezek, K., Leutgeb, J.K., Moser, E.I., McNaughton, B.L., and Moser, M.B. (2010). Attractor-map versus autoassociation based attractor dynamics in the hippocampal network. J Neurophysiol 104, 35-50.

Cravens, C.J., Vargas-Pinto, N., Christian, K.M., and Nakazawa, K. (2006). CA3 NMDA receptors are crucial for rapid and automatic representation of context memory. Eur J Neurosci 24, 1771-1780.

Creer, D.J., Romberg, C., Saksida, L.M., van Praag, H., and Bussey, T.J. (2010). Running enhances spatial pattern separation in mice. Proc Natl Acad Sci USA 107, 2367-2372.

Csicsvari, J., Hirase, H., Czurko, A., Mamiya, A., and Buzsaki, G. (1999a). Fast Network Oscillations in the Hippocampal CA1 Region of the Behaving Rat. J Neurosci 19, RC20.

Csicsvari, J., Hirase, H., Czurko, A., Mamiya, A., and Buzsaki, G. (1999b). Oscillatory coupling of hippocampal pyramidal cells and interneurons in the behaving rat. J Neurosci 19, 274-287.

Csicsvari, J., Hirase, H., Mamiya, A., and Buzsaki, G. (2000). Ensemble patterns of hippocampal CA3-CA1 neurons during sharp wave-associated population events. Neuron 28, 585-594.

Csicsvari, J., Jamieson, B., Wise, K.D., and Buzsaki, G. (2003). Mechanisms of gamma oscillations in the hippocampus of the behaving rat. Neuron 37, 311-322.

Csicsvari, J., O'Neill, J., Allen, K., and Senior, T. (2007). Place-selective firing contributes to the reverse-order reactivation of CA1 pyramidal cells during sharp waves in open-field exploration. Eur J Neurosci 26, 704-716.

Cui, Z., Gerfen, C.R., and Young, W.S., 3rd (2013). Hypothalamic and other connections with dorsal CA2 area of the mouse hippocampus. J Comp Neurol 521, 1844-1866.

Cutsuridis, V., and Taxidis, J. (2013). Deciphering the role of CA1 inhibitory circuits in sharp wave-ripple complexes. Front Syst Neurosci 7, 13.

Danielson, N.B., Kaifosh, P., Zaremba, J.D., Lovett-Barron, M., Tsai, J., Denny, C.A., Balough, E.M., Goldberg, A.R., Drew, L.J., Hen, R., et al. (2016). Distinct contribution of adult-born hippocampal granule cells to context encoding. Neuron.

Davidson, T.J., Kloosterman, F., and Wilson, M.A. (2009). Hippocampal replay of extended experience. Neuron 63, 497-507.

de Hoz, L., Knox, J., and Morris, R.G. (2003). Longitudinal axis of the hippocampus: both septal and temporal poles of the hippocampus support water maze spatial learning depending on the training protocol. Hippocampus 13, 587-603.

de Hoz, L., and Martin, S.J. (2014). Double dissociation between the contributions of the septal and temporal hippocampus to spatial learning: the role of prior experience. Hippocampus 24, 990-1005.

de Lavilleon, G., Lacroix, M.M., Rondi-Reig, L., and Benchenane, K. (2015). Explicit memory creation during sleep demonstrates a causal role of place cells in navigation. Nat Neurosci 18, 493-495.

Deadwyler, S.A., and Hampson, R.E. (2004). Differential but complementary mnemonic functions of the hippocampus and subiculum. Neuron 42, 465-476.

Deller, T., Martinez, A., Nitsch, R., and Frotscher, M. (1996). A novel entorhinal projection to the rat dentate gyrus: direct innervation of proximal dendrites and cell bodies of granule cells and GABAergic neurons. J Neurosci 16, 3322-3333.

Deshmukh, S.S., and Knierim, J.J. (2011). Representation of non-spatial and spatial information in the lateral entorhinal cortex. Frontiers in behavioral neuroscience 5, 69.

Deshmukh, S.S., and Knierim, J.J. (2013). Influence of local objects on hippocampal representations: Landmark vectors and memory. Hippocampus 23, 253-267.

Deshmukh, S.S., Yoganarasimha, D., Voicu, H., and Knierim, J.J. (2010). Theta modulation in the medial and the lateral entorhinal cortices. J Neurophysiol 104, 994-1006.

DeVito, L.M., Konigsberg, R., Lykken, C., Sauvage, M., Young, W.S., 3rd, and Eichenbaum, H. (2009). Vasopressin 1b receptor knock-out impairs memory for temporal order. J Neurosci 29, 2676-2683.

Diba, K., and Buzsaki, G. (2007). Forward and reverse hippocampal place-cell sequences during ripples. Nat Neurosci 10, 1241-1242.

Dolleman-Van der Weel, M.J., and Witter, M.P. (1996). Projections from the nucleus reuniens thalami to the entorhinal cortex, hippocampal field CA1, and the subiculum in the rat arise from different populations of neurons. J Comp Neurol 364, 637--650.

Dong, H.W., Swanson, L.W., Chen, L., Fanselow, M.S., and Toga, A.W. (2009). Genomic-anatomic evidence for distinct functional domains in hippocampal field CA1. Proc Natl Acad Sci USA 106, 11794-11799.

Dudek, S.M., Alexander, G.M., and Farris, S. (2016). Rediscovering area CA2: unique properties and functions. Nat Rev Neurosci 17, 89-102.

Duncan, K., Ketz, N., Inati, S.J., and Davachi, L. (2012). Evidence for area CA1 as a match/mismatch detector: a high-resolution fMRI study of the human hippocampus. Hippocampus 22, 389-398.

Dupret, D., O'Neill, J., Pleydell-Bouverie, B., and Csicsvari, J. (2010). The reorganization and reactivation of hippocampal maps predict spatial memory performance. Nat Neurosci 13, 995-1002.

Dupret, D., Revest, J.M., Koehl, M., Ichas, F., De Giorgi, F., Costet, P., Abrous, D.N., and Piazza, P.V. (2008). Spatial relational memory requires hippocampal adult neurogenesis. PLoS One 3, e1959.

Duvarci, S., and Pare, D. (2014). Amygdala microcircuits controlling learned fear. Neuron 82, 966-980.

Ego-Stengel, V., and Wilson, M.A. (2007). Spatial selectivity and theta phase precession in CA1 interneurons. Hippocampus 17, 161-174.

Ego-Stengel, V., and Wilson, M.A. (2010). Disruption of ripple-associated hippocampal activity during rest impairs spatial learning in the rat. Hippocampus 20, 1-10.

Eichenbaum, H. (2014). Time cells in the hippocampus: a new dimension for mapping memories. Nat Rev Neurosci 15, 732-744.

Eichenbaum, H., and Cohen, N.J. (2001). From Conditioning to Conscious Recollection (New York: Oxford University Press).

Eichenbaum, H., and Cohen, N.J. (2014). Can we reconcile the declarative memory and spatial navigation views on hippocampal function? Neuron 83, 764-770.

Eichenbaum, H., Kuperstein, M., Fagan, A., and Nagode, J. (1987). Cue-sampling and goal-approach correlates of hippocampal unit activity in rats performing an odor-discrimination task. J Neurosci 7, 716-732.

Eichenbaum, H., Sauvage, M., Fortin, N., Komorowski, R., and Lipton, P. (2012). Towards a functional organization of episodic memory in the medial temporal lobe. Neurosci Biobehav Rev 36, 1597-1608.

Eller, J., Zarnadze, S., Bauerle, P., Dugladze, T., and Gloveli, T. (2015). Cell type-specific separation of subicular principal neurons during network activities. PLoS One 10, e0123636.

Eschenko, O., Molle, M., Born, J., and Sara, S.J. (2006). Elevated sleep spindle density after learning or after retrieval in rats. J Neurosci 26, 12914-12920.

Eschenko, O., Ramadan, W., Molle, M., Born, J., and Sara, S.J. (2008). Sustained increase in hippocampal sharp-wave ripple activity during slow-wave sleep after learning. Learn Mem 15, 222-228.

Esposito, M.S., Piatti, V.C., Laplagne, D.A., Morgenstern, N.A., Ferrari, C.C., Pitossi, F.J., and Schinder, A.F. (2005). Neuronal differentiation in the adult hippocampus recapitulates embryonic development. J Neurosci 25, 10074-10086.

Fanselow, M.S., and Dong, H.W. (2010). Are the dorsal and ventral hippocampus functionally distinct structures? Neuron 65, 7-19.

Felix-Ortiz, A.C., Beyeler, A., Seo, C., Leppla, C.A., Wildes, C.P., and Tye, K.M. (2013). BLA to vHPC inputs modulate anxiety-related behaviors. Neuron 79, 658-664.

Felix-Ortiz, A.C., and Tye, K.M. (2014). Amygdala inputs to the ventral hippocampus bidirectionally modulate social behavior. J Neurosci 34, 586-595.

Fell, J., and Axmacher, N. (2011). The role of phase synchronization in memory processes. Nat Rev Neurosci 12, 105-118.

Feng, T., Silva, D., and Foster, D.J. (2015). Dissociation between the experience-dependent development of hippocampal theta sequences and single-trial phase precession. J Neurosci 35, 4890-4902.

Fenton, A.A., Kao, H.Y., Neymotin, S.A., Olypher, A., Vayntrub, Y., Lytton, W.W., and Ludvig, N. (2008). Unmasking the CA1 ensemble place code by exposures to small and large environments: more place cells and multiple, irregularly arranged, and expanded place fields in the larger space. J Neurosci 28, 11250-11262.

Ferbinteanu, J., and McDonald, R.J. (2001). Dorsal/ventral hippocampus, fornix, and conditioned place preference. Hippocampus 11, 187-200.

Ferbinteanu, J., and Shapiro, M.L. (2003). Prospective and retrospective memory coding in the hippocampus. Neuron 40, 1227-1239.

Finch, D.M., Nowlin, N.L., and Babb, T.L. (1983). Demonstration of axonal projections of neurons in the rat hippocampus and subiculum by intracellular injection of HRP. Brain Res 271, 201--216.

Foster, D.J., and Wilson, M.A. (2006). Reverse replay of behavioural sequences in hippocampal place cells during the awake state. Nature 440, 680-683.

Foster, T.C., Castro, C.A., and McNaughton, B.L. (1989). Spatial selectivity of rat hippocampal neurons: dependence on preparedness for movement. Science 244, 1580-1582.

Fox, S.E., and Ranck, J.B., Jr. (1981). Electrophysiological characteristics of hippocampal complex-spike cells and theta cells. Exp Brain Res 41, 399-410.

Frank, L.M., Brown, E.N., and Wilson, M. (2000). Trajectory encoding in the hippocampus and entorhinal cortex. Neuron 27, 169-178.

Frank, L.M., Stanley, G.B., and Brown, E.N. (2004). Hippocampal plasticity across multiple days of exposure to novel environments. J Neurosci 24, 7681-7689.

Freeman, W.J. (2007). Definitions of state variables and state space for brain-computer interface : Part 1. Multiple hierarchical levels of brain function. Cogn Neurodyn 1, 3-14.

Freund, T.F., and Antal, M. (1988). GABA-containing neurons in the septum control inhibitory interneurons in the hippocampus. Nature 336, 170-173.

Freund, T.F., and Buzsaki, G. (1996). Interneurons of the hippocampus. Hippocampus 6, 347-470.

Fries, P. (2005). A mechanism for cognitive dynamics: neuronal communication through neuronal coherence. Trends Cogn Sci 9, 474-480.

Frotscher, M., and Leranth, C. (1985). Cholinergic innervation of the rat hippocampus as revealed by choline acetyltransferase immunocytochemistry: a combined light and electron microscopic study. J Comp Neurol 239, 237-246.

Fyhn, M., Molden, S., Hollup, S., Moser, M.B., and Moser, E. (2002). Hippocampal neurons responding to first-time dislocation of a target object. Neuron 35, 555-566.

Gallagher, M., and Chiba, A.A. (1996). The amygdala and emotion. Curr Opin Neurobiol 6, 221-227.

Garthe, A., Behr, J., and Kempermann, G. (2009). Adult-generated hippocampal neurons allow the flexible use of spatially precise learning strategies. PLoS One 4, e5464.

Ge, S., Sailor, K.A., Ming, G.L., and Song, H. (2008). Synaptic integration and plasticity of new neurons in the adult hippocampus. J Physiol 586, 3759-3765.

Gerstner, W., Kempter, R., van Hemmen, J.L., and Wagner, H. (1996). A neuronal learning rule for sub-millisecond temporal coding. Nature 383, 76--81.

Gilbert, P.E., and Brushfield, A.M. (2009). The role of the CA3 hippocampal subregion in spatial memory: a process oriented behavioral assessment. Prog Neuropsychopharmacol Biol Psych 33, 774-781.

Gillespie, A.K., Jones, E.A., Lin, Y.-H., Karlsson, M.P., Kay, K., Yoon, S.Y., Tong, L.M., Nova, P., Carr, J.S., Frank, L.M., et al. (in press). Apolipoprotein E4 causes age-dependent disruption of slow gamma oscillations during hippocampal sharp-wave ripples. Neuron.

Girardeau, G., Benchenane, K., Wiener, S.I., Buzsaki, G., and Zugaro, M.B. (2009). Selective suppression of hippocampal ripples impairs spatial memory. Nat Neurosci 12, 1222-1223.

Givens, B.S., and Olton, D.S. (1990). Cholinergic and GABAergic modulation of medial septal area: effect on working memory. Behav Neurosci 104, 849-855.

Gold, A.E., and Kesner, R.P. (2005). The role of the CA3 subregion of the dorsal hippocampus in spatial pattern completion in the rat. Hippocampus 15, 808-814.

Gomperts, S.N., Kloosterman, F., and Wilson, M.A. (2015). VTA neurons coordinate with the hippocampal reactivation of spatial experience. eLife 4.

Gonzales, R.B., DeLeon Galvan, C.J., Rangel, Y.M., and Claiborne, B.J. (2001). Distribution of thorny excrescences on CA3 pyramidal neurons in the rat hippocampus. J Comp Neurol 430, 357-368.

Grastyan, E., Lissak, K., Madarasz, I., and Donhoffer, H. (1959). Hippocampal electrical activity during the development of conditioned reflexes. Electroencephalogr Clin Neurophysiol 11, 409-430.

Gray, C.M., Maldonado, P.E., Wilson, M., and McNaughton, B. (1995). Tetrodes markedly improve the reliability and yield of multiple single- unit isolation from multi-unit recordings in cat striate cortex. J Neurosci Methods 63, 43-54.

Green, J.D., and Arduini, A.A. (1954). Hippocampal electrical activity in arousal. J Neurophysiol 17, 533-557.

Groenewegen, H.J., Vermeulen-Van der Zee, E., te Kortschot, A., and Witter, M.P. (1987). Organization of the projections from the subiculum to the ventral striatum in the rat. A study using anterograde transport of Phaseolus vulgaris leucoagglutinin. Neuroscience 23, 103-120.

Grosmark, A.D., Mizuseki, K., Pastalkova, E., Diba, K., and Buzsaki, G. (2012). REM sleep reorganizes hippocampal excitability. Neuron 75, 1001-1007.

Gu, Y., Arruda-Carvalho, M., Wang, J., Janoschka, S.R., Josselyn, S.A., Frankland, P.W., and Ge, S. (2012). Optical controlling reveals time-dependent roles for adult-born dentate granule cells. Nat Neurosci 15, 1700-1706.

Gulyas, A.I., Hajos, N., Katona, I., and Freund, T.F. (2003). Interneurons are the local targets of hippocampal inhibitory cells which project to the medial septum. Eur J Neurosci 17, 1861--1872.

Gupta, A.S., van der Meer, M.A., Touretzky, D.S., and Redish, A.D. (2010). Hippocampal replay is not a simple function of experience. Neuron 65, 695-705.

Gupta, A.S., van der Meer, M.A., Touretzky, D.S., and Redish, A.D. (2012). Segmentation of spatial experience by hippocampal theta sequences. Nat Neurosci 15, 1032-1039.

Guzowski, J.F., Knierim, J.J., and Moser, E.I. (2004). Ensemble dynamics of hippocampal regions CA3 and CA1. Neuron 44, 581-584.

Guzowski, J.F., McNaughton, B.L., Barnes, C.A., and Worley, P.F. (1999). Environment-specific expression of the immediate-early gene Arc in hippocampal neuronal ensembles. Nat Neurosci 2, 1120-1124.

Hafting, T., Fyhn, M., Bonnevie, T., Moser, M.B., and Moser, E.I. (2008). Hippocampus-independent phase precession in entorhinal grid cells. Nature 453, 1248-1252.

Hafting, T., Fyhn, M., Molden, S., Moser, M.B., and Moser, E.I. (2005). Microstructure of a spatial map in the entorhinal cortex. Nature 436, 801-806.

Hales, J.B., Schlesiger, M.I., Leutgeb, J.K., Squire, L.R., Leutgeb, S., and Clark, R.E. (2014). Medial entorhinal cortex lesions only partially disrupt hippocampal place cells and hippocampus-dependent place memory. Cell reports 9, 893-901.

Harris, A.Z., and Gordon, J.A. (2015). Long-range neural synchrony in behavior. Annu Rev Neurosci 38, 171-194.

Hasselmo, M.E. (2005). What is the function of hippocampal theta rhythm?-Linking behavioral data to phasic properties of field potential and unit recording data. Hippocampus 15, 936-949.

Hasselmo, M.E., Bodelon, C., and Wyble, B.P. (2002). A proposed function for hippocampal theta rhythm: separate phases of encoding and retrieval enhance reversal of prior learning. Neural Comput 14, 793-817.

Hasselmo, M.E., and Schnell, E. (1994). Laminar selectivity of the cholinergic suppression of synaptic transmission in rat hippocampal region CA1: computational modeling and brain slice physiology. J Neurosci 14, 3898-3914.

Henke, P.G. (1990). Hippocampal pathway to the amygdala and stress ulcer development. Brain Res Bull 25, 691-695.

Henze, D.A., and Buzsaki, G. (2007). Hilar mossy cells: functional identification and activity in vivo. Prog Brain Res 163, 199-810.

Herkenham, M. (1978). The connections of the nucleus reuniens thalami: evidence for a direct thalamo-hippocampal pathway in the rat. J Comp Neurol 177, 589-610.

Hill, A.J. (1978). First occurrence of hippocampal spatial firing in a new environment. Exp Neurol 62, 282-297.

Hitti, F.L., and Siegelbaum, S.A. (2014). The hippocampal CA2 region is essential for social memory. Nature 508, 88-92.

Hok, V., Lenck-Santini, P.P., Roux, S., Save, E., Muller, R.U., and Poucet, B. (2007). Goal-related activity in hippocampal place cells. J Neurosci 27, 472-482.

Hopfield, J.J. (1995). Pattern recognition computation using action potential timing for stimulus representation. Nature 376, 33--36.

Huxter, J., Burgess, N., and O'Keefe, J. (2003). Independent rate and temporal coding in hippocampal pyramidal cells. Nature 425, 828-832.

Hyman, J.M., Wyble, B.P., Goyal, V., Rossi, C.A., and Hasselmo, M.E. (2003). Stimulation in hippocampal region CA1 in behaving rats yields long-term potentiation when delivered to the peak of theta and long-term depression when delivered to the trough. J Neurosci 23, 11725--11731.

Igarashi, K.M., Lu, L., Colgin, L.L., Moser, M.B., and Moser, E.I. (2014). Coordination of entorhinal-hippocampal ensemble activity during associative learning. Nature 510, 143-147.

Isaac, J.T., Buchanan, K.A., Muller, R.U., and Mellor, J.R. (2009). Hippocampal place cell firing patterns can induce long-term synaptic plasticity in vitro. J Neurosci 29, 6840-6850.

Ishizuka, N. (2001). Laminar organization of the pyramidal cell layer of the subiculum in the rat. J Comp Neurol 435, 89--110.

Ishizuka, N., Cowan, W.M., and Amaral, D.G. (1995). A quantitative analysis of the dendritic organization of pyramidal cells in the rat hippocampus. J Comp Neurol 362, 17-45.

Ishizuka, N., Weber, J., and Amaral, D.G. (1990). Organization of intrahippocampal projections originating from CA3 pyramidal cells in the rat. J Comp Neurol 295, 580-623.

Isomura, Y., Sirota, A., Ozen, S., Montgomery, S., Mizuseki, K., Henze, D.A., and Buzsaki, G. (2006). Integration and segregation of activity in entorhinal-hippocampal subregions by neocortical slow oscillations. Neuron 52, 871-882.

Ito, H.T., Zhang, S.J., Witter, M.P., Moser, E.I., and Moser, M.B. (2015). A prefrontal-thalamo-hippocampal circuit for goal-directed spatial navigation. Nature 522, 50-55.

Itskov, V., Pastalkova, E., Mizuseki, K., Buzsaki, G., and Harris, K.D. (2008). Theta-mediated dynamics of spatial information in hippocampus. J Neurosci 28, 5959-5964.

Jackson, J., Goutagny, R., and Williams, S. (2011). Fast and slow gamma rhythms are intrinsically and independently generated in the subiculum. J Neurosci 31, 12104-12117.

Jackson, J.C., Johnson, A., and Redish, A.D. (2006). Hippocampal sharp waves and reactivation during awake states depend on repeated sequential experience. J Neurosci 26, 12415-12426.

Jadhav, S.P., Kemere, C., German, P.W., and Frank, L.M. (2012). Awake hippocampal sharp-wave ripples support spatial memory. Science 336, 1454-1458.

Jadhav, S.P., Rothschild, G., Roumis, D.K., and Frank, L.M. (2016). Coordinated Excitation and Inhibition of Prefrontal Ensembles during Awake Hippocampal Sharp-Wave Ripple Events. Neuron 90, 113-127.

Janak, P.H., and Tye, K.M. (2015). From circuits to behaviour in the amygdala. Nature 517, 284-292.

Jarosiewicz, B., McNaughton, B.L., and Skaggs, W.E. (2002). Hippocampal population activity during the small-amplitude irregular activity state in the rat. J Neurosci 22, 1373-1384.

Jarsky, T., Mady, R., Kennedy, B., and Spruston, N. (2008). Distribution of bursting neurons in the CA1 region and the subiculum of the rat hippocampus. J Comp Neurol 506, 535-547.

Jensen, O., and Lisman, J.E. (2000). Position reconstruction from an ensemble of hippocampal place cells: contribution of theta phase coding. J Neurophysiol 83, 2602-2609.

Jessberger, S., Clark, R.E., Broadbent, N.J., Clemenson, G.D., Jr., Consiglio, A., Lie, D.C., Squire, L.R., and Gage, F.H. (2009). Dentate gyrus-specific knockdown of adult neurogenesis impairs spatial and object recognition memory in adult rats. Learn Mem 16, 147-154.

Ji, D., and Wilson, M.A. (2007). Coordinated memory replay in the visual cortex and hippocampus during sleep. Nat Neurosci 10, 100-107.

Jog, M.S., Connolly, C.I., Kubota, Y., Iyengar, D.R., Garrido, L., Harlan, R., and Graybiel, A.M. (2002). Tetrode technology: advances in implantable hardware, neuroimaging, and data analysis techniques. J Neurosci Methods 117, 141--152.

Johnson, A., and Redish, A.D. (2007). Neural ensembles in CA3 transiently encode paths forward of the animal at a decision point. J Neurosci 27, 12176-12189.

Johnston, S.T., Shtrahman, M., Parylak, S., Goncalves, J.T., and Gage, F.H. (2016). Paradox of pattern separation and adult neurogenesis: A dual role for new neurons balancing memory resolution and robustness. Neurobiol Learn Mem 129, 60-68.

Jones, M.W., and McHugh, T.J. (2011). Updating hippocampal representations: CA2 joins the circuit. Trends Neurosci 34, 526-535.

Jones, M.W., and Wilson, M.A. (2005). Theta rhythms coordinate hippocampal-prefrontal interactions in a spatial memory task. PLoS Biol 3, e402.

Jung, M.W., and McNaughton, B.L. (1993). Spatial selectivity of unit activity in the hippocampal granular layer. Hippocampus 3, 165-182.

Jung, M.W., Wiener, S.I., and McNaughton, B.L. (1994). Comparison of spatial firing characteristics of units in dorsal and ventral hippocampus of the rat. J Neurosci 14, 7347-7356.

Jutras, M.J., Fries, P., and Buffalo, E.A. (2013). Oscillatory activity in the monkey hippocampus during visual exploration and memory formation. Proc Natl Acad Sci USA 110, 13144-13149.

Kajikawa, Y., and Schroeder, C.E. (2011). How local is the local field potential? Neuron 72, 847-858.

Kajiwara, R., Wouterlood, F.G., Sah, A., Boekel, A.J., Baks-te Bulte, L.T., and Witter, M.P. (2008). Convergence of entorhinal and CA3 inputs onto pyramidal neurons and interneurons in hippocampal area CA1--an anatomical study in the rat. Hippocampus 18, 266-280.

Kali, S., and Dayan, P. (2000). The involvement of recurrent connections in area CA3 in establishing the properties of place fields: a model. J Neurosci 20, 7463-7477.

Kali, S., and Freund, T.F. (2005). Distinct properties of two major excitatory inputs to hippocampal pyramidal cells: a computational study. Eur J Neurosci 22, 2027-2048.

Kamondi, A., Acsady, L., Wang, X.J., and Buzsaki, G. (1998). Theta oscillations in somata and dendrites of hippocampal pyramidal cells in vivo: activity-dependent phase-precession of action potentials. Hippocampus 8, 244-261.

Kaplan, R., Adhikari, M.H., Hindriks, R., Mantini, D., Murayama, Y., Logothetis, N.K., and Deco, G. (2016). Hippocampal sharp-wave ripples influence selective activation of the default mode network. Curr Biol 26, 686-691.

Karlsson, M.P., and Frank, L.M. (2008). Network dynamics underlying the formation of sparse, informative representations in the hippocampus. J Neurosci 28, 14271-14281.

Karlsson, M.P., and Frank, L.M. (2009). Awake replay of remote experiences in the hippocampus. Nat Neurosci 12, 913-918.

Kay, K., Sosa, M., Chung, J.E., Karlsson, M.P., Larkin, M.C., and Frank, L.M. (2016). A hippocampal network for spatial coding during immobility and sleep. Nature 531, 185-190.

Keinath, A.T., Wang, M.E., Wann, E.G., Yuan, R.K., Dudman, J.T., and Muzzio, I.A. (2014). Precise spatial coding is preserved along the longitudinal hippocampal axis. Hippocampus 24, 1533-1548.

Kemere, C., Carr, M.F., Karlsson, M.P., and Frank, L.M. (2013). Rapid and continuous modulation of hippocampal network state during exploration of new places. PLoS One 8, e73114.

Kemp, I.R., and Kaada, B.R. (1975). The relation of hippocampal theta activity to arousal, attentive behaviour and somato-motor movements in unrestrained cats. Brain Res 95, 323-342.

Kennedy, P.J., and Shapiro, M.L. (2009). Motivational states activate distinct hippocampal representations to guide goal-directed behaviors. Proc Natl Acad Sci USA 106, 10805-10810.

Kerr, K.M., Agster, K.L., Furtak, S.C., and Burwell, R.D. (2007). Functional neuroanatomy of the parahippocampal region: the lateral and medial entorhinal areas. Hippocampus 17, 697-708.

Kesner, R.P. (2007). Behavioral functions of the CA3 subregion of the hippocampus. Learn Mem 14, 771-781.

Kheirbek, M.A., Drew, L.J., Burghardt, N.S., Costantini, D.O., Tannenholz, L., Ahmari, S.E., Zeng, H., Fenton, A.A., and Hen, R. (2013). Differential control of learning and anxiety along the dorsoventral axis of the dentate gyrus. Neuron 77, 955-968.

Kim, S.M., Ganguli, S., and Frank, L.M. (2012). Spatial information outflow from the hippocampal circuit: distributed spatial coding and phase precession in the subiculum. J Neurosci 32, 11539-11558.

Kim, Y., and Spruston, N. (2012). Target-specific output patterns are predicted by the distribution of regular-spiking and bursting pyramidal neurons in the subiculum. Hippocampus 22, 693-706.

Kjelstrup, K.B., Solstad, T., Brun, V.H., Hafting, T., Leutgeb, S., Witter, M.P., Moser, E.I., and Moser, M.B. (2008). Finite scale of spatial representation in the hippocampus. Science 321, 140-143.

Kjelstrup, K.G., Tuvnes, F.A., Steffenach, H.A., Murison, R., Moser, E.I., and Moser, M.B. (2002). Reduced fear expression after lesions of the ventral hippocampus. Proc Natl Acad Sci USA 99, 10825-10830.

Klausberger, T., and Somogyi, P. (2008). Neuronal diversity and temporal dynamics: the unity of hippocampal circuit operations. Science 321, 53-57.

Knierim, J.J., Lee, I., and Hargreaves, E.L. (2006). Hippocampal place cells: parallel input streams, subregional processing, and implications for episodic memory. Hippocampus 16, 755-764.

Knierim, J.J., and Neunuebel, J.P. (2016). Tracking the flow of hippocampal computation: Pattern separation, pattern completion, and attractor dynamics. Neurobiol Learn Mem 129, 38-49.

Kobayashi, T., Nishijo, H., Fukuda, M., Bures, J., and Ono, T. (1997). Task-dependent representations in rat hippocampal place neurons. J Neurophysiol 78, 597-613.

Kocsis, B., and Vertes, R.P. (1997). Phase relations of rhythmic neuronal firing in the supramammillary nucleus and mammillary body to the hippocampal theta activity in urethane anesthetized rats. Hippocampus 7, 204-214.

Koenig, J., Linder, A.N., Leutgeb, J.K., and Leutgeb, S. (2011). The spatial periodicity of grid cells is not sustained during reduced theta oscillations. Science 332, 592-595.

Kohara, K., Pignatelli, M., Rivest, A.J., Jung, H.Y., Kitamura, T., Suh, J., Frank, D., Kajikawa, K., Mise, N., Obata, Y., et al. (2014). Cell type-specific genetic and optogenetic tools reveal hippocampal CA2 circuits. Nat Neurosci 17, 269-279.

Kohler, C. (1985). Intrinsic projections of the retrohippocampal region in the rat brain. I. The subicular complex. J Comp Neurol 236, 504--522.

Komorowski, R.W., Garcia, C.G., Wilson, A., Hattori, S., Howard, M.W., and Eichenbaum, H. (2013). Ventral hippocampal neurons are shaped by experience to represent behaviorally relevant contexts. J Neurosci 33, 8079-8087.

Komorowski, R.W., Manns, J.R., and Eichenbaum, H. (2009). Robust conjunctive item-place coding by hippocampal neurons parallels learning what happens where. J Neurosci 29, 9918-9929.

Kopell, N., Ermentrout, G.B., Whittington, M.A., and Traub, R.D. (2000). Gamma rhythms and beta rhythms have different synchronization properties. Proc Natl Acad Sci USA 97, 1867--1872.

Kraus, B.J., Robinson, R.J., 2nd, White, J.A., Eichenbaum, H., and Hasselmo, M.E. (2013). Hippocampal "time cells": time versus path integration. Neuron 78, 1090-1101.

Kropff, E., Carmichael, J.E., Moser, M.B., and Moser, E.I. (2015). Speed cells in the medial entorhinal cortex. Nature 523, 419-424.

Kudrimoti, H.S., Barnes, C.A., and McNaughton, B.L. (1999). Reactivation of hippocampal cell assemblies: effects of behavioral state, experience, and EEG dynamics. J Neurosci 19, 4090-4101.

Kumaran, D., and Maguire, E.A. (2007). Which computational mechanisms operate in the hippocampus during novelty detection? Hippocampus 17, 735-748.

Kwag, J., and Paulsen, O. (2009). Bidirectional control of spike timing by GABA(A) receptor-mediated inhibition during theta oscillation in CA1 pyramidal neurons. Neuroreport 20, 1209-1213.

Lansink, C.S., Goltstein, P.M., Lankelma, J.V., Joosten, R.N., McNaughton, B.L., and Pennartz, C.M. (2008). Preferential reactivation of motivationally relevant information in the ventral striatum. J Neurosci 28, 6372-6382.

Lansink, C.S., Goltstein, P.M., Lankelma, J.V., McNaughton, B.L., and Pennartz, C.M. (2009). Hippocampus leads ventral striatum in replay of place-reward information. PLoS Biol 7, e1000173.

Larimer, P., and Strowbridge, B.W. (2008). Nonrandom local circuits in the dentate gyrus. J Neurosci 28, 12212-12223.

Larkin, M.C., Lykken, C., Tye, L.D., Wickelgren, J.G., and Frank, L.M. (2014). Hippocampal output area CA1 broadcasts a generalized novelty signal during an object-place recognition task. Hippocampus 24, 773-783.

Laurberg, S. (1979). Commissural and intrinsic connections of the rat hippocampus. J Comp Neurol 184, 685-708.

Lee, A.K., and Wilson, M.A. (2002). Memory of sequential experience in the hippocampus during slow wave sleep. Neuron 36, 1183-1194.

Lee, H., Wang, C., Deshmukh, S.S., and Knierim, J.J. (2015). Neural Population Evidence of Functional Heterogeneity along the CA3 Transverse Axis: Pattern Completion versus Pattern Separation. Neuron 87, 1093-1105.

Lee, I., Jerman, T.S., and Kesner, R.P. (2005). Disruption of delayed memory for a sequence of spatial locations following CA1- or CA3-lesions of the dorsal hippocampus. Neurobiol Learn Mem 84, 138-147.

Lee, I., and Kesner, R.P. (2003). Differential roles of dorsal hippocampal subregions in spatial working memory with short versus intermediate delay. Behav Neurosci 117, 1044-1053.

Lee, I., and Kesner, R.P. (2004). Differential contributions of dorsal hippocampal subregions to memory acquisition and retrieval in contextual fear-conditioning. Hippocampus 14, 301-310.

Lee, I., Rao, G., and Knierim, J.J. (2004a). A double dissociation between hippocampal subfields: differential time course of CA3 and CA1 place cells for processing changed environments. Neuron 42, 803-815.

Lee, I., Yoganarasimha, D., Rao, G., and Knierim, J.J. (2004b). Comparison of population coherence of place cells in hippocampal subfields CA1 and CA3. Nature 430, 456-459.

Lee, S.E., Simons, S.B., Heldt, S.A., Zhao, M., Schroeder, J.P., Vellano, C.P., Cowan, D.P., Ramineni, S., Yates, C.K., Feng, Y., et al. (2010). RGS14 is a natural suppressor of both synaptic plasticity in CA2 neurons and hippocampal-based learning and memory. Proc Natl Acad Sci USA 107, 16994-16998.

Lein, E.S., Callaway, E.M., Albright, T.D., and Gage, F.H. (2005). Redefining the boundaries of the hippocampal CA2 subfield in the mouse using gene expression and 3-dimensional reconstruction. J Comp Neurol 485, 1-10.

Lein, E.S., Zhao, X., and Gage, F.H. (2004). Defining a molecular atlas of the hippocampus using DNA microarrays and high-throughput in situ hybridization. J Neurosci 24, 3879-3889.

Lenck-Santini, P.P., Rivard, B., Muller, R.U., and Poucet, B. (2005). Study of CA1 place cell activity and exploratory behavior following spatial and nonspatial changes in the environment. Hippocampus 15, 356-369.

Lengyel, M., Kwag, J., Paulsen, O., and Dayan, P. (2005). Matching storage and recall: hippocampal spike timing-dependent plasticity and phase response curves. Nat Neurosci 8, 1677-1683.

Leutgeb, J.K., Leutgeb, S., Moser, M.B., and Moser, E.I. (2007). Pattern separation in the dentate gyrus and CA3 of the hippocampus. Science 315, 961-966.

Leutgeb, J.K., Leutgeb, S., Treves, A., Meyer, R., Barnes, C.A., McNaughton, B.L., Moser, M.B., and Moser, E.I. (2005a). Progressive transformation of hippocampal neuronal representations in "morphed" environments. Neuron 48, 345-358.

Leutgeb, S., and Leutgeb, J.K. (2007). Pattern separation, pattern completion, and new neuronal codes within a continuous CA3 map. Learn Mem 14, 745-757.

Leutgeb, S., Leutgeb, J.K., Barnes, C.A., Moser, E.I., McNaughton, B.L., and Moser, M.B. (2005b). Independent codes for spatial and episodic memory in hippocampal neuronal ensembles. Science 309, 619-623.

Leutgeb, S., Leutgeb, J.K., Moser, M.B., and Moser, E.I. (2005c). Place cells, spatial maps and the population code for memory. Curr Opin Neurobiol 15, 738-746.

Leutgeb, S., Leutgeb, J.K., Treves, A., Moser, M.B., and Moser, E.I. (2004). Distinct ensemble codes in hippocampal areas CA3 and CA1. Science 305, 1295-1298.

Lever, C., Burton, S., Jeewajee, A., O'Keefe, J., and Burgess, N. (2009). Boundary vector cells in the subiculum of the hippocampal formation. J Neurosci 29, 9771-9777.

Lever, C., Wills, T., Cacucci, F., Burgess, N., and O'Keefe, J. (2002). Long-term plasticity in hippocampal place-cell representation of environmental geometry. Nature 416, 90-94.

Li, S., Cullen, W.K., Anwyl, R., and Rowan, M.J. (2003). Dopamine-dependent facilitation of LTP induction in hippocampal CA1 by exposure to spatial novelty. Nat Neurosci 6, 526-531.

Li, X.G., Somogyi, P., Ylinen, A., and Buzsaki, G. (1994). The hippocampal CA3 network: an in vivo intracellular labeling study. J Comp Neurol 339, 181--208.

Li, Y., Aimone, J.B., Xu, X., Callaway, E.M., and Gage, F.H. (2012). Development of GABAergic inputs controls the contribution of maturing neurons to the adult hippocampal network. Proc Natl Acad Sci USA 109, 4290-4295.

Lisman, J. (2003). Long-term potentiation: outstanding questions and attempted synthesis. Philos Trans R Soc Lond B Biol Sci 358, 829-842.

Lisman, J.E. (1999). Relating hippocampal circuitry to function: recall of memory sequences by reciprocal dentate-CA3 interactions. Neuron 22, 233-242.

Lisman, J.E., and Grace, A.A. (2005). The hippocampal-VTA loop: controlling the entry of information into long-term memory. Neuron 46, 703-713.

Lisman, J.E., and Otmakhova, N.A. (2001). Storage, recall, and novelty detection of sequences by the hippocampus: elaborating on the SOCRATIC model to account for normal and aberrant effects of dopamine. Hippocampus 11, 551-568.

Logothetis, N.K., Eschenko, O., Murayama, Y., Augath, M., Steudel, T., Evrard, H.C., Besserve, M., and Oeltermann, A. (2012). Hippocampal-cortical interaction during periods of subcortical silence. Nature 491, 547-553.

Lorente de Nó, R. (1933). Studies on the structure of the cerebral cortex. I. The area entorhinalis. J Psychol Neurol 45, 381-438.

Lorente de Nó, R. (1934). Studies on the structure of the cerebral cortex. II. Continuation of the study of the ammonic system. J Psychol Neurol 46, 113-177.

Loughlin, S.E., Foote, S.L., and Bloom, F.E. (1986). Efferent projections of nucleus locus coeruleus: topographic organization of cells of origin demonstrated by three-dimensional reconstruction. Neuroscience 18, 291-306.

Louie, K., and Wilson, M.A. (2001). Temporally structured replay of awake hippocampal ensemble activity during rapid eye movement sleep. Neuron 29, 145-156.

Loureiro, M., Lecourtier, L., Engeln, M., Lopez, J., Cosquer, B., Geiger, K., Kelche, C., Cassel, J.C., and Pereira de Vasconcelos, A. (2012). The ventral hippocampus is necessary for expressing a spatial memory. Brain Struct Funct 217, 93-106.

Lu, L., Igarashi, K.M., Witter, M.P., Moser, E.I., and Moser, M.B. (2015). Topography of place maps along the CA3-to-CA2 axis of the hippocampus. Neuron 87, 1078-1092.

Lubenov, E.V., and Siapas, A.G. (2009). Hippocampal theta oscillations are travelling waves. Nature 459, 534-539.

MacDonald, C.J., Carrow, S., Place, R., and Eichenbaum, H. (2013). Distinct hippocampal time cell sequences represent odor memories in immobilized rats. J Neurosci 33, 14607-14616.

MacDonald, C.J., Lepage, K.Q., Eden, U.T., and Eichenbaum, H. (2011). Hippocampal "time cells" bridge the gap in memory for discontiguous events. Neuron 71, 737-749.

Maier, N., Nimmrich, V., and Draguhn, A. (2003). Cellular and network mechanisms underlying spontaneous sharp wave-ripple complexes in mouse hippocampal slices. J Physiol 550, 873-887.

Malhotra, S., Cross, R.W., and van der Meer, M.A. (2012). Theta phase precession beyond the hippocampus. Rev Neurosci 23, 39-65.

Mankin, E.A., Diehl, G.W., Sparks, F.T., Leutgeb, S., and Leutgeb, J.K. (2015). Hippocampal CA2 activity patterns change over time to a larger extent than between spatial contexts. Neuron 85, 190-201.

Mankin, E.A., Sparks, F.T., Slayyeh, B., Sutherland, R.J., Leutgeb, S., and Leutgeb, J.K. (2012). Neuronal code for extended time in the hippocampus. Proc Natl Acad Sci USA 109, 19462-19467.

Manns, J.R., and Eichenbaum, H. (2009). A cognitive map for object memory in the hippocampus. Learn Mem 16, 616-624.

Marin-Burgin, A., Mongiat, L.A., Pardi, M.B., and Schinder, A.F. (2012). Unique processing during a period of high excitation/inhibition balance in adult-born neurons. Science 335, 1238-1242.

Markram, H., Lubke, J., Frotscher, M., and Sakmann, B. (1997). Regulation of synaptic efficacy by coincidence of postsynaptic APs and EPSPs. Science 275, 213-215.

Markus, E.J., Qin, Y.L., Leonard, B., Skaggs, W.E., Mcnaughton, B.L., and Barnes, C.A. (1995). Interactions between Location and Task Affect the Spatial and Directional Firing of Hippocampal-Neurons. J Neurosci 15, 7079-7094.

Marr, D. (1971). Simple memory: a theory for archicortex. Philos Trans R Soc Lond B Biol Sci 262, 23-81.

Martig, A.K., and Mizumori, S.J. (2011). Ventral tegmental area disruption selectively affects CA1/CA2 but not CA3 place fields during a differential reward working memory task. Hippocampus 21, 172-184.

McAvoy, K., Besnard, A., and Sahay, A. (2015). Adult hippocampal neurogenesis and pattern separation in DG: a role for feedback inhibition in modulating sparseness to govern population-based coding. Front Syst Neurosci 9, 120.

McClelland, J.L., and Goddard, N.H. (1996). Considerations arising from a complementary learning systems perspective on hippocampus and neocortex. Hippocampus 6, 654-665.

McKenzie, S., Frank, A.J., Kinsky, N.R., Porter, B., Riviere, P.D., and Eichenbaum, H. (2014). Hippocampal representation of related and opposing memories develop within distinct, hierarchically organized neural schemas. Neuron 83, 202-215.

McNaughton, B.L., and Barnes, C.A. (1977). Physiological identification and analysis of dentate granule cell responses to stimulation of the medial and lateral perforant pathways in the rat. J Comp Neurol 175, 439-454.

McNaughton, B.L., Barnes, C.A., Meltzer, J., and Sutherland, R.J. (1989). Hippocampal granule cells are necessary for normal spatial learning but not for spatially-selective pyramidal cell discharge. Exp Brain Res 76, 485-496.

McNaughton, B.L., Barnes, C.A., and O'Keefe, J. (1983). The contributions of position, direction, and velocity to single unit activity in the hippocampus of freely-moving rats. Exp Brain Res 52, 41-49.

McNaughton, B.L., Battaglia, F.P., Jensen, O., Moser, E.I., and Moser, M.B. (2006). Path integration and the neural basis of the 'cognitive map'. Nat Rev Neurosci 7, 663-678.

Mcnaughton, B.L., and Morris, R.G. (1987). Hippocampal Synaptic Enhancement and Information-Storage within a Distributed Memory System. Trends Neurosci 10, 408-415.

Meeter, M., Murre, J.M., and Talamini, L.M. (2004). Mode shifting between storage and recall based on novelty detection in oscillating hippocampal circuits. Hippocampus 14, 722-741.

Megias, M., Emri, Z., Freund, T.F., and Gulyas, A.I. (2001). Total number and distribution of inhibitory and excitatory synapses on hippocampal CA1 pyramidal cells. Neuroscience 102, 527-540.

Mehta, M.R., Lee, A.K., and Wilson, M.A. (2002). Role of experience and oscillations in transforming a rate code into a temporal code. Nature 417, 741-746.

Mehta, M.R., Quirk, M.C., and Wilson, M.A. (2000). Experience-dependent asymmetric shape of hippocampal receptive fields. Neuron 25, 707--715.

Meibach, R.C., and Siegel, A. (1977). Efferent connections of the hippocampal formation in the rat. Brain Res 124, 197-224.

Mercer, A., Eastlake, K., Trigg, H.L., and Thomson, A.M. (2012). Local circuitry involving parvalbumin-positive basket cells in the CA2 region of the hippocampus. Hippocampus 22, 43-56.

Mercer, A., Trigg, H.L., and Thomson, A.M. (2007). Characterization of neurons in the CA2 subfield of the adult rat hippocampus. J Neurosci 27, 7329-7338.

Milstein, A.D., Bloss, E.B., Apostolides, P.F., Vaidya, S.P., Dilly, G.A., Zemelman, B.V., and Magee, J.C. (2015). Inhibitory Gating of Input Comparison in the CA1 Microcircuit. Neuron 87, 1274-1289.

Mishkin, M. (1978). Memory in monkeys severely impaired by combined but not by separate removal of amygdala and hippocampus. Nature 273, 297-298.

Mitchell, S.J., Rawlins, J.N., Steward, O., and Olton, D.S. (1982). Medial septal area lesions disrupt theta rhythm and cholinergic staining in medial entorhinal cortex and produce impaired radial arm maze behavior in rats. J Neurosci 2, 292-302.

Mitzdorf, U. (1985). Current source-density method and application in cat cerebral cortex: investigation of evoked potentials and EEG phenomena. Physiol Rev 65, 37-100.

Mizumori, S.J., McNaughton, B.L., Barnes, C.A., and Fox, K.B. (1989). Preserved spatial coding in hippocampal CA1 pyramidal cells during reversible suppression of CA3c output: evidence for pattern completion in hippocampus. J Neurosci 9, 3915-3928.

Mizuseki, K., Sirota, A., Pastalkova, E., and Buzsaki, G. (2009). Theta oscillations provide temporal windows for local circuit computation in the entorhinal-hippocampal loop. Neuron 64, 267-280.

Moita, M.A., Rosis, S., Zhou, Y., LeDoux, J.E., and Blair, H.T. (2003). Hippocampal place cells acquire location-specific responses to the conditioned stimulus during auditory fear conditioning. Neuron 37, 485-497.

Molle, M., Eschenko, O., Gais, S., Sara, S.J., and Born, J. (2009). The influence of learning on sleep slow oscillations and associated spindles and ripples in humans and rats. Eur J Neurosci 29, 1071-1081.

Montgomery, S.M., Betancur, M.I., and Buzsaki, G. (2009). Behavior-dependent coordination of multiple theta dipoles in the hippocampus. J Neurosci 29, 1381-1394.

Montgomery, S.M., and Buzsaki, G. (2007). Gamma oscillations dynamically couple hippocampal CA3 and CA1 regions during memory task performance. Proc Natl Acad Sci USA 104, 14495-14500.

Montgomery, S.M., Sirota, A., and Buzsaki, G. (2008). Theta and gamma coordination of hippocampal networks during waking and rapid eye movement sleep. J Neurosci 28, 6731-6741.

Morris, R.G., Garrud, P., Rawlins, J.N., and O'Keefe, J. (1982). Place navigation impaired in rats with hippocampal lesions. Nature 297, 681-683.

Morris, R.G., Schenk, F., Tweedie, F., and Jarrard, L.E. (1990). Ibotenate lesions of hippocampus and/or subiculum: dissociating components of allocentric spatial learning. Eur J Neurosci 2, 1016-1028.

Moser, E., Moser, M.B., and Andersen, P. (1993). Spatial learning impairment parallels the magnitude of dorsal hippocampal lesions, but is hardly present following ventral lesions. J Neurosci 13, 3916-3925.

Moser, M.B., and Moser, E.I. (1998). Functional differentiation in the hippocampus. Hippocampus 8, 608-619.

Moser, M.B., Moser, E.I., Forrest, E., Andersen, P., and Morris, R.G. (1995). Spatial learning with a minislab in the dorsal hippocampus. Proc Natl Acad Sci USA 92, 9697-9701.

Muenzinger, K.F. (1938). Vicarious trial and error at a point of choice. I. A general survey of its relation to learning efficiency. J Genet Psychol 12, 75-86.

Muller, R.U., and Kubie, J.L. (1987). The effects of changes in the environment on the spatial firing of hippocampal complex-spike cells. J Neurosci 7, 1951-1968.

Muller, R.U., Kubie, J.L., and Ranck, J.B., Jr. (1987). Spatial firing patterns of hippocampal complex-spike cells in a fixed environment. J Neurosci 7, 1935-1950.

Nadasdy, Z., Hirase, H., Czurko, A., Csicsvari, J., and Buzsaki, G. (1999). Replay and time compression of recurring spike sequences in the hippocampus. J Neurosci 19, 9497-9507.

Nakashiba, T., Buhl, D.L., McHugh, T.J., and Tonegawa, S. (2009). Hippocampal CA3 output is crucial for ripple-associated reactivation and consolidation of memory. Neuron 62, 781-787.

Nakashiba, T., Cushman, J.D., Pelkey, K.A., Renaudineau, S., Buhl, D.L., McHugh, T.J., Rodriguez Barrera, V., Chittajallu, R., Iwamoto, K.S., McBain, C.J., et al. (2012). Young dentate granule cells mediate pattern separation, whereas old granule cells facilitate pattern completion. Cell 149, 188-201.

Nakashiba, T., Young, J.Z., McHugh, T.J., Buhl, D.L., and Tonegawa, S. (2008). Transgenic inhibition of synaptic transmission reveals role of CA3 output in hippocampal learning. Science 319, 1260-1264.

Nakazawa, K., Quirk, M.C., Chitwood, R.A., Watanabe, M., Yeckel, M.F., Sun, L.D., Kato, A., Carr, C.A., Johnston, D., Wilson, M.A., et al. (2002). Requirement for hippocampal CA3 NMDA receptors in associative memory recall. Science 297, 211-218.

Nakazawa, K., Sun, L.D., Quirk, M.C., Rondi-Reig, L., Wilson, M.A., and Tonegawa, S. (2003). Hippocampal CA3 NMDA receptors are crucial for memory acquisition of one-time experience. Neuron 38, 305-315.

Neunuebel, J.P., and Knierim, J.J. (2012). Spatial firing correlates of physiologically distinct cell types of the rat dentate gyrus. J Neurosci 32, 3848-3858.

Neunuebel, J.P., and Knierim, J.J. (2014). CA3 retrieves coherent representations from degraded input: direct evidence for CA3 pattern completion and dentate gyrus pattern separation. Neuron 81, 416-427.

Neunuebel, J.P., Yoganarasimha, D., Rao, G., and Knierim, J.J. (2013). Conflicts between local and global spatial frameworks dissociate neural representations of the lateral and medial entorhinal cortex. J Neurosci 33, 9246-9258.

Nitz, D., and McNaughton, B. (2004). Differential modulation of CA1 and dentate gyrus interneurons during exploration of novel environments. J Neurophysiol 91, 863-872.

Nokia, M.S., Mikkonen, J.E., Penttonen, M., and Wikgren, J. (2012). Disrupting neural activity related to awake-state sharp wave-ripple complexes prevents hippocampal learning. Frontiers in behavioral neuroscience 6, 84.

O'Keefe, J. (1976). Place units in the hippocampus of the freely moving rat. Exp Neurol 51, 78-109.

O'Keefe, J., and Dostrovsky, J. (1971). The hippocampus as a spatial map. Preliminary evidence from unit activity in the freely-moving rat. Brain Res 34, 171-175.

O'Keefe, J., and Nadel, L. (1978). The hippocampus as a cognitive map (London: Oxford University Press).

O'Keefe, J., and Recce, M.L. (1993). Phase relationship between hippocampal place units and the EEG theta rhythm. Hippocampus 3, 317-330.

O'Mara, S. (2005). The subiculum: what it does, what it might do, and what neuroanatomy has yet to tell us. J Anat 207, 271-282.

O'Mara, S. (2006). Controlling hippocampal output: the central role of subiculum in hippocampal information processing. Behav Brain Res 174, 304-312.

O'Neill, J., Pleydell-Bouverie, B., Dupret, D., and Csicsvari, J. (2010). Play it again: reactivation of waking experience and memory. Trends Neurosci 33, 220-229.

O'Neill, J., Senior, T., and Csicsvari, J. (2006). Place-selective firing of CA1 pyramidal cells during sharp wave/ripple network patterns in exploratory behavior. Neuron 49, 143-155.

O'Neill, J., Senior, T.J., Allen, K., Huxter, J.R., and Csicsvari, J. (2008). Reactivation of experience-dependent cell assembly patterns in the hippocampus. Nat Neurosci 11, 209-215.

Ochiishi, T., Saitoh, Y., Yukawa, A., Saji, M., Ren, Y., Shirao, T., Miyamoto, H., Nakata, H., and Sekino, Y. (1999). High level of adenosine A1 receptor-like immunoreactivity in the CA2/CA3a region of the adult rat hippocampus. Neuroscience 93, 955-967.

Olton, D.S., Branch, M., and Best, P.J. (1978). Spatial correlates of hippocampal unit activity. Exp Neurol 58, 387-409.

Olton, D.S., and Papas, B.C. (1979). Spatial memory and hippocampal function. Neuropsychologia 17, 669-682.

Olypher, A.V., Lansky, P., Muller, R.U., and Fenton, A.A. (2003). Quantifying location-specific information in the discharge of rat hippocampal place cells. J Neurosci Methods 127, 123-135.

Osborne, L.C., Palmer, S.E., Lisberger, S.G., and Bialek, W. (2008). The neural basis for combinatorial coding in a cortical population response. J Neurosci 28, 13522-13531.

Padilla-Coreano, N., Bolkan, S.S., Pierce, G.M., Blackman, D.R., Hardin, W.D., Garcia-Garcia, A.L., Spellman, T.J., and Gordon, J.A. (2016). Direct Ventral Hippocampal-Prefrontal Input Is Required for Anxiety-Related Neural Activity and Behavior. Neuron 89, 857-866.

Pagani, J.H., Zhao, M., Cui, Z., Avram, S.K., Caruana, D.A., Dudek, S.M., and Young, W.S. (2015). Role of the vasopressin 1b receptor in rodent aggressive behavior and synaptic plasticity in hippocampal area CA2. Mol Psychiatry 20, 490-499.

Pan, W.X., and McNaughton, N. (2002). The role of the medial supramammillary nucleus in the control of hippocampal theta activity and behaviour in rats. Eur J Neurosci 16, 1797-1809.

Papp, G., Witter, M.P., and Treves, A. (2007). The CA3 network as a memory store for spatial representations. Learn Mem 14, 732-744.

Park, E., Dvorak, D., and Fenton, A.A. (2011). Ensemble place codes in hippocampus: CA1, CA3, and dentate gyrus place cells have multiple place fields in large environments. PLoS One 6, e22349.

Pastalkova, E., Itskov, V., Amarasingham, A., and Buzsaki, G. (2008). Internally generated cell assembly sequences in the rat hippocampus. Science 321, 1322-1327.

Patel, J., Fujisawa, S., Berenyi, A., Royer, S., and Buzsaki, G. (2012). Traveling theta waves along the entire septotemporal axis of the hippocampus. Neuron 75, 410-417.

Patel, J., Schomburg, E.W., Berenyi, A., Fujisawa, S., and Buzsaki, G. (2013). Local generation and propagation of ripples along the septotemporal axis of the hippocampus. J Neurosci 33, 17029-17041.

Pavlides, C., and Winson, J. (1989). Influences of hippocampal place cell firing in the awake state on the activity of these cells during subsequent sleep episodes. J Neurosci 9, 2907-2918.

Paz, R., and Pare, D. (2013). Physiological basis for emotional modulation of memory circuits by the amygdala. Curr Opin Neurobiol 23, 381-386.

Penttonen, M., Kamondi, A., Sik, A., Acsady, L., and Buzsaki, G. (1997). Feed-forward and feed-back activation of the dentate gyrus in vivo during dentate spikes and sharp wave bursts. Hippocampus 7, 437-450.

Petrulis, A., Alvarez, P., and Eichenbaum, H. (2005). Neural correlates of social odor recognition and the representation of individual distinctive social odors within entorhinal cortex and ventral subiculum. Neuroscience 130, 259-274.

Petsche, H., and Stumpf, C. (1962). The origin of theta-rhytm in the rabbit hippocampus. Wien Klin Wochenschr 74, 696-700.

Pfeiffer, B.E., and Foster, D.J. (2013). Hippocampal place-cell sequences depict future paths to remembered goals. Nature 497, 74-79.

Pfeiffer, B.E., and Foster, D.J. (2015). PLACE CELLS. Autoassociative dynamics in the generation of sequences of hippocampal place cells. Science 349, 180-183.

Pikkarainen, M., Ronkko, S., Savander, V., Insausti, R., and Pitkanen, A. (1999). Projections from the lateral, basal, and accessory basal nuclei of the amygdala to the hippocampal formation in rat. J Comp Neurol 403, 229-260.

Piskorowski, R.A., and Chevaleyre, V. (2012). Synaptic integration by different dendritic compartments of hippocampal CA1 and CA2 pyramidal neurons. Cell Mol Life Sci 69, 75-88.

Pitkanen, A., Pikkarainen, M., Nurminen, N., and Ylinen, A. (2000). Reciprocal connections between the amygdala and the hippocampal formation, perirhinal cortex, and postrhinal cortex in rat - A review. Ann Ny Acad Sci 911, 369-391.

Pothuizen, H.H., Zhang, W.N., Jongen-Relo, A.L., Feldon, J., and Yee, B.K. (2004). Dissociation of function between the dorsal and the ventral hippocampus in spatial learning abilities of the rat: a within-subject, within-task comparison of reference and working spatial memory. Eur J Neurosci 19, 705-712.

Potvin, O., Allen, K., Thibaudeau, G., Dore, F.Y., and Goulet, S. (2006). Performance on spatial working memory tasks after dorsal or ventral hippocampal lesions and adjacent damage to the subiculum. Behav Neurosci 120, 413-422.

Potvin, O., Dore, F.Y., and Goulet, S. (2007). Contributions of the dorsal hippocampus and the dorsal subiculum to processing of idiothetic information and spatial memory. Neurobiol Learn Mem 87, 669-678.

Poucet, B., Thinus-Blanc, C., and Muller, R.U. (1994). Place cells in the ventral hippocampus of rats. Neuroreport 5, 2045-2048.

Rajasethupathy, P., Sankaran, S., Marshel, J.H., Kim, C.K., Ferenczi, E., Lee, S.Y., Berndt, A., Ramakrishnan, C., Jaffe, A., Lo, M., et al. (2015). Projections from neocortex mediate top-down control of memory retrieval. Nature 526, 653-659.

Ramadan, W., Eschenko, O., and Sara, S.J. (2009). Hippocampal sharp wave/ripples during sleep for consolidation of associative memory. PLoS One 4, e6697.

Ramón y Cajal, S. (1893). Estructura del asta de Ammon y fascia dentata. Ann Soc Esp Hist Nat 22.

Rangel, L.M., Quinn, L.K., Chiba, A.A., Gage, F.H., and Aimone, J.B. (2013). A hypothesis for temporal coding of young and mature granule cells. Front Neurosci 7, 75.

Renno-Costa, C., Lisman, J.E., and Verschure, P.F. (2014). A signature of attractor dynamics in the CA3 region of the hippocampus. PLoS Comput Biol 10, e1003641.

Richard, G.R., Titiz, A., Tyler, A., Holmes, G.L., Scott, R.C., and Lenck-Santini, P.P. (2013). Speed modulation of hippocampal theta frequency correlates with spatial memory performance. Hippocampus 23, 1269-1279.

Richmond, M.A., Yee, B.K., Pouzet, B., Veenman, L., Rawlins, J.N., Feldon, J., and Bannerman, D.M. (1999). Dissociating context and space within the hippocampus: effects of complete, dorsal, and ventral excitotoxic hippocampal lesions on conditioned freezing and spatial learning. Behav Neurosci 113, 1189-1203.

Rolls, E.T. (2007). An attractor network in the hippocampus: theory and neurophysiology. Learn Mem 14, 714-731.

Rosene, D.L., and Van Hoesen, G.W. (1977). Hippocampal efferents reach widespread areas of cerebral cortex and amygdala in the rhesus monkey. Science 198, 315-317.

Roumis, D.K., and Frank, L.M. (2015). Hippocampal sharp-wave ripples in waking and sleeping states. Curr Opin Neurobiol 35, 6-12.

Rowland, D.C., Weible, A.P., Wickersham, I.R., Wu, H., Mayford, M., Witter, M.P., and Kentros, C.G. (2013). Transgenically targeted rabies virus demonstrates a major monosynaptic projection from hippocampal area CA2 to medial entorhinal layer II neurons. J Neurosci 33, 14889-14898.

Royer, S., Sirota, A., Patel, J., and Buzsaki, G. (2010). Distinct representations and theta dynamics in dorsal and ventral hippocampus. J Neurosci 30, 1777-1787.

Sadowski, J.H., Jones, M.W., and Mellor, J.R. (2016). Sharp-wave ripples orchestrate the induction of synaptic plasticity during reactivation of place cell firing patterns in the hippocampus. Cell Rep 14, 1916-1929.

Sahay, A., Scobie, K.N., Hill, A.S., O'Carroll, C.M., Kheirbek, M.A., Burghardt, N.S., Fenton, A.A., Dranovsky, A., and Hen, R. (2011). Increasing adult hippocampal neurogenesis is sufficient to improve pattern separation. Nature 472, 466-470.

San Antonio, A., Liban, K., Ikrar, T., Tsyganovskiy, E., and Xu, X. (2014). Distinct physiological and developmental properties of hippocampal CA2 subfield revealed by using anti-Purkinje cell protein 4 (PCP4) immunostaining. J Comp Neurol 522, 1333-1354.

Sargolini, F., Fyhn, M., Hafting, T., McNaughton, B.L., Witter, M.P., Moser, M.B., and Moser, E.I. (2006). Conjunctive representation of position, direction, and velocity in entorhinal cortex. Science 312, 758-762.

Sasaki, T., Leutgeb, S., and Leutgeb, J.K. (2015). Spatial and memory circuits in the medial entorhinal cortex. Curr Opin Neurobiol 32, 16-23.

Savanthrapadian, S., Meyer, T., Elgueta, C., Booker, S.A., Vida, I., and Bartos, M. (2014). Synaptic properties of SOM- and CCK-expressing cells in dentate gyrus interneuron networks. J Neurosci 34, 8197-8209.

Savelli, F., Yoganarasimha, D., and Knierim, J.J. (2008). Influence of boundary removal on the spatial representations of the medial entorhinal cortex. Hippocampus 18, 1270-1282.

Scharfman, H.E. (1994). Evidence from simultaneous intracellular recordings in rat hippocampal slices that area CA3 pyramidal cells innervate dentate hilar mossy cells. J Neurophysiol 72, 2167-2180.

Scharfman, H.E. (2007). The CA3 "backprojection" to the dentate gyrus. Prog Brain Res 163, 627-637.

Scharfman, H.E., and Myers, C.E. (2012). Hilar mossy cells of the dentate gyrus: a historical perspective. Frontiers in neural circuits 6, 106.

Scheffer-Teixeira, R., Belchior, H., Caixeta, F.V., Souza, B.C., Ribeiro, S., and Tort, A.B. (2012). Theta phase modulates multiple layer-specific oscillations in the CA1 region. Cereb Cortex 22, 2404-2414.

Schiller, D., Eichenbaum, H., Buffalo, E.A., Davachi, L., Foster, D.J., Leutgeb, S., and Ranganath, C. (2015). Memory and space: towards an understanding of the cognitive map. J Neurosci 35, 13904-13911.

Schlesiger, M.I., Cannova, C.C., Boublil, B.L., Hales, J.B., Mankin, E.A., Brandon, M.P., Leutgeb, J.K., Leibold, C., and Leutgeb, S. (2015). The medial entorhinal cortex is necessary for temporal organization of hippocampal neuronal activity. Nat Neurosci 18, 1123-1132.

Schlesiger, M.I., Cressey, J.C., Boublil, B., Koenig, J., Melvin, N.R., Leutgeb, J.K., and Leutgeb, S. (2013). Hippocampal activation during the recall of remote spatial memories in radial maze tasks. Neurobiol Learn Mem 106, 324-333.

Schmidt, B., Hinman, J.R., Jacobson, T.K., Szkudlarek, E., Argraves, M., Escabi, M.A., and Markus, E.J. (2013). Dissociation between dorsal and ventral hippocampal theta oscillations during decision-making. J Neurosci 33, 6212-6224.

Schmidt-Hieber, C., Jonas, P., and Bischofberger, J. (2004). Enhanced synaptic plasticity in newly generated granule cells of the adult hippocampus. Nature 429, 184-187.

Scoville, W.B., and Milner, B. (1957). Loss of recent memory after bilateral hippocampal lesions. J Neurol Neurosurg Psychiatry 20, 11-21.

Sekino, Y., Obata, K., Tanifuji, M., Mizuno, M., and Murayama, J. (1997). Delayed signal propagation via CA2 in rat hippocampal slices revealed by optical recording. J Neurophysiol 78, 1662-1668.

Sharp, P.E. (1996). Multiple spatial/behavioral correlates for cells in the rat postsubiculum: multiple regression analysis and comparison to other hippocampal areas. Cereb Cortex 6, 238-259.

Sharp, P.E. (2006). Subicular place cells generate the same "map" for different environments: Comparison with hippocampal cells. Behav Brain Res 174, 206-214.

Sharp, P.E., and Green, C. (1994). Spatial correlates of firing patterns of single cells in the subiculum of the freely moving rat. J Neurosci 14, 2339-2356.

Shen, J., Kudrimoti, H.S., McNaughton, B.L., and Barnes, C.A. (1998). Reactivation of neuronal ensembles in hippocampal dentate gyrus during sleep after spatial experience. J Sleep Res 7 Suppl 1, 6-16.

Shors, T.J., Miesegaes, G., Beylin, A., Zhao, M., Rydel, T., and Gould, E. (2001). Neurogenesis in the adult is involved in the formation of trace memories. Nature 410, 372-376.

Siapas, A.G., Lubenov, E.V., and Wilson, M.A. (2005). Prefrontal phase locking to hippocampal theta oscillations. Neuron 46, 141-151.

Siapas, A.G., and Wilson, M.A. (1998). Coordinated interactions between hippocampal ripples and cortical spindles during slow-wave sleep. Neuron 21, 1123-1128.

Siegle, J.H., and Wilson, M.A. (2014). Enhancement of encoding and retrieval functions through theta phase-specific manipulation of hippocampus. eLife 3, e03061.

Sik, A., Penttonen, M., Ylinen, A., and Buzsaki, G. (1995). Hippocampal CA1 interneurons: an in vivo intracellular labeling study. J Neurosci 15, 6651-6665.

Sik, A., Ylinen, A., Penttonen, M., and Buzsaki, G. (1994). Inhibitory CA1-CA3-hilar region feedback in the hippocampus. Science 265, 1722-1724.

Silva, D., Feng, T., and Foster, D.J. (2015). Trajectory events across hippocampal place cells require previous experience. Nature neuroscience 18, 1772-1779.

Simons, S.B., Escobedo, Y., Yasuda, R., and Dudek, S.M. (2009). Regional differences in hippocampal calcium handling provide a cellular mechanism for limiting plasticity. Proc Natl Acad Sci USA 106, 14080-14084.

Singer, A.C., Carr, M.F., Karlsson, M.P., and Frank, L.M. (2013). Hippocampal SWR Activity Predicts Correct Decisions during the Initial Learning of an Alternation Task. Neuron 77, 1163-1173.

Singer, A.C., and Frank, L.M. (2009). Rewarded outcomes enhance reactivation of experience in the hippocampus. Neuron 64, 910-921.

Singer, A.C., Karlsson, M.P., Nathe, A.R., Carr, M.F., and Frank, L.M. (2010). Experience-dependent development of coordinated hippocampal spatial activity representing the similarity of related locations. J Neurosci 30, 11586-11604.

Sirota, A., Csicsvari, J., Buhl, D., and Buzsaki, G. (2003). Communication between neocortex and hippocampus during sleep in rodents. Proc Natl Acad Sci USA 100, 2065--2069.

Skaggs, W.E., and McNaughton, B.L. (1996). Replay of neuronal firing sequences in rat hippocampus during sleep following spatial experience. Science 271, 1870-1873.

Skaggs, W.E., McNaughton, B.L., Permenter, M., Archibeque, M., Vogt, J., Amaral, D.G., and Barnes, C.A. (2007). EEG sharp waves and sparse ensemble unit activity in the macaque hippocampus. J Neurophysiol 98, 898-910.

Skaggs, W.E., McNaughton, B.L., Wilson, M.A., and Barnes, C.A. (1996). Theta phase precession in hippocampal neuronal populations and the compression of temporal sequences. Hippocampus 6, 149-172.

Solstad, T., Boccara, C.N., Kropff, E., Moser, M.B., and Moser, E.I. (2008). Representation of geometric borders in the entorhinal cortex. Science 322, 1865-1868.

Spruston, N. (2008). Pyramidal neurons: dendritic structure and synaptic integration. Nat Rev Neurosci 9, 206-221.

Squire, L.R., and Wixted, J.T. (2011). The cognitive neuroscience of human memory since H.M. Annu Rev Neurosci 34, 259-288.

Staff, N.P., Jung, H.Y., Thiagarajan, T., Yao, M., and Spruston, N. (2000). Resting and active properties of pyramidal neurons in subiculum and CA1 of rat hippocampus. J Neurophysiol 84, 2398--2408.

Stark, E., Roux, L., Eichler, R., Senzai, Y., Royer, S., and Buzsaki, G. (2014). Pyramidal cell-interneuron interactions underlie hippocampal ripple oscillations. Neuron 83, 467-480.

Stensola, H., Stensola, T., Solstad, T., Froland, K., Moser, M.B., and Moser, E.I. (2012). The entorhinal grid map is discretized. Nature 492, 72-78.

Steriade, M., Nunez, A., and Amzica, F. (1993). A novel slow (< 1 Hz) oscillation of neocortical neurons in vivo: depolarizing and hyperpolarizing components. J Neurosci 13, 3252-3265.

Stevenson, E.L., and Caldwell, H.K. (2014). Lesions to the CA2 region of the hippocampus impair social memory in mice. Eur J Neurosci 40, 3294-3301.

Steward, O., and Scoville, S.A. (1976). Cells of origin of entorhinal cortical afferents to the hippocampus and fascia dentata of the rat. J Comp Neurol 169, 347-370.

Stewart, M., and Fox, S.E. (1990). Do septal neurons pace the hippocampal theta rhythm? Trends Neurosci 13, 163-168.

Strange, B.A., Witter, M.P., Lein, E.S., and Moser, E.I. (2014). Functional organization of the hippocampal longitudinal axis. Nat Rev Neurosci 15, 655-669.

Sullivan, D., Csicsvari, J., Mizuseki, K., Montgomery, S., Diba, K., and Buzsaki, G. (2011). Relationships between Hippocampal Sharp Waves, Ripples, and Fast Gamma Oscillation: Influence of Dentate and Entorhinal Cortical Activity. J Neurosci 31, 8605-8616.

Sun, Y., Nguyen, A.Q., Nguyen, J.P., Le, L., Saur, D., Choi, J., Callaway, E.M., and Xu, X. (2014). Cell-type-specific circuit connectivity of hippocampal CA1 revealed through Cre-dependent rabies tracing. Cell reports 7, 269-280.

Suzuki, S.S., and Smith, G.K. (1987). Spontaneous EEG spikes in the normal hippocampus. I. Behavioral correlates, laminar profiles and bilateral synchrony. Electroencephalogr Clin Neurophysiol 67, 348-359.

Swanson, L.W., and Cowan, W.M. (1977). An autoradiographic study of the organization of the efferent connections of the hippocampal formation in the rat. J Comp Neurol 172, 49-84.

Takacs, V.T., Klausberger, T., Somogyi, P., Freund, T.F., and Gulyas, A.I. (2012). Extrinsic and local glutamatergic inputs of the rat hippocampal CA1 area differentially innervate pyramidal cells and interneurons. Hippocampus 22, 1379-1391.

Tamamaki, N., Abe, K., and Nojyo, Y. (1988). Three-dimensional analysis of the whole axonal arbors originating from single CA2 pyramidal neurons in the rat hippocampus with the aid of a computer graphic technique. Brain Res 452, 255-272.

Tao, C., Zhang, G., Xiong, Y., and Zhou, Y. (2015). Functional dissection of synaptic circuits: in vivo patch-clamp recording in neuroscience. Frontiers in neural circuits 9, 23.

Taube, J.S. (2007). The head direction signal: origins and sensory-motor integration. Annu Rev Neurosci 30, 181-207.

Temprana, S.G., Mongiat, L.A., Yang, S.M., Trinchero, M.F., Alvarez, D.D., Kropff, E., Giacomini, D., Beltramone, N., Lanuza, G.M., and Schinder, A.F. (2015). Delayed coupling to feedback inhibition during a critical period for the integration of adult-born granule cells. Neuron 85, 116-130.

Tesche, C.D., and Karhu, J. (2000). Theta oscillations index human hippocampal activation during a working memory task. Proc Natl Acad Sci USA 97, 919-924.

Thompson, L.T., and Best, P.J. (1990). Long-term stability of the place-field activity of single units recorded from the dorsal hippocampus of freely behaving rats. Brain Res 19; 509, 299-308.

Tolman, E.C. (1938). The determiners of behavior at a choice point. Psychological review 45, 1-41.

Tort, A.B., Komorowski, R., Eichenbaum, H., and Kopell, N. (2010). Measuring phase-amplitude coupling between neuronal oscillations of different frequencies. J Neurophysiol 104, 1195-1210.

Tort, A.B., Komorowski, R.W., Manns, J.R., Kopell, N.J., and Eichenbaum, H. (2009). Theta-gamma coupling increases during the learning of item-context associations. Proc Natl Acad Sci USA 106, 20942-20947.

Toth, K., Borhegyi, Z., and Freund, T.F. (1993). Postsynaptic targets of GABAergic hippocampal neurons in the medial septum-diagonal band of broca complex. J Neurosci 13, 3712-3724.

Toth, K., and Freund, T.F. (1992). Calbindin D28k-containing nonpyramidal cells in the rat hippocampus: their immunoreactivity for GABA and projection to the medial septum. Neuroscience 49, 793-805.

Treves, A., and Rolls, E. (1991). What determines the capacity of autoassociative memories in the brain? Comp Neural Sys 2, 371-397.

Treves, A., and Rolls, E.T. (1992). Computational constraints suggest the need for two distinct input systems to the hippocampal CA3 network. Hippocampus 2, 189-199.

Treves, A., and Rolls, E.T. (1994). Computational analysis of the role of the hippocampus in memory. Hippocampus 4, 374-391.

Tronel, S., Belnoue, L., Grosjean, N., Revest, J.M., Piazza, P.V., Koehl, M., and Abrous, D.N. (2012). Adult-born neurons are necessary for extended contextual discrimination. Hippocampus 22, 292-298.

Trouche, S., Koren, V., Doig, N.M., Ellender, T.J., El-Gaby, M., Lopes-Dos-Santos, V., Reeve, H.M., Perestenko, P.V., Garas, F.N., Magill, P.J., et al. (2019). A Hippocampus-Accumbens Tripartite Neuronal Motif Guides Appetitive Memory in Space. Cell 176, 1393-1406.

Ulanovsky, N., and Moss, C.F. (2007). Hippocampal cellular and network activity in freely moving echolocating bats. Nat Neurosci 10, 224-233.

Valero, M., Cid, E., Averkin, R.G., Aguilar, J., Sanchez-Aguilera, A., Viney, T.J., Gomez-Dominguez, D., Bellistri, E., and de la Prida, L.M. (2015). Determinants of different deep and superficial CA1 pyramidal cell dynamics during sharp-wave ripples. Nat Neurosci 18, 1281-1290.

Van Cauter, T., Poucet, B., and Save, E. (2008). Unstable CA1 place cell representation in rats with entorhinal cortex lesions. Eur J Neurosci 27, 1933-1946.

van der Meer, M.A., and Redish, A.D. (2011). Theta phase precession in rat ventral striatum links place and reward information. J Neurosci 31, 2843-2854.

van Strien, N.M., Cappaert, N.L., and Witter, M.P. (2009). The anatomy of memory: an interactive overview of the parahippocampal-hippocampal network. Nat Rev Neurosci 10, 272-282.

Vanderwolf, C.H. (1969). Hippocampal electrical activity and voluntary movement in the rat. Electroencephalogr Clin Neurophysiol 26, 407-418.

VanElzakker, M., Fevurly, R.D., Breindel, T., and Spencer, R.L. (2008). Environmental novelty is associated with a selective increase in Fos expression in the output elements of the hippocampal formation and the perirhinal cortex. Learn Mem 15, 899-908.

Vazdarjanova, A., and Guzowski, J.F. (2004). Differences in hippocampal neuronal population responses to modifications of an environmental context: evidence for distinct, yet complementary, functions of CA3 and CA1 ensembles. J Neurosci 24, 6489-6496.

Vellano, C.P., Lee, S.E., Dudek, S.M., and Hepler, J.R. (2011). RGS14 at the interface of hippocampal signaling and synaptic plasticity. Trends Pharmacol Sci 32, 666-674.

Vertes, R.P., Hoover, W.B., Szigeti-Buck, K., and Leranth, C. (2007). Nucleus reuniens of the midline thalamus: link between the medial prefrontal cortex and the hippocampus. Brain Res Bull 71, 601-609.

Vinogradova, O.S. (2001). Hippocampus as comparator: role of the two input and two output systems of the hippocampus in selection and registration of information. Hippocampus 11, 578-598.

Wang, M.E., Fraize, N.P., Yin, L., Yuan, R.K., Petsagourakis, D., Wann, E.G., and Muzzio, I.A. (2013). Differential roles of the dorsal and ventral hippocampus in predator odor contextual fear conditioning. Hippocampus 23, 451-466.

Watrous, A.J., Lee, D.J., Izadi, A., Gurkoff, G.G., Shahlaie, K., and Ekstrom, A.D. (2013). A comparative study of human and rat hippocampal low-frequency oscillations during spatial navigation. Hippocampus 23, 656-661.

Weeden, C.S., Roberts, J.M., Kamm, A.M., and Kesner, R.P. (2015). The role of the ventral dentate gyrus in anxiety-based behaviors. Neurobiol Learn Mem 118, 143-149.

Wersinger, S.R., Ginns, E.I., O'Carroll, A.M., Lolait, S.J., and Young, W.S., 3rd (2002). Vasopressin V1b receptor knockout reduces aggressive behavior in male mice. Mol Psychiatry 7, 975-984.

Wersinger, S.R., Kelliher, K.R., Zufall, F., Lolait, S.J., O'Carroll, A.M., and Young, W.S., 3rd (2004). Social motivation is reduced in vasopressin 1b receptor null mice despite normal performance in an olfactory discrimination task. Horm Behav 46, 638-645.

Wespatat, V., Tennigkeit, F., and Singer, W. (2004). Phase sensitivity of synaptic modifications in oscillating cells of rat visual cortex. J Neurosci 24, 9067-9075.

Wierzynski, C.M., Lubenov, E.V., Gu, M., and Siapas, A.G. (2009). State-dependent spike-timing relationships between hippocampal and prefrontal circuits during sleep. Neuron 61, 587-596.

Wikenheiser, A.M., and Redish, A.D. (2015). Hippocampal theta sequences reflect current goals. Nat Neurosci 18, 289-294.

Wilson, D.I., Langston, R.F., Schlesiger, M.I., Wagner, M., Watanabe, S., and Ainge, J.A. (2013). Lateral entorhinal cortex is critical for novel object-context recognition. Hippocampus 23, 352-366.

Wilson, M.A., and McNaughton, B.L. (1994). Reactivation of hippocampal ensemble memories during sleep. Science 265, 676-679.

Winson, J. (1972). Interspecies differences in the occurrence of theta. Behav Biol 7, 479-487.

Winson, J., and Abzug, C. (1978). Neuronal Transmission through Hippocampal Pathways Dependent on Behavior. J Neurophys 41, 716-732.

Witter, M.P. (1986). A survey of the anatomy of the hippocampal formation, with emphasis on the septotemporal organization of its intrinsic and extrinsic connections. Advances in experimental medicine and biology 203, 67-82.

Witter, M.P. (1993). Organization of the entorhinal-hippocampal system: a review of current anatomical data. Hippocampus 3 Spec No, 33--44.

Witter, M.P. (2006). Connections of the subiculum of the rat: Topography in relation to columnar and laminar organization. Behav Brain Res 174, 251-264.

Witter, M.P. (2007). Intrinsic and extrinsic wiring of CA3: indications for connectional heterogeneity. Learn Mem 14, 705-713.

Witter, M.P., and Amaral, D.G. (2004). Hippocampal formation. In The rat nervous system, G. Paxinos, ed. (San Diego, CA: Elsevier Academic Press), pp. 635-704.

Witter, M.P., Groenewegen, H.J., Lopes da Silva, F.H., and Lohman, A.H. (1989). Functional organization of the extrinsic and intrinsic circuitry of the parahippocampal region. Prog Neurobiol 33, 161-253.

Witter, M.P., Wouterlood, F.G., Naber, P.A., and Van Haeften, T. (2000). Anatomical organization of the parahippocampal-hippocampal network. Ann N Y Acad Sci 911, 1-24.

Wojtowicz, J.M., Askew, M.L., and Winocur, G. (2008). The effects of running and of inhibiting adult neurogenesis on learning and memory in rats. Eur J Neurosci 27, 1494-1502.

Wood, E.R., Dudchenko, P.A., Robitsek, R.J., and Eichenbaum, H. (2000). Hippocampal neurons encode information about different types of memory episodes occurring in the same location. Neuron 27, 623-633.

Wu, X., and Foster, D.J. (2014). Hippocampal replay captures the unique topological structure of a novel environment. J Neurosci 34, 6459-6469.

Yartsev, M.M., Witter, M.P., and Ulanovsky, N. (2011). Grid cells without theta oscillations in the entorhinal cortex of bats. Nature 479, 103-107.

Ylinen, A., Bragin, A., Nadasdy, Z., Jando, G., Szabo, I., Sik, A., and Buzsaki, G. (1995). Sharp wave-associated high-frequency oscillation (200 Hz) in the intact hippocampus: network and intracellular mechanisms. J Neurosci 15, 30-46.

Yoganarasimha, D., Rao, G., and Knierim, J.J. (2011). Lateral entorhinal neurons are not spatially selective in cue-rich environments. Hippocampus 21, 1363-1374.

Young, B.J., Fox, G.D., and Eichenbaum, H. (1994). Correlates of hippocampal complex-spike cell activity in rats performing a nonspatial radial maze task. J Neurosci 14, 6553-6563.

Young, W.S., Li, J., Wersinger, S.R., and Palkovits, M. (2006). The vasopressin 1b receptor is prominent in the hippocampal area CA2 where it is unaffected by restraint stress or adrenalectomy. Neuroscience 143, 1031-1039.

Zhang, S.J., Ye, J., Miao, C., Tsao, A., Cerniauskas, I., Ledergerber, D., Moser, M.B., and Moser, E.I. (2013). Optogenetic dissection of entorhinal-hippocampal functional connectivity. Science 340, 1232627.

Zhang, W.N., Bast, T., and Feldon, J. (2001). The ventral hippocampus and fear conditioning in rats: different anterograde amnesias of fear after infusion of N-methyl-D-aspartate or its noncompetitive antagonist MK-801 into the ventral hippocampus. Behav Brain Res 126, 159-174.

Zhao, M., Choi, Y.S., Obrietan, K., and Dudek, S.M. (2007). Synaptic plasticity (and the lack thereof) in hippocampal CA2 neurons. J Neurosci 27, 12025-12032.

Zhao, X., Lein, E.S., He, A., Smith, S.C., Aston, C., and Gage, F.H. (2001). Transcriptional profiling reveals strict boundaries between hippocampal subregions. J Comp Neurol 441, 187-196.

Zheng, C., Bieri, K.W., Hsiao, Y.T., and Colgin, L.L. (2016). Spatial Sequence Coding Differs during Slow and Fast Gamma Rhythms in the Hippocampus. Neuron 89, 398-408.

Zheng, C., Bieri, K.W., Trettel, S.G., and Colgin, L.L. (2015). The relationship between gamma frequency and running speed differs for slow and fast gamma rhythms in freely behaving rats. Hippocampus 25, 924-938.

Ziv, Y., Burns, L.D., Cocker, E.D., Hamel, E.O., Ghosh, K.K., Kitch, L.J., El Gamal, A., and Schnitzer, M.J. (2013). Long-term dynamics of CA1 hippocampal place codes. Nat Neurosci 16, 264-266.

CHAPTER 2

Dorsal and ventral hippocampal sharp-wave ripples activate distinct

nucleus accumbens networks

2.1 Abstract

Memories of positive experiences link places, events, and reward outcomes. These memories recruit interactions between the hippocampus and nucleus accumbens (NAc). Both dorsal and ventral hippocampus (dH and vH) project to the NAc, but it remains unknown whether dH and vH act in concert or separately to engage NAc representations related to space and reward. We recorded simultaneously from the dH, vH, and NAc of rats during an appetitive spatial task and focused on hippocampal sharp-wave ripples (SWRs) to identify times of memory reactivation across brain regions. Here we show that dH and vH awake SWRs occur asynchronously and activate distinct and opposing patterns of NAc spiking. Only NAc neurons activated during dH SWRs were tuned to task- and reward-related information. These temporally and anatomically separable hippocampal-NAc interactions point to distinct channels of mnemonic processing in the NAc, with the dH-NAc channel specialized for spatial task and reward information.

2.2 Introduction

Episodic memories entail the integration of diverse aspects of experience, such as places, events, context, and reward outcomes. The hippocampus is critical for these memories and coordinates mnemonic processing in many downstream brain regions (Buzsaki and Moser, 2013; Eichenbaum, 2017; Sosa et al., 2016). Within the hippocampus, different aspects of experience are thought to be preferentially processed in different subdivisions, with the dorsal hippocampus (dH) specialized for precise spatial representations and the ventral hippocampus (vH) specialized for contextual and emotional representations (Ciocchi et al., 2015; de Hoz and Martin, 2014; Fanselow and Dong, 2010; Jimenez et al., 2018; Kjelstrup et al., 2008; Komorowski et al., 2013; Moser and Moser, 1998; Royer et al., 2010; Strange et al., 2014).

Memories linking space and reward are thought to depend on hippocampal communication with the nucleus accumbens (NAc), a striatal region known to represent reward and the value of chosen actions (Carelli, 2002; Chersi and Burgess, 2015; Humphries and Prescott, 2010; Ito et al., 2008; LeGates et al., 2018; Pennartz et al., 2009; Pennartz et al., 2011; Sjulson et al., 2018; Trouche et al., 2019). The most prominent anatomical projections from the hippocampus to the NAc arise from the vH, and optogenetic manipulations of this pathway can drive or block conditioned place preference behavior (Britt et al., 2012; LeGates et al., 2018). Inactivation of vH can also affect reward memories (Riaz et al., 2017), and vH neurons that project to the NAc are modulated at locations associated with reward (Ciocchi et al., 2015). Taken together, these findings have suggested a role for the vH-NAc pathway in processing information related to locations and rewards. Interestingly, the dH also projects to the NAc, albeit much more sparsely (Brog et al., 1993; Humphries and Prescott, 2010; Li et al., 2018; Strange et al., 2014; Trouche et al., 2019), and a recent study demonstrated that optogenetic inhibition of projections from dH (specifically from dorsal CA1) to the NAc impairs recall of a spatial-reward association (Trouche et al., 2019).

Thus, both dH and vH have been linked to spatial-reward memory. These links are based in large part on manipulations that target entire pathways or structures, but these manipulations lead to large scale changes in neural activity patterns that are not seen in the intact system. Studies examining activity under normal conditions have reported coordinated firing between neurons of the dH and NAc in the context of

spatially-guided appetitive behaviors (Lansink et al., 2016; Sjulson et al., 2018; Tabuchi et al., 2000; Trouche et al., 2019; van der Meer and Redish, 2011), but whether neural activity patterns in the vH and NAc are coordinated during behavior has not yet been explored. More broadly, whether vH, dH, or both recruit representations related to spatial and/or reward information in the NAc under normal conditions remains unclear.

Addressing these issues requires identifying specific NAc neurons that are engaged in the context of dH- or vH-specific information processing. Hippocampal sharp-wave ripples (SWRs) are discrete events that are well suited for this identification. These high-frequency (150-250 Hz) oscillations occur during sleep and times of awake immobility and are known to coincide with the sequential reactivation of place cell ensembles (Buzsaki, 2015; Diba and Buzsaki, 2007; Foster and Wilson, 2006; Joo and Frank, 2018). Moreover, SWRs have been shown to engage extrahippocampal structures (Girardeau et al., 2017; Gomperts et al., 2015; Jadhav et al., 2016; Ji and Wilson, 2007; Pennartz et al., 2004; Rothschild et al., 2017; Yu et al., 2017), thus providing a mechanism for time-compressed memory retrieval across the brain.

SWRs can be detected in both dH and vH, and during sleep these events can propagate along the entire dorsoventral axis in either direction or be isolated (Patel et al., 2013). However, the relationship between dH SWRs (dSWRs) and vH SWRs (vSWRs) during waking has not been explored. Previous work has also reported the activation of NAc neurons during dH SWRs in sleep and found that these neurons tended to fire near reward sites during task performance (Lansink et al., 2008; Lansink et al., 2009; Pennartz et al., 2004; Sjulson et al., 2018). Whether NAc neurons are engaged during awake dSWRs or during either awake or sleep vSWRs remains unknown. Importantly, it is also unknown whether dSWRs and vSWRs engage similar or different NAc populations.

Here we report that dSWRs and vSWRs occur asynchronously in the awake state and engage largely distinct subpopulations of NAc neurons. Surprisingly, when individual neurons were modulated during both types of SWRs, they were most often activated during dSWRs and suppressed during vSWRs or vice-versa. We also found that dSWR-activated NAc neurons encoded information related to reward history and progression along spatial paths to goals. By contrast, the vSWR-activated neurons showed an

absence of spatial-specificity and reward encoding, indicating that dH and vH coordinate distinct neural representations in the NAc. We propose that these circuit dynamics could provide a substrate for the independent storage and retrieval of distinct aspects of experience.

2.3 Results

Temporal asynchrony of awake dH and vH SWRs during a spatial memory task

Identifying the nature of coordination between the dH-NAc and vH-NAc pathways requires a simultaneous survey of all three regions. We therefore recorded from dH, vH, and NAc using chronically implanted tetrode arrays in rats (**Fig. 2.1 [A], Fig. S1**), in the context of both a dynamic spatial memory task and interleaved sleep periods in a separate rest box (**Fig. 2.1 [B]**). We utilized a "Multiple-W" task (Singer and Frank, 2009) in which a rat must first learn which three of six maze arms are reward locations and alternate between them to receive liquid food reward on each correct well visit (**Fig. 2.1 [C]**). Learning this alternation requires hippocampal-dependent memory (Kim and Frank, 2009) as well as the association of specific locations with reward, a type of association thought to involve the hippocampal-NAc circuit (Chersi and Burgess, 2015; Floresco et al., 1997; Humphries and Prescott, 2010; Ito et al., 2008; Pennartz et al., 2011). Once the animal acquired the first alternation sequence to ~80% correct, we introduced a new sequence shifted over by one arm (**Fig. 2.1 [C]**), requiring the animal to transfer the alternation rule to a new set of reward locations. Sequences were thereafter switched across task epochs for the remainder of the experiment (example switch day in **Fig. 2.1 [B]**) to continually promote adaptive, spatially-guided reward-seeking behavior.

This task is known to engage dSWRs, particularly during reward consumption (Singer et al., 2013; Singer and Frank, 2009), but the occurrence of vSWRs during awake behavior had not been previously described. We therefore examined awake SWRs detected in dH or vH during periods of immobility on the task, which occurred primarily at the reward wells (example in **Fig. 2.1 [D]**). Both dSWRs and vSWRs showed the expected spectral properties (**Fig. S2 [A-B]**) and increases in multiunit activity (Buzsaki, 2015; Patel et al., 2013), both locally in CA1 as well as in CA3 (**Fig. S2 [C-D]**), indicating strong, transient
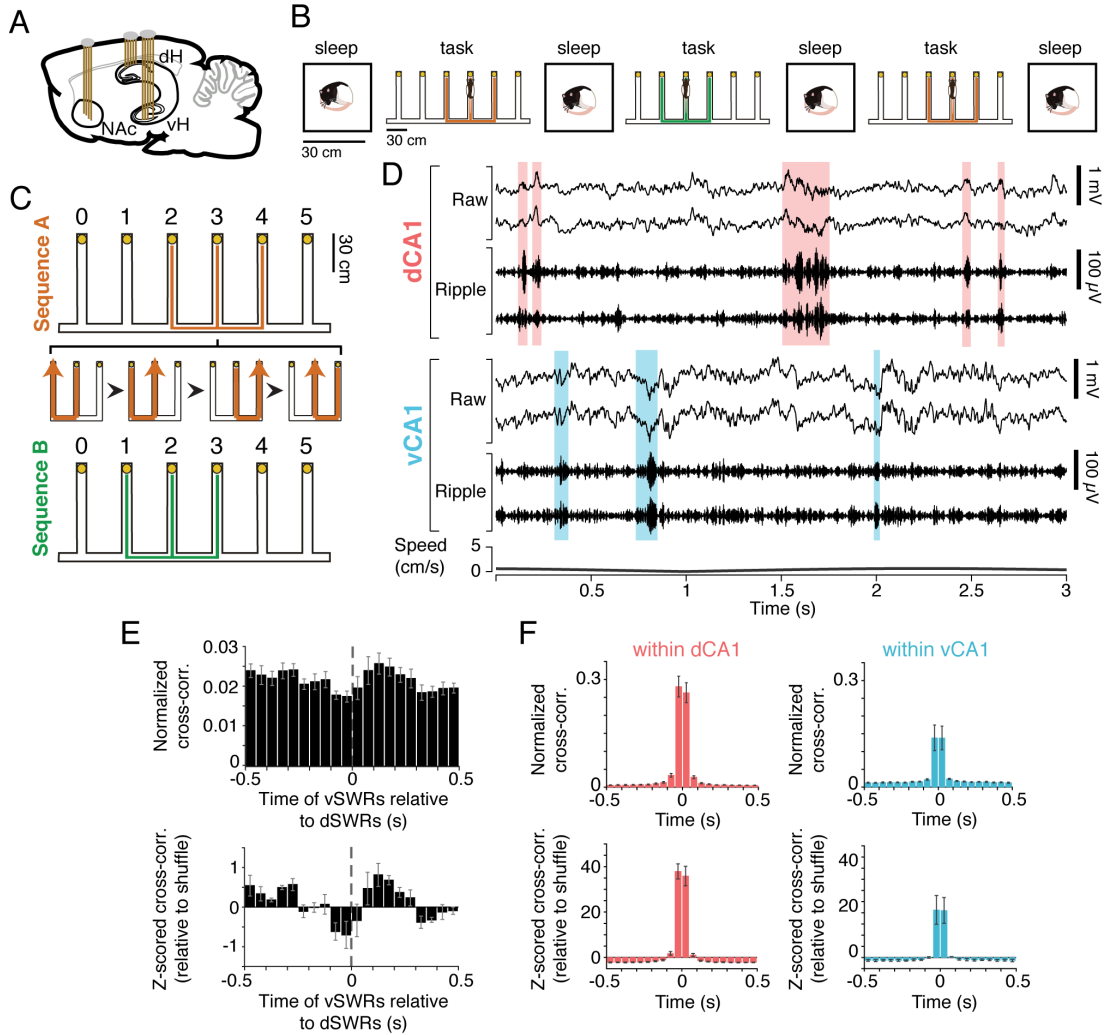
Figure 2.1 | Awake dorsal and ventral hippocampal SWRs occur asynchronously.
(A) Sagittal schematic of tetrodes targeting NAc, dH, and vH in the rat brain. **(B)** Behavioral structure for an example "Switch" day. Task epochs (sessions) on the Multiple-W maze are flanked by sleep epochs in a separate rest box. On an "Acquisition" day, the rat would repeat the same W sequence in each task epoch. **(C)** Schematic of the Multiple-W task. Yellow circles indicate visually identical reward wells. The animal was required to alternate visits from the center well of the "W" to the outer two wells to receive a liquid food reward on each correct well visit. Expanded section depicts four consecutive correct trials. Animals acquired one sequence (either A or B, counterbalanced across animals) to ~80% correct ("Acquisition" days) before the second sequence was introduced on the first "Switch" day. **(D)** Example dSWRs and vSWRs during awake immobility at a reward well (Rat 4). The raw (1-400 Hz) and ripple-filtered (150-250 Hz) local field potential is shown for two tetrodes each in dorsal CA1 (dCA1) and ventral CA1 (vCA1). Shaded regions highlight detected dSWRs (pink) and vSWRs (blue). Bottom plot depicts the speed of the animal. **(E)** Mean cross-correlation histogram (CCH) between onset times of dSWRs and vSWRs across animals (n=5 rats). Top: CCH normalized by the number of dSWRs. The y-axis signifies the fraction of dSWRs that have a vSWR occurring within each time bin. Bottom: CCH z-scored relative to shuffled vSWR onset times. Z-score 0 reflects mean of shuffles. Error bars indicate s.e.m. **(F)** Mean CCH showing high synchrony of awake SWRs between pairs of tetrodes within dCA1 (left, n=5 rats) or vCA1 (right, n=3 rats with >1 tetrode in vCA1). Top: CCH normalized by the number of SWRs on one tetrode. Bottom: CCH z-scored relative to shuffle. SWRs here were detected on individual tetrodes. Error bars indicate s.e.m. See also Figures S1, S2 and S3A.

activation of the local hippocampal networks. Also consistent with previous characterization in sleep (Patel et al., 2013), awake vSWRs occurred more frequently but were of smaller amplitude and shorter duration than dSWRs (**Fig. S2 [E-G]**).

Strikingly, despite the existence of dorsoventral connectivity within the hippocampus (van Strien et al., 2009; Witter, 2007) and observations of occasional synchrony between dSWRs and vSWRs during sleep (Patel et al., 2013), dSWRs and vSWRs occurred asynchronously during awake immobility on the task (**Fig. 2.1 [D-E]**). Only ~3.7% of dSWRs occurred within 50 ms of a vSWR, which was no more than expected from a shuffle of SWR times (**Fig. 2.1 [E]**). This pattern was observed in each animal (n=5, **Fig. S3 [A]**), despite small anatomical differences in recording sites (**Fig. S1 [C,E-F]**). This dorsoventral asynchrony was in stark contrast to the prominent synchrony between pairs of recording sites within dH or within vH (**Fig. 2.1 [F]**), indicating temporally separable dH and vH outputs to downstream brain areas during awake SWRs.

Distinct modulation of dSWRs and vSWRs by novelty and reward

DSWRs and vSWRs also showed different patterns of modulation relative to novelty and reward. We examined SWR occurrence on rewarded and error trials as function of the animals' performance on the Multiple-W task (**Fig. 2.2 [A], Fig. S4**), as improving performance parallels decreasing novelty and increasing familiarity with both the task and the environment. We first noted that dSWRs and vSWRs remained asynchronous on both rewarded and error trials (**Fig. S3 [B]**). Previous findings established that new and rewarding experiences strongly enhance the rate of dSWRs (Ambrose et al., 2016; Singer and Frank, 2009), and as expected, dSWRs were more prevalent when the environment was novel and following receipt of reward (**Fig. 2.2 [B], Fig. S3 [C]**). Given the strong anatomical projections from the vH to limbic brain areas involved in reward processing (Fanselow and Dong, 2010; Humphries and Prescott, 2010; Strange et al., 2014), we expected a similar pattern of enhancement for vSWRs.
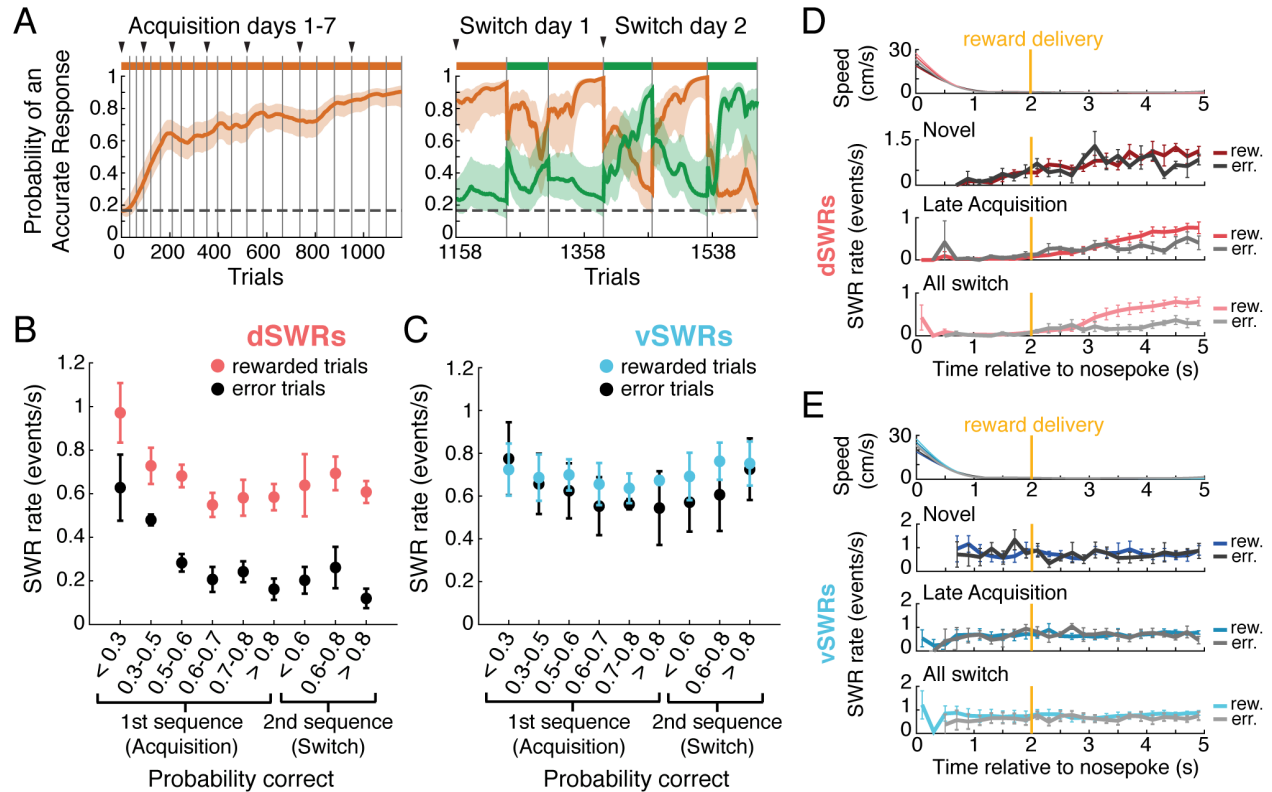
Figure 2.2 | Awake dSWRs and vSWRs are differently modulated by reward and novelty.
(A) Example behavior (Rat 5) on the Multiple-W expressed as the probability that the rat is making an accurate choice on each trial according to Sequence A (orange) or B (green) (see Methods). Solid line indicates the mode of the probability distribution, shaded region indicates the 90% confidence interval. Colored bars above the plot indicate the rewarded sequence, grey vertical lines mark epoch boundaries, black triangles mark the start of each day, and the horizontal dotted line indicates chance performance (0.167). For clarity, only 2 full switch days are shown on the right (see Figure S4 for the complete behavior from each animal). **(B)** Change in dSWR rate on rewarded vs. error trials (well visits), calculated per time spent immobile at reward wells (minimum 1 s). Each point represents the mean SWR rate across animals ± s.e.m. within that learning stage (n=4 rats in Acquisition stages 0.7-0.8, >0.8; n=5 rats all other stages; see Methods). Learning stages are defined by each animal's probability of performing the rewarded sequence correctly on each trial (see Figure S4), and is used here as a proxy for novelty. For Switch performance, SWR rate is shown only for the second sequence when it was rewarded. **(C)** Similar to (B), but for vSWR rate in each learning stage (n=4 rats in Acquisition stages 0.7-0.8, >0.8; n=5 rats all other stages). **(D)** Timing of dSWRs relative to nosepoke, by behavioral stage. Gold line indicates reward delivery or its expected time on error trials, 2 s after nosepoke at the well. Top: mean speed in each behavioral stage; note that each rat's head takes ~1 s to fully decelerate and dip into the reward well. Below: mean SWR rate across animals in 200 ms bins for rewarded and error trials, during the first 100 trials of Multiple-W behavior ("Novel"), trials occurring at >0.6 probability correct on the first sequence ("Late Acquisition"), and during all Switch epochs ("All switch"). Shades of red are rewarded trials, shades of grey are error trials. **(E)** Timing of vSWRs relative to nosepoke, by behavioral stage. Speed data at top are repeated from (D). Note that since reward rate is only calculated when at least 2 s of data are present below 4 cm/s in each bin, empty bins indicate too little data to calculate an SWR rate. Shades of blue are rewarded trials, shades of grey are error trials. See also Figures S3B-D and S4.

Instead, vSWRs maintained a similar rate on rewarded and error trials and were not enhanced during early novelty (**Fig. 2.2 [C], Fig. S3 [D]**). The onset time of dSWRs and vSWRs also differed relative to arrival at the reward wells. We utilized a 2-second delay between nosepoke and reward delivery to separate the time of immobility from the time of reward. While dSWRs shifted later following initial learning such that they began only after receipt of reward (**Fig. 2.2 [D]**), vSWRs were detected as soon as the animal stopped moving at all stages of learning (**Fig. 2.2 [E]**). Together, these results indicate that dSWRs and vSWRs are differently regulated by novelty and reward.

NAc subpopulations are oppositely modulated during dSWRs and vSWRs

The temporal separation and distinct modulation patterns of awake dSWRs and vSWRs provided the opportunity to determine whether these events differentially engaged the NAc. It is unknown whether and how NAc neurons are modulated during awake dSWRs or during either awake or sleep vSWRs. To sample the respective target regions of the sparse dH projection and the much more prominent vH projection, we recorded from both the NAc core and shell (**Fig. S1 [D]**). We then classified NAc single units into putative medium-sized spiny neurons (MSNs) and fast-spiking interneurons (FSIs) based on firing rate and waveform properties (**Fig. S5 [A]**) (Atallah et al., 2014; Berke, 2008) and examined their activity aligned to the times of awake dSWRs and vSWRs.

We found that 51% of MSNs either significantly increased or decreased their firing rates around the times of dSWRs and/or vSWRs. Strikingly, the observed firing rate changes were often opposite for dSWRs and vSWRs, such that 10.6% of cells were significantly dSWR-activated and vSWR-suppressed (D+V-) or dSWR-suppressed and vSWR-activated (D-V+) (**Fig. 2.3 [A-B]**). This bidirectional and opposing modulation was quite surprising, as it indicates that SWRs from dH and vH have opposing influences on the same neurons. Crucially, the fraction of oppositely modulated cells was significantly larger than would be expected by total chance overlap of independent dSWR- (D+, D-) and vSWR-modulated (V+, V-) subgroups, while the fraction of co-positively modulated cells (3.2% D+V+) was not greater than chance. In addition, many cells were significantly modulated during only dSWRs or vSWRs

but not both (**Fig. 2.3 [B]**). Across the full population of MSNs (**Fig. 2.3 [C], Fig. S6 [A]**), we found a significant anti-correlation in SWR modulation amplitudes (**Fig. 2.3 [D]**), demonstrating that dSWRs and vSWRs are consistently associated with opposite activity changes at the level of individual NAc MSNs. We also noted that MSN activity changes predominantly followed dH or vH neuronal activation during SWRs, consistent with hippocampus to NAc information flow (**Fig. S6 [B]**).

This opposing modulation could not be explained by the temporal proximity of dSWRs and vSWRs. We excluded the small number of dSWRs and vSWRs that occurred within 250 ms of one another and confirmed that the opposition persisted during isolated SWRs (**Fig. S6 [E-G]**). We also verified that our results held when we applied a conservative criterion (see Methods) to ensure that each cell was included only once (**Fig. S6 [H-J]**), accounting for the possibility of recording the same neurons across days.

The same patterns of modulation were seen when we examined FSIs (**Fig. 2.3 [E]**), applying the same criterion to ensure that each cell was included only once. The majority of FSIs were SWR-modulated (85%), and we identified FSIs that were D+V-, D-V+, or only D+ or V+, but none that were D+V+ (**Fig. 2.3 [F]**). The FSI population as a whole also showed anti-correlated modulation during dSWRs versus vSWRs (**Fig. 2.3 [G-H], Fig. S6 [C-D]**).

For both MSNs and FSIs, SWR-modulation was anatomically distributed in a pattern consistent with reported dH and vH projections to the NAc (Britt et al., 2012; Brog et al., 1993; Groenewegen et al., 1987; Humphries and Prescott, 2010; Pennartz et al., 2011; Strange et al., 2014; Trouche et al., 2019), with V+ neurons present mostly in the medial shell and parts of the core and D+ neurons restricted to the core and lateral shell (**Fig. S5 [C-D]**). Together, these findings reveal that dSWRs and vSWRs engage largely distinct subpopulations of multiple cell types in the NAc, and when these populations overlap, their modulation is opposite for dSWRs versus vSWRs.
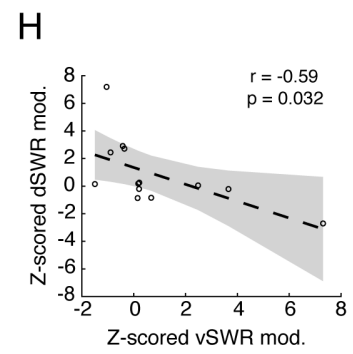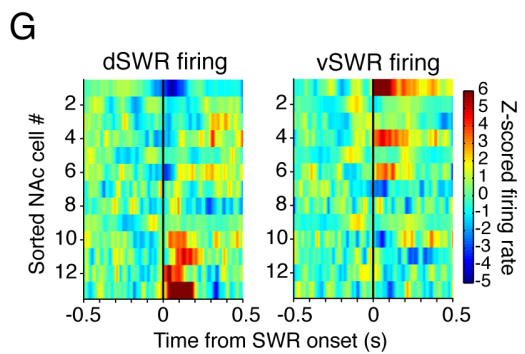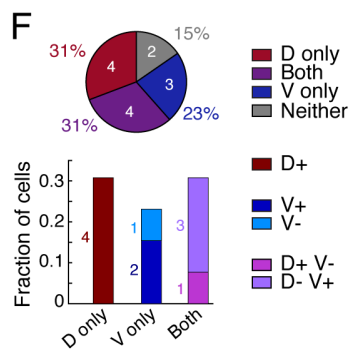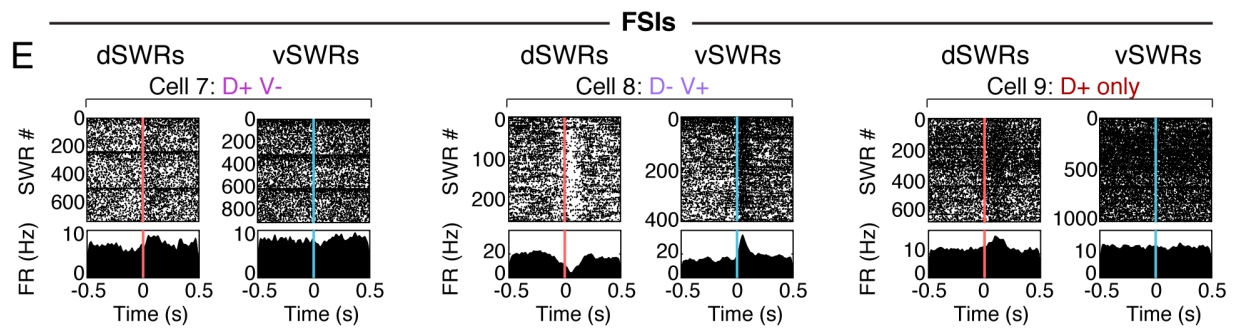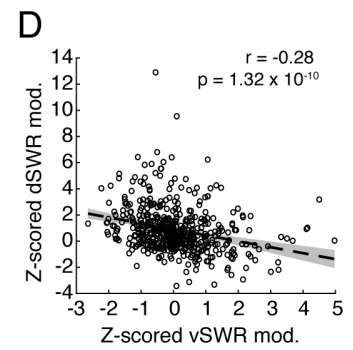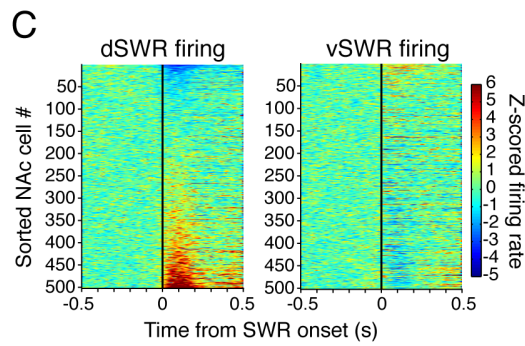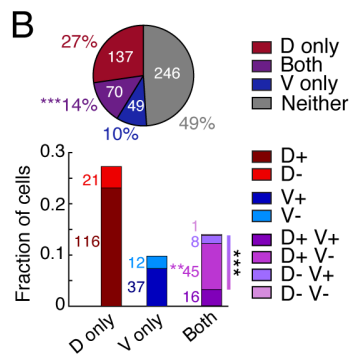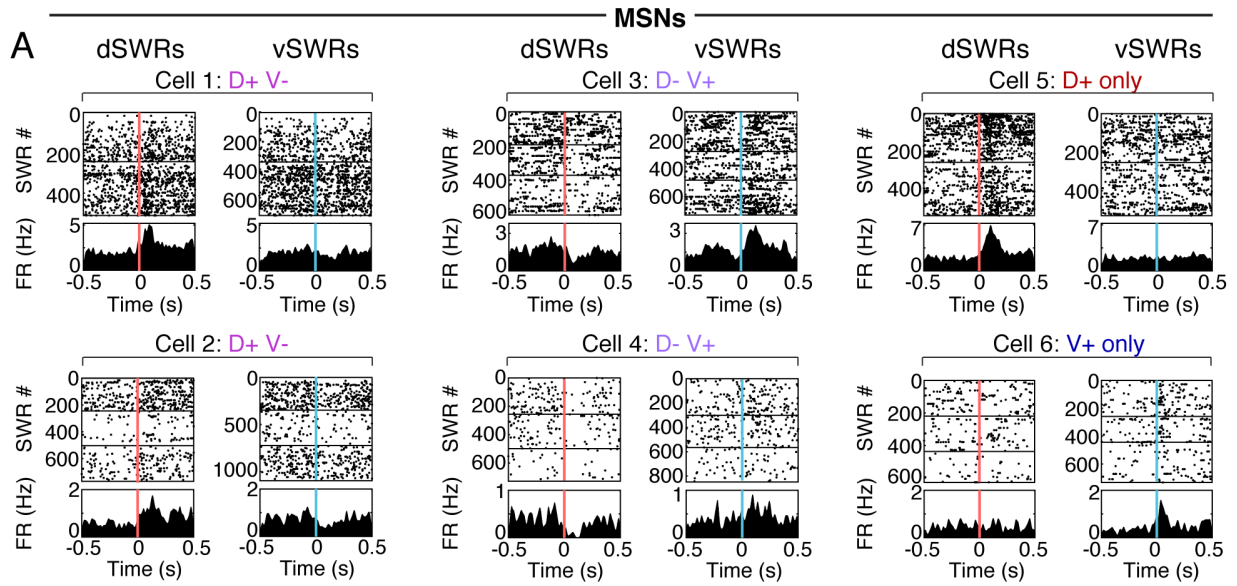
Figure 2.3 | Opposing patterns of NAc modulation during awake dH vs. vH SWRs.
(A) Examples of single NAc MSNs showing significant modulation during awake SWRs. Spike rasters and peri-event time histograms (PETHs) are aligned to the onset of dSWRs (left within each cell, pink line) or vSWRs (right within each cell, blue line). Horizontal lines separate task epochs in which each cell was isolated. Categories at the top of each cell indicate directions of significant modulation (positive or negative). All modulations in these examples are significant at p<0.01 (shuffle test). **(B)** Proportions of significantly SWR-modulated NAc MSNs. Top: fractions modulated during dSWRs only (D only), vSWRs only (V only), Both, or Neither dSWRs nor vSWRs, regardless of the direction of modulation. Cell counts are shown in white. Significantly more cells are modulated during Both than would be expected by chance overlap of dSWR- and vSWR-modulated cells (***p=5.44x10^{-4}, z-test for proportions). Bottom: directional modulation of MSNs. Cell counts are shown next to each bar. The fractions of D+V- cells alone and total "opposing" cells (gradient bar, D+V- and D-V+) are higher than would be expected by chance (**p=0.0017 and ***p=6.12x10^{-4}, respectively, z-tests for proportions). All fractions are out of 502 MSNs that fired at least 50 spikes around both dSWRs and vSWRs, from all 5 rats. **(C)** NAc MSN population shows opposing modulation during dSWRs vs. vSWRs. Left: dSWR-aligned z-scored PETHs for each MSN ordered by its modulation amplitude (mean z-scored firing rate in the 200 ms following SWR onset). Right: vSWR-aligned z-scored PETHs for the same ordered MSNs shown on the left. Z-scores are calculated within cell relative to the pre-SWR period (-500 to 0 ms). **(D)** Anti-correlation between dSWR and vSWR modulation amplitudes of MSNs. Each point represents a single cell. Dotted line and shaded regions represent a linear fit with 95% confidence intervals. Pearson's correlation coefficient (r) and p-value are shown in upper right. **(E)** Examples of single NAc FSIs showing significant modulation during SWRs. Format and modulation categories as in (A), top row. All modulations are significant at p<0.01 (shuffle test). **(F)** Proportions of significantly SWR-modulated FSIs after exclusion of potential duplicates from recording the same cell across days, which could bias this small population of cells (see Methods). Fractions are out of 13 FSIs from 5 rats. Similar to (B). **(G)** NAc FSI population shows opposing modulation during dSWRs vs. vSWRs. Similar to (C). **(H)** Anti-correlation between dSWR and vSWR modulation amplitudes of FSIs. Similar to (D). See also Figures S5 and S6.

Distinct task firing patterns in MSNs activated during dSWRs versus vSWRs

Given previous observations implicating the vH-NAc pathway in spatial-reward associations (Britt et al., 2012; Ciocchi et al., 2015; LeGates et al., 2018), we expected that V+ NAc neurons would show patterns of spiking consistent with encoding information about spatial locations and their relationship to reward. Here again this prediction was incorrect. Instead, we found that only D+ NAc neurons expressed reliable and robust representations related to spatial locations between reward sites.

To examine the dSWR- and vSWR-activated populations independently, we grouped together all cells that were D+ (only D+ or D+V-) and separately, all cells that were V+ (only V+ or D-V+), excluding the small number of D+V+ cells. We then examined the firing patterns of each population on the six rewarded trajectories across the two alternation sequences of the task (**Fig. 2.4 [A]**, top), as a function of both time and distance. To assess firing as a function of time, each trial was split into normalized

progression of time spent at the reward well starting the trajectory, from nosepoke to when the animal turns around ("well," excluding spikes during SWRs), and time spent during movement between wells, from turnaround to next nosepoke ("path") (**Fig. 2.4 [A]**, bottom). To assess spatial distance, each trajectory was converted to a one-dimensional distance from its start well to end well (linearized position), and only movement times were considered. In both approaches we applied several controls for behavioral variability (see Methods).

First, we found that D+ MSNs tended to fire very similarly across distinct trajectories. We quantified firing similarity as a mean coefficient of determination (r^2) across all trajectory pairs on which a given cell was active. D+ MSNs with high r^2 values were "tuned" to the same relative point of progression through each trajectory in both time and distance (examples in **Fig. 2.4 [B]**, left), regardless of actual spatial location or egocentric movement direction to the left or right (**Fig. S7 [A]**). This firing yielded a two-dimensional spatial rate map (**Fig. 2.4 [C]**, left) that resembles the path equivalence observed in dH place cells in geometrically repetitive environments (Frank et al., 2000; Singer et al., 2010), consistent with D+ cells receiving dH input. The preferred trajectory stage varied across D+ cells but was consistent across trajectories for a given cell, such that D+ population activity spanned the full extent of each trajectory. We also observed an abundance of D+ cells tuned to either the departure from reward wells (turnaround) or to the latter half of the path leading to the next reward well (**Fig. 2.4 [D]**), suggesting a preferential representation of trajectory initiation and final approach to reward. At the population level, D+ MSNs showed significantly higher firing similarity across trajectories compared to both the V+ MSNs and unmodulated (N) MSNs (**Fig. 2.4 [F-G], Fig. S7 [E-F]**).

By contrast, many V+ MSNs showed low rate, sparse firing patterns that were largely uncorrelated across distinct trajectories (**Fig. 2.4 [B-C]**, right). Only a small minority of V+ cells displayed some reliability across trajectories, and these were most often tuned to departures from reward wells (**Fig. 2.4 [E]**). Importantly, the sparse firing of V+ cells did not mirror the broad spatial representations seen in the vH, where a single cell can be active across a large fraction of an environment (Ciocchi et al., 2015; Keinath et al., 2014; Kjelstrup et al., 2008; Komorowski et al., 2013; Royer et al., 2010). We computed each cell's
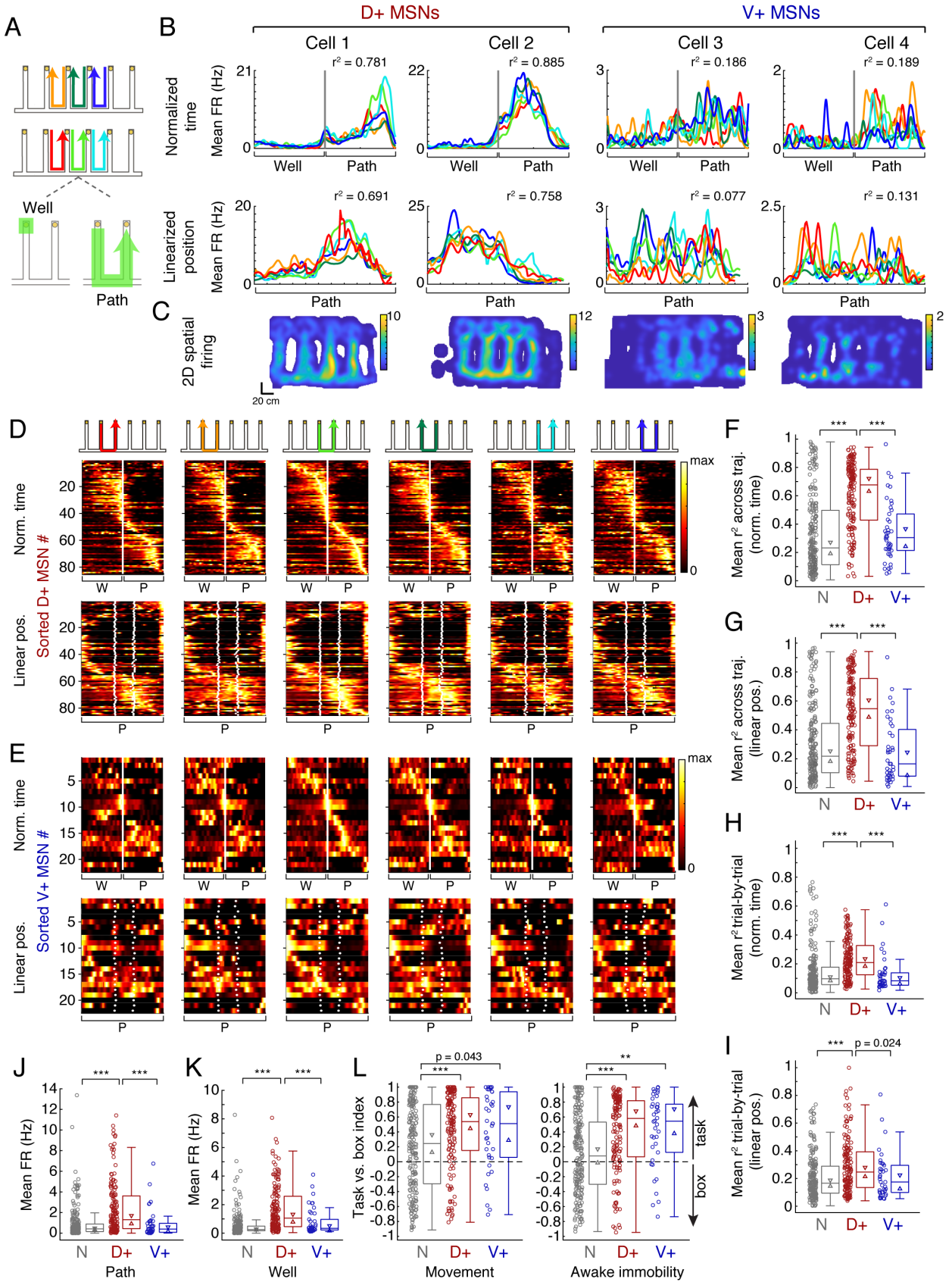
114

Figure 2.4 | Selective encoding of task-related information in the dH-NAc network.
(A) Schematic of the 6 rewarded trajectories across Sequence A and B, defined spatially by start and end reward well and directionally by left (top) or right (middle) movement between wells. Bottom: An example trajectory split into its well and path components, where well is the time from nosepoke to turnaround (departure) and path is the time from turnaround to next nosepoke. **(B)** Example NAc MSNs from the D+ and V+ populations showing high (D+, left) vs. low (V+, right) firing similarity (r^2) across trajectories. Trajectories are color coded according to the key in (A). Cell numbers do not correspond to Figure 2. Top row: trajectories are plotted as a function of normalized trial time. Grey vertical line marks 100% of the well period and beginning of the path period (turnaround), and the end of the path period starts a new well visit. Bottom row: trajectories are plotted as a function of linearized position during movement from each trajectory's start well to end well. Note that well times fall into the first and last position bins of the path since there is no position change at the well. X-axis for each plot covers 220 cm. Each cell's r^2 across all possible pairs of trajectories is shown in upper right. **(C)** Occupancy-normalized spatial firing for the example cells shown in (B), across the whole day. Color scale indicates maximum spatial firing rate in Hz. **(D)** Heterogeneity of trajectory stages represented by D+ MSNs across the six trajectories, shown in cartoons. Top row: normalized trial time; white line indicates turnaround time. Bottom row: linearized position; white dots indicate junctions of the maze between vertical and horizontal segments. Distance on the x-axis is normalized here. Firing rates are normalized to each cell's maximum as calculated by either method, and cells are sorted by the bin of their peak firing on the third trajectory (light green) in normalized trial time. Only cells which were active on enough trials of all six trajectories are shown here, such that these cells predominantly correspond to the Switch phase of the task (n=85 cells). W = well, P = path. **(E)** Heterogeneity and sparsity of firing of V+ MSNs, format as in (D) (n=22 cells sufficiently active across all 6 trajectories, predominantly in the Switch phase). **(F)** Mean r^2 across trajectories, in normalized trial time, by SWR-modulation category. Circles are individual cells, boxes show interquartile range, horizontal lines mark the median, triangles mark the 95% confidence interval of the median, whiskers mark non-outlier extremes. N (n=226 cells) vs. D+ (n=154 cells): ***p=5.45x10^{-19}; D+ vs. V+ (n=42 cells): ***p=6.33x10^{-9}. All tests between populations in F-L are Wilcoxon rank-sum tests with Bonferroni correction for multiple comparisons, setting significance level at p<0.017. **(G)** Mean r^2 across trajectories, in linearized position. N (n=220 cells) vs. D+ (n=152 cells): ***p=1.47x10^{-14}; D+ vs. V+ (n=40 cells): ***p=7.19x10^{-9}. Boxes as in (F). **(H)** Mean r^2 trial-by-trial, in normalized trial time. N (n=211 cells) vs. D+ (n=151 cells): ***p=2.35x10^{-12}; D+ vs. V+ (n=40 cells): ***p=5.09x10^{-7}. **(I)** Mean r^2 trial-by-trial, in linearized position. N (n=194 cells) vs. D+ (n=147 cells): ***4.70x10^{-5}; D+ vs. V+ (n=38 cells): p=0.024. **(J)** Mean firing rate on the path. N (n=226 cells) vs. D+ (n=154 cells): ***p=1.57x10^{-12}; D+ vs. V+ (n=42 cells): ***p=5.70x10^{-6}. **(K)** Mean firing rate during well periods outside of SWRs, same cells as in (J). N vs. D+: ***p=4.94x10^{-22}; D+ vs. V+: ***p=3.69x10^{-5}; V+ vs. N: p=0.024. **(L)** Comparison of firing rate during movement (left) or awake immobility (right) in the sleep box vs. on the task, expressed as an index where values >0 indicate higher firing rate on the task. Only task-active cells that were also active during the specified behavior in the sleep box are included. Movement: N (n=198 cells) vs. D+ (n=142 cells): ***p=9.43x10^{-4}; N vs. V+ (n=38 cells): p=0.043. Immobility: N (n=199 cells) vs. D+ (n=142 cells): ***p=2.43x10^{-6}; N vs. V+ (n=38 cells): **p=0.0011. See also Figure S7.

two-dimensional spatial coverage, normalizing for peak spatial firing rates, and found that V+ cells did not

cover a larger total proportion of the environment than the D+ cells or N cells (**Fig. 2.4 [C], Fig. S7 [B]**).

Instead, individual V+ cells showed diffuse spiking that could be preferential to the path or well (**Fig. S7**

[C]) or a specific direction (**Fig. S7 [A,D]**) on average. Critically, the timing and location of this firing

along the trajectory was typically unreliable across trials, and correlations in trial-to-trial firing were lower than those of the D+ population (**Fig. 2.4 [H-I]**). This variability resulted in patterns that were not tuned to a specific part of the trajectory, and indicates that the V+ population lacks consistent encoding of either spatial information or trial progression. Moreover, we found no evidence for consistent relationships between fluctuations in V+ firing and task-relevant variables such as accuracy of the upcoming trial, preference for a specific trajectory or maze segment, or performance of the currently or previously rewarded alternation sequence (data not shown).

Furthermore, the D+ population had much higher mean firing rates on both the path and well components suggesting greater task engagement overall (**Fig. 2.4 [J-K], Fig. S7 [G-H]**). Importantly, these higher firing rates could not account for the observed differences in firing similarity across trajectories (**Fig. S7 [I-J]**). Thus, in the context of our task, D+ cells (and D+V+ cells, **Fig. S7 [K]**) are much more active and express clear task-related firing properties that are not evident in cells that are V+ (and not D+). Interestingly, however, both D+ and V+ cells were more active on the task than during putative awake times in the sleep box, both during movement and during brief periods of immobility, as compared to N cells (**Fig. 2.4 [L]**). This suggests that despite an absence of specificity for trajectory features, V+ cells represent a population distinct from NAc cells that are not SWR-modulated.

dSWR-activated MSNs uniquely encode reward history

We next investigated whether D+ or V+ cells would preferentially signal reward-related information in the Multiple-W task, which involves reward associations with specific spatial paths. In particular, we aimed to test the longstanding hypothesis that vH would most strongly engage valence-related representations downstream (Ciocchi et al., 2015; Fanselow and Dong, 2010; Jimenez et al., 2018; Riaz et al., 2017; Royer et al., 2010; Strange et al., 2014), including reward information in the NAc.

Contrary to this hypothesis, we observed a strong and differential effect of reward history only on D+ MSNs. We computed a reward history preference index for each MSN from the difference in its mean firing rate curve on paths following a rewarded well visit versus an error visit, controlling for movement

speed. We found that the D+ population fired more on paths following reward than following an error (examples in **Fig. 2.5 [A]**), demonstrating a clear reward history preference that was not seen in the V+ or N populations (**Fig. 2.5 [A-B], Fig. S7 [L-N]**). This preference persisted when we additionally controlled for upcoming choice and reward expectation, by examining only trials going from the outer wells to the center well of each W sequence, as returns to the center well are always rewarded (**Fig. S7 [O]**). Specifically, ~21% of D+ cells exhibited a significant firing rate increase on paths following reward compared to error (permutation test). While many of these cells were tuned to the turnaround from the well (as in Cell 1, **Fig. 2.5 [A]**), this D+ subpopulation covered the full extent of a given path (**Fig. S7 [P]**). This pattern implies that the reward history signal persists until the next path is complete.

At the same time, we were surprised to find an overall lack of enhanced firing during receipt of reward at the reward sites, given previous work suggesting reward-site-specificity for NAc neurons activated during dSWRs in sleep (Lansink et al., 2008; Lansink et al., 2009). While we found individual examples of MSNs that had higher firing rates during rewarded as opposed to unrewarded times at the wells in both the D+ and V+ populations, we also found cells that showed higher firing during errors (**Fig. 2.5 [C,E]**). Importantly, neither the D+ nor V+ populations were enriched for cells showing reward-specific firing at the wells (**Fig. 2.5 [D,F]**). When examined in unnormalized time, the D+ neurons tended to fire more when reward was not delivered on error trials (**Fig. 2.5 [F]**), likely because of their activity preceding turns away from the reward wells. These findings suggest that D+ neurons multiplex a signal of past reward outcome with their encoding of trajectory features rather than encoding reward receipt *per se*. Moreover, reward representation is largely absent in the V+ population, contrary to our initial hypothesis.

D+ and V+ MSNs comprise distinct neuronal networks

If the D+ and V+ physiological subtypes reflect distinct populations that are part of distinct anatomical networks, we would expect them to show coordinated spiking activity within each population but not across populations. We therefore examined patterns of co-firing outside of SWRs. During movement on the task, pairs of D+ MSNs showed a stronger tendency to be coactive than D+/V+ pairs, as
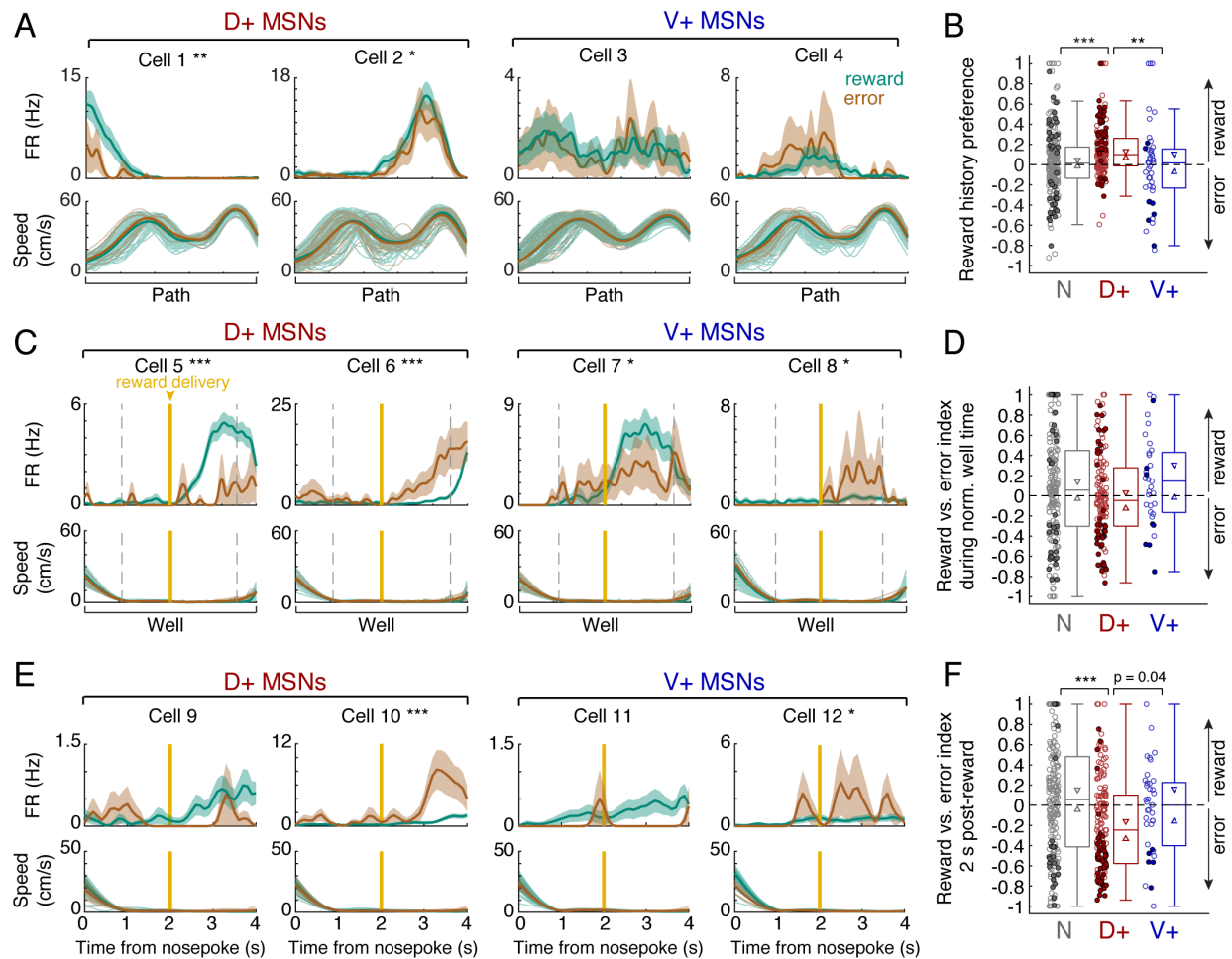
Figure 2.5 | Selective encoding of past reward outcome on the path in the dH-NAc network.
(A) Example path firing patterns of D+ and V+ NAc MSNs as a function of reward history, defined as whether or not the well visit starting the trajectory was rewarded. Top: firing rate of each cell (mean ± s.e.m. across trials) on all paths following a reward (teal) vs. all paths following an error (brown). Cell numbers do not correspond to previous figures. Reward history preference: Cell 1: 0.52, Cell 2: 0.15, Cell 3: 0.018 (p=0.81), Cell 4: -0.26 (p=0.053). *p<0.05, **p<0.01 (permutation test). Bottom: faded lines indicate speed profiles of individual paths following reward and error, thick lines indicate mean speeds.
(B) Distributions of reward history preference by SWR-modulation category. Filled circles indicate significantly reward-preferring (>0) or error-preferring (<0) cells, open circles indicate non-significant cells. The D+ population (n=159 cells) is significantly shifted toward positive values (p=6.00x10^{-11}, one-tailed signed-rank test). N (n=235 cells) vs. D+: ***p=1.29x10^{-4}; D+ vs. V+ (n=45 cells): **p=0.003 (Wilcoxon rank-sum tests). **(C)** Examples of individual D+ and V+ MSNs showing higher firing rate for rewarded well visits (left of each category) or for error visits (right of each category), as a function of normalized well time. Gold vertical line marks reward delivery or time of expected reward delivery on error trials. Top: firing rate (mean ± s.e.m. across trials). Reward vs. error index: Cell 5: 0.65, Cell 6: -0.69, Cell 7: 0.21, Cell 8: -0.48. *p<0.05, ***p<0.001 (permutation test). Bottom: speed, format as in (A). Dotted grey lines flank the time period analyzed for significance, when both rewarded and error mean speeds are <2 cm/s. **(D)** Distributions of reward vs. error index during normalized well time, by SWR-modulation category. Filled circles indicate significantly reward-preferring (>0) or error-preferring (<0) cells, open circles indicate non-significant cells (N n=188 cells, D+ n=131 cells, V+ n=33 cells). **(E)** Examples of

individual D+ and V+ MSNs showing higher firing rate for rewarded well visits (left of each category) or for error visits (right of each category), as a function of time since nosepoke. Format as in (C). Reward vs. error index: Cell 9: 0.60 (p=0.093), Cell 10: -0.69, Cell 11: 0.77 (p=0.22), Cell 12: -0.48. *p<0.05, ***p<0.001 (permutation test in the 2-4 s window). **(F)** Distributions of reward vs. error index during 2 s following reward delivery time, by SWR-modulation category (N n=196 cells, D+ n=147 cells, V+ n=37 cells). The D+ population is significantly shifted negative of zero by this metric (p=9.05×10^{-7}, one-tailed signed-rank test) and shows significantly less post-reward preference than the N population (***p=1.85×10^{-5}, Wilcoxon rank-sum test). See also Figure S7.

measured by the magnitude of their cross-correlation at zero-lag (**Fig. 2.6 [A,C]**). No such difference was seen for V+ MSN pairs as compared to D+/V+ pairs (**Fig. 2.6 [B-C]**), perhaps because of the overall low levels of activity of V+ neurons in our task (**Fig. 2.4 [J-K]**) and because we had so few co-recorded V+ cells (10 pairs). These findings suggest that the D+ MSN population constitutes a specific network distinct from the V+ MSN population.

The co-firing of D+ MSNs during movement also predicted their coactivity during SWRs, similar to SWR reactivation of hippocampal place cells (Karlsson and Frank, 2009; O'Neill et al., 2006; O'Neill et al., 2008; Wilson and McNaughton, 1994) and reactivation across the hippocampus and prefrontal cortex (Jadhav et al., 2016; Tang et al., 2017). We quantified SWR coactivity of cell pairs using a coactivity z-score (Cheng and Frank, 2008; Singer and Frank, 2009), which measures how likely two cells are to spike together normalized by how often each one spikes independently during SWRs. The cross-correlation strength of spiking during movement was positively correlated with SWR coactivity z-score, for both pairs of D+ MSNs and for pairs of D+ MSNs and dH pyramidal cells (**Fig. S5 [B]**; **Fig. 2.6 [D]**, left and center). This SWR coactivity is consistent with coordinated reactivation across brain regions during dSWRs. We had too few V+ pairs and too few single units in vH to observe inter-regional reactivation. Nevertheless, all but one V+/V+ pair showed a positive coactivity z-score during vSWRs (**Fig. 2.6 [D]**, right), suggesting the presence of co-reactivation of V+ MSNs.
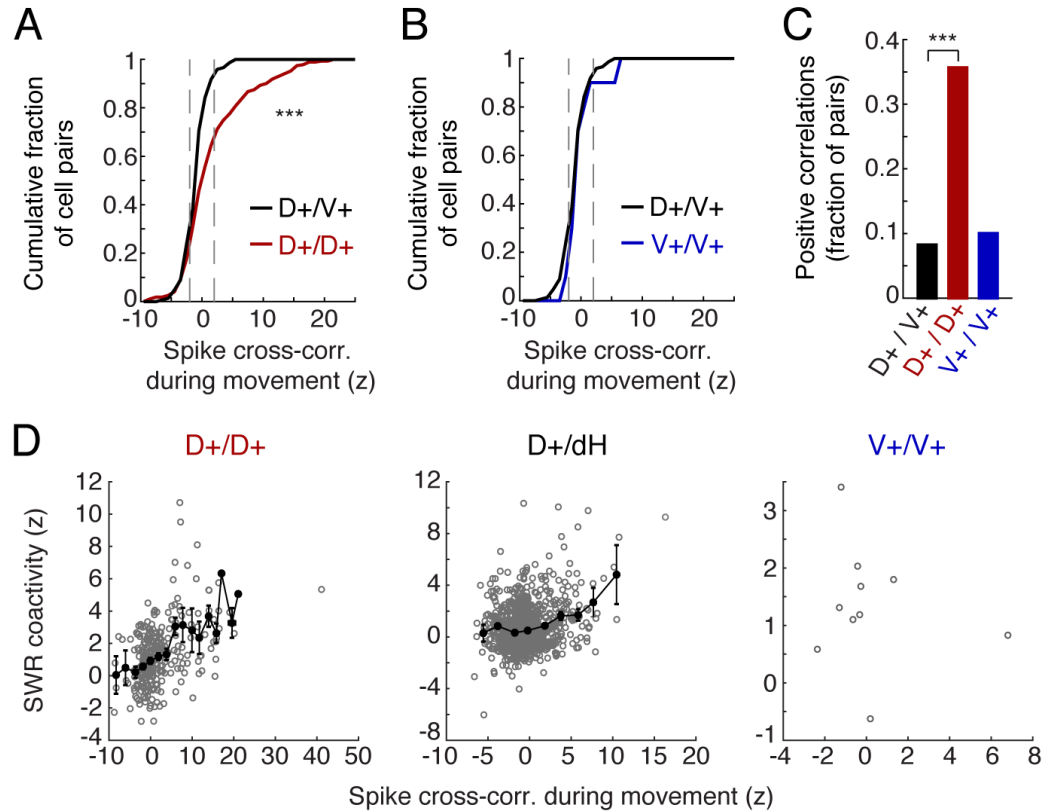
Figure 2.6 | Coordinated spiking in the dH-NAc network.
(A) Cumulative distributions of z-scored spike cross-correlations during movement (mean at zero lag ±10 ms) between pairs of MSNs. Left: pairs of D+ MSNs (D+/D+) vs. pairs of D+ and V+ MSNs (D+/V+). The D+/D+ distribution is significantly shifted to the right of the D+/V+ distribution (***p=1.00x10^{-6}, Wilcoxon rank-sum test; n=272 D+/D+ pairs, 146 D+/V+ pairs). **(B)** Cumulative distributions of z-scored spike cross-correlations during movement between pairs of V+ MSNs (V+/V+) vs. D+/V+ pairs. The V+/V+ distribution is not significantly different from the D+/V+ distribution (Wilcoxon rank-sum test; n=10 V+/V+ pairs). The D+/V+ distribution is repeated from (A). In (A) and (B), only z-scores up to 25 are shown for clarity. **(C)** Fraction of cell pairs exhibiting positive spike cross-correlations (≥2 z-scores, mean at zero lag ±10 ms) during movement. D+/D+ vs. D+/V+: ***p=1.11x10^{-9}; D+/D+ vs. V+/V+: p=0.094 (z-tests for proportions). **(D)** Spike coactivity during movement (cross-correlation z-score at zero-lag) vs. coactivity z-score during SWRs. Left: D+/D+ MSN pairs (same as in **A**), with SWR coactivity calculated during dSWRs (Spearman's rho=0.415, p=1.30x10^{-12}). Center: Pairs of D+ MSNs and dH (dCA1) pyramidal cells, with SWR coactivity calculated during dSWRs (n=990 pairs, rho=0.118, p=2.22x10^{-4}). Black points are binned averages (2 z-score bins on the x-axis). Right: V+/V+ MSNs (same as in **B**), with SWR coactivity calculated during vSWRs (rho= -0.103, p=0.785).

Patterns of SWR-modulation and network activity are maintained during sleep

Finally, we asked whether D+ and V+ neurons constitute separate networks across both waking task performance and sleep. During sleep, we observed greater synchrony between dSWRs and vSWRs than during wake (example in **Fig. 2.7 [A]**). While synchronous SWRs occurred more often than expected from a shuffle of SWR times, they still comprised a small minority of events, with only ~6.7% of dSWRs occurring within 50 ms of a vSWR (**Fig. 2.7 [B,D]**). This degree of synchrony was substantially smaller than the synchrony observed within dH or within vH (**Fig. 2.7 [C]**).

Because many SWRs remained isolated within the hippocampal subdivisions, we excluded all pairs of dSWRs and vSWRs that occurred within 250 ms of each other to examine the modulation of NAc neurons. In the remaining, temporally isolated SWRs in sleep, we found that 30% of MSNs were significantly modulated during either dSWRs, vSWRs, or both, and that this modulation was predominantly positive. Notably, although the proportion of single MSNs showing opposing modulation during dSWRs versus vSWRs (1.6%) was smaller than in wake, it was again greater than chance (**Fig. 2.7 [E]**). Furthermore, the population-level opposition and anti-correlation of MSN activity during dSWRs versus vSWRs remained apparent (**Fig. 2.7 [F-G]**). A majority of FSIs (~62%) were again modulated during either dSWRs or vSWRs (**Fig. 2.7 [H]**). While this anti-correlation was no longer significant for FSIs (**Fig. 2.7 [I-J]**), the absence of a relationship between dSWR and vSWR modulation suggests that dSWR- and vSWR-engaged FSIs are largely separate populations in sleep.

We hypothesized that if SWR modulation reflects network-level connectivity between dH, vH, and NAc subpopulations, then on average, individual NAc neurons should respond similarly during SWRs in wake and sleep. This was indeed the case; for both dSWRs and vSWRs, the amplitude and direction of NAc MSN modulation in wake and sleep was positively correlated, across the full population of cells active in both states (**Fig. 2.7 [K]**). Moreover, D+ MSNs demonstrated preserved co-firing outside of SWRs in sleep, with significantly more positively correlated pairs as compared to D+/V+ pairs (**Fig. 2.7 [L-M]**). Together, these findings suggest that D+ and V+ neurons comprise largely distinct NAc networks, coordinated in opposition during SWRs from dH and vH across behavioral states.

A

dCA1
Raw
Ripple

1 mV
100 μV

vCA1
Raw
Ripple

1 mV
100 μV

Speed (cm/s)

B

Normalized cross-corr.

Z-scored cross-corr. (relative to shuffle)

Time of vSWRs relative to dSWRs (s)

C

within dCA1

within vCA1

Normalized cross-corr.

Time

D

Z-scored cross-corr.

Rat 1   Rat 2   Rat 3   Rat 4   Rat 5

Time of vSWRs relative to dSWRs (s)

E

18%
***3%
9%
70%

219
43
114
865

D only
Both
V only
Neither

Fraction of cells

D+
D−
V+
V−
D+ V+
D+ V−
D− V+
D− V−

28
191
15
99
*17
3
3
20

D only   V only   Both

F

MSNs during sleep

dSWR firing   vSWR firing

Sorted NAc cell #

Time from SWR onset (s)

Z-scored firing rate

G

r = −0.20
p = 3.51x10⁻¹²

Z-scored dSWR mod.

Z-scored vSWR mod.

H

31%
23%
8%
38%

4
3
1
5

D only
Both
V only
Neither

Fraction of cells

D+
D−
V+
D+ V+
D− V+

4
1
2
1
1

D only   V only   Both

I

FSIs during sleep

dSWR firing   vSWR firing

Sorted NAc cell #

Time from SWR onset (s)

Z-scored firing rate

J

r = −0.14
p = 0.64

Z-scored dSWR mod.

Z-scored vSWR mod.

K

r = 0.44
p = 1.77x10⁻¹⁸

Sleep Z-scored dSWR mod.

Z-scored dSWR mod. Awake

r = 0.31
p = 9.12x10⁻¹⁰

Sleep Z-scored vSWR mod.

Z-scored vSWR mod. Awake

L

Cumulative fraction of cell pairs

D+/V+
D+/D+

***

D+/V+
V+/V+

Spike cross-corr. outside SWRs (z)

M

*

Positive correlations (fraction of pairs)
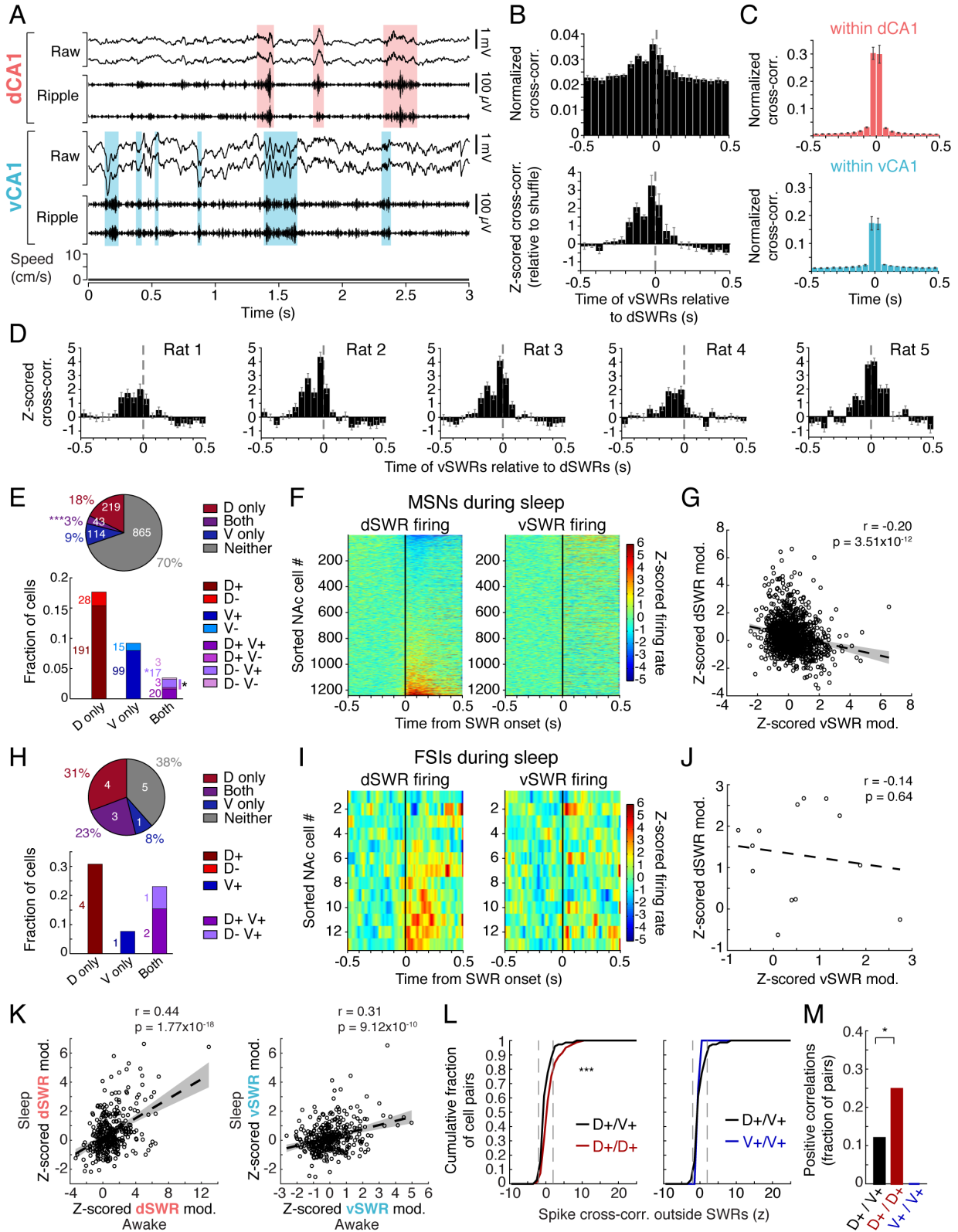
D+ / V+
D+ / D+
V+ / V+

123

Figure 2.7 | Hippocampal-NAc network patterns are maintained during sleep, despite increased synchrony between dSWRs and vSWRs.
(A) Example of dCA1 and vCA1 SWRs during sleep from the same tetrodes and same rat as Figure 1D (Rat 4). Shaded regions highlight detected dSWRs (pink) and vSWRs (blue). **(B)** Mean cross-correlation histogram (CCH) for sleep vSWRs vs. dSWRs across animals. Top: normalized by the number of dSWRs. Bottom: CCH z-scored relative to shuffled vSWR onset times. Error bars indicate s.e.m. (n=5 rats). **(C)** Mean CCH for sleep SWRs between tetrodes within dCA1 (top, n=5 rats) or vCA1 (bottom, n=3 rats with >1 tetrode in vCA1), normalized by the number of SWRs on one tetrode. Error bars indicate s.e.m. across included animals. **(D)** Z-scored CCH (relative to shuffle) of sleep vSWRs vs. dSWRs in each animal. Error bars indicate s.e.m. across days (n=15-19 days) for each animal. Note the tendency of vSWRs to lead dSWRs in 4 of the 5 rats. **(E)** Proportions of NAc MSNs showing significant modulation during asynchronous dSWRs and vSWRs in sleep, similar to Figure 3B. Top: fractions of modulated MSNs regardless of the direction of modulation. Cell counts are shown in white. Significantly more cells are modulated during Both than would be expected by chance overlap of dSWR- and vSWR-modulated cells (***p=1.50×10^{-4}, z-test for proportions). Bottom: directional modulation of NAc MSNs. Cell counts are shown next to each bar. The fraction of D-V+ cells alone and total "opposing" cells (gradient bar, D+V- and D-V+) are higher than would be expected by chance (*p=0.012 and *p=0.037, respectively, z-tests for proportions). All fractions are out of 1241 MSNs that fired at least 50 spikes around both dSWRs and vSWRs in sleep, from all 5 rats. **(F)** NAc MSN population activity shows opposing modulation during asynchronous dSWRs and vSWRs in sleep, similar to Figure 3C. Left: dSWR-aligned z-scored PETHs for each MSN ordered by its modulation amplitude. Right: vSWR-aligned z-scored PETHs for the same ordered MSNs shown on the left. **(G)** Anti-correlation between dSWR and vSWR modulation amplitudes of MSNs, similar to Figure 3D. Each point represents a single cell. Dotted line and shaded regions represent a linear fit with 95% confidence intervals. Pearson's correlation coefficient (r) and p-value are shown in upper right. **(H)** Similar to (E), but for fractions of FSIs showing significant modulation during asynchronous SWRs in sleep, after removal of potential duplicate cells. Fractions are out of 13 FSIs. **(I)** Similar to (F) but for FSI population in sleep. **(J)** Similar to (G) but for FSI population in sleep. **(K)** SWR-modulation direction and amplitude of individual NAc MSNs is significantly correlated between SWRs during awake immobility on the task and during sleep, for both dSWRs (left) and vSWRs (right). Each point represents a single cell, and only cells active in both wake and sleep are included (n=368 cells). Dotted line and shaded regions represent a linear fit with 95% confidence intervals. Pearson's correlation coefficient (r) and p-value are shown in upper right. **(L)** Cumulative distributions of z-scored spike cross-correlations during sleep outside SWRs (mean at zero lag ±10 ms), between pairs of MSNs defined by D+ and V+ categories in wake. Left: pairs of D+ MSNs (D+/D+) vs. pairs of D+ and V+ MSNs (D+/V+). Right: pairs of V+ MSNs (V+/V+) vs. D+/V+ pairs. The D+/D+ distribution is significantly shifted to the right of the D+/V+ distribution (***p=5.73×10^{-5}, Wilcoxon rank-sum test), similar to wake. D+/V+ distributions are repeated from left to right for clarity. Only cells that were active in both wake and sleep are included (n=161 D+/D+ pairs, 75 D+/V+ pairs, 3 V+/V+ pairs). **(M)** Fraction of cell pairs exhibiting positive spike cross-correlations (≥2 z-scores, mean at zero lag ±10 ms) in sleep outside SWRs. D+/D+ vs. D+/V+: *p=0.024; D+/D+ vs. V+/V+: p=0.32 (z-tests for proportions).

2.4 Discussion

Our findings demonstrate that dorsal and ventral hippocampal SWRs (dSWRs and vSWRs) occur asynchronously during waking and activate distinct subpopulations in the NAc. Contrary to our initial hypotheses, vSWRs are not modulated by novelty and reward, and V+ (vSWR-activated) MSNs show no evident or reliable tuning to spatial locations, progression through a trial, or reward history. By contrast, dSWRs are both novelty and reward modulated, and D+ (dSWR-activated) MSNs show strong encoding of information related to both the spatial progression through a trial and past reward.

Our results also indicate that D+ and V+ neurons, including both MSNs and FSIs, constitute distinct and largely opposing networks. D+ cells are typically unmodulated or suppressed during vSWRs and V+ cells are typically unmodulated or suppressed during dSWRs. Further, the D+ network exhibits strong coordinated spiking activity both during movement and during SWR reactivation with dorsal hippocampal pyramidal cells, while D+ and V+ MSN pairs showed no such coordination. These findings establish that SWR-related communication in the dH-NAc and vH-NAc pathways occurs at separate moments in time and engages distinct NAc circuits, with only the dH-activated NAc neurons showing clear encoding of variables related to spatial task performance and reward.

An absence of spatial and reward representations in the vH-NAc network

We found no indication that the V+ NAc population encodes task-relevant variables related to spatial paths or reward. This was surprising given that the vH has long been viewed as the hippocampal subdivision dedicated to the emotional and valence components of episodic memory (Fanselow and Dong, 2010; Moser and Moser, 1998; Strange et al., 2014), and the NAc is often associated with reward and task-predictors of reward (Carelli, 2002; Humphries and Prescott, 2010; Pennartz et al., 1994). As some NAc-projecting vH neurons show modulation at reward sites (Ciocchi et al., 2015), we expected that vH-associated NAc neurons would show similar patterns, yet this was not the case. Moreover, inactivation studies of the vH-NAc circuit have yielded deficits in spatial reward-seeking behavior and memory (Britt et al., 2012; Floresco et al., 1997; Ito et al., 2008; LeGates et al., 2018; Riaz et al., 2017). By contrast, in

the Multiple-W task, V+ NAc neurons were much less active than D+ neurons and lacked the task-relevant representations seen in D+ neurons of path progression and reward history. Our findings are, however, consistent with a recent report that vH is overall suppressed during goal-directed behavior which requires work to obtain reward (Yoshida et al., 2019). The observed low activity levels of V+ MSNs therefore suggest that these neurons receive minimal excitation from vH during our goal-directed task.

What could explain the discrepancy between these physiological findings and results of previous manipulation studies? First, we found that the vH-NAc and dH-NAc pathways can act in opposition, which implies that stimulating or inactivating one pathway will likely influence activity in the other. This interaction makes it difficult to assign a unique function to a given pathway. Second, it has been demonstrated that activation of multiple glutamatergic inputs to the NAc can be positively reinforcing (Britt et al., 2012), such that optogenetic activations of the vH-NAc pathway do not necessarily drive behavior specific to a spatial association. Additionally, in one of the aforementioned studies, the vH-NAc pathway was optogenetically inhibited during learning with a social reward rather than a food reward (LeGates et al., 2018), raising the possibility that different reward types could differentially recruit vH-NAc sub-circuits.

We note, however, that our findings do not preclude the involvement of the vH-NAc network in other tasks, such as those that rely on discrimination between environments defined by proximal contextual cues such as odors and textures (Komorowski et al., 2013; Riaz et al., 2017). A growing body of work examining vH and its projections also suggests a specialization for aversive experiences and anxiety (Adhikari et al., 2011; Bannerman et al., 2004; Ciocchi et al., 2015; Jimenez et al., 2018; Keinath et al., 2014; Kheirbek et al., 2013; Kjelstrup et al., 2002; Padilla-Coreano et al., 2016; Parfitt et al., 2017). This raises the possibility that the vH-NAc network could be specialized for variables perhaps present but not immediately relevant to our task, such as associations between overall context and emotional state. Furthermore, as the NAc is remarkably heterogeneous (Carelli, 2002; Castro and Bruchas, 2019; Pennartz et al., 1994), the vH may engage other representation types in subregions of the NAc not sampled here.

Spatial-reward memory in the dH-NAc network

The spatial path and reward history representations of D+ NAc neurons are consistent with prior studies suggesting that dH-NAc communication links spatial locations and paths to reward (Berke et al., 2004; Lansink et al., 2009; Lansink et al., 2016; Sjulson et al., 2018; Tabuchi et al., 2000; van der Meer and Redish, 2011). Recent work demonstrated that direct dH input to the NAc is indeed necessary for spatial-reward memory in a conditioned place preference paradigm, and that during memory retrieval the dH recruits NAc ensembles (Trouche et al., 2019). Our findings complement these results in several important ways.

First, we demonstrated that coordinated reactivation between dH pyramidal cells and NAc cells is present during awake dSWRs and recruits a specific NAc network. This reactivation may contribute to the active storage of associations during the experience as well as to the retrieval of associations for decision-making processes (Joo and Frank, 2018). We also found that NAc MSNs can be inhibited during SWRs. This inhibition is likely mediated by lateral connections with other MSNs or by local FSIs, consistent with our observation that FSIs are likewise SWR-modulated. As individual FSIs innervate large populations of MSNs (Tepper et al., 2018), FSIs may play an important role in coordinating NAc responses to hippocampal inputs (Trouche et al., 2019), including during SWRs.

Second, we found that individual D+ neurons are active at "path equivalent" (Frank et al., 2000; Singer et al., 2010) locations on multiple trajectories, and can thus be understood as encoding progression along spatial paths between reward sites. We propose that the task elements represented by our D+ MSNs correspond to repeated goal-directed actions of the animal that occur in specific locations on each spatial path. For instance, the turnaround from the reward well initiates the next approach to reward and thus is the first in a set of goal-directed actions. As the animal learns to repeat these actions at specific locations and with specific timing on each spatial path, they become generalized across the task. Such patterns that generalize across task elements rooted in space have been reported in dorsal and ventral striatum (Berke et al., 2009; Lansink et al., 2012; Lavoie and Mizumori, 1994; Mulder et al., 2004; van der Meer et al., 2010), but they have not been previously linked to dSWR activation. Moreover, these D+ MSN firing patterns

mirror those seen in the subset of medial prefrontal cortical neurons activated during dSWRs (Yu et al., 2018), suggesting that dSWRs may broadly engage generalized task-related representations across the brain. Our findings are thus consistent with a role for dSWRs in binding discrete spatial sequences to goal-directed action sequences.

Furthermore, we found that NAc representations activated during awake dSWRs are not restricted to reward sites or reward approach. Based on previous work (Lansink et al., 2008; Lansink et al., 2009), we expected that NAc cells encoding receipt of reward or the reward location itself would preferentially activate during awake dSWRs. Instead, we found that D+ neurons do not reliably encode the delivery, consumption, or location of reward, but are modulated by past receipt of reward. Importantly, our task included a 2-second delay between the animal's arrival at a reward site and reward delivery, and we specifically measured reward modulation relative to time- and velocity-matched error trials, allowing us to separate location and reward-delivery signals. In addition, we note that as dSWRs are modulated by reward themselves and activate NAc neurons, some fraction of reward-specific spikes previously reported likely occurred during awake dSWRs (or vSWRs).

Interestingly, the anatomical distribution of D+ MSNs and FSIs largely in the NAc core is consistent with recent work showing that dopamine release corresponding to reward rate and motivation is localized to this region (Mohebi et al., 2019). This dopamine release is a potential mechanism of the reward history signal we observed in D+ MSNs. Moreover, as dopamine has been shown to regulate the excitability of NAc neurons to external inputs (Goto and Grace, 2005), dopamine release in the core may facilitate the binding of dorsal hippocampal spatial signals to NAc representations.

Storage and retrieval of different aspects of experience

We propose that the opposition between the dH-NAc and vH-NAc networks during SWRs is well suited to support the processing of different aspects of experience at different times. During a given experience, all of its many aspects (location, events, emotional state, etc.) could be stored simultaneously to create a complete episodic memory. Alternatively, each aspect could be stored either at different

moments in time or in distinct neural circuits to facilitate the flexible retrieval of each piece of information in the future. Given the evidence for functional divergence across dH and vH, we speculate that dSWRs and vSWRs send information about largely distinct features of experience to downstream structures. The temporal asynchrony of dSWRs and vSWRs could thus be a mechanism to keep those features separate as they are stored and/or retrieved during pauses in behavior, as only some of that information may be relevant to the task at hand. This temporal separation of hippocampal output may be mirrored during movement. Theta oscillations (~5-11 Hz) travel as a wave across the dorsoventral axis of the hippocampus, such that at the dorsal and ventral poles, they are 180 degrees out of phase with each other (Patel et al., 2012). Our results suggest that these out of phase outputs would drive activity in distinct sets of NAc MSNs and FSIs. More broadly, the opposing recruitment we see during SWRs could facilitate the compartmentalization of episodic memory components. Conversely, during sleep, the greater synchrony of dSWRs and vSWRs may reflect the consolidation of a more complete memory.
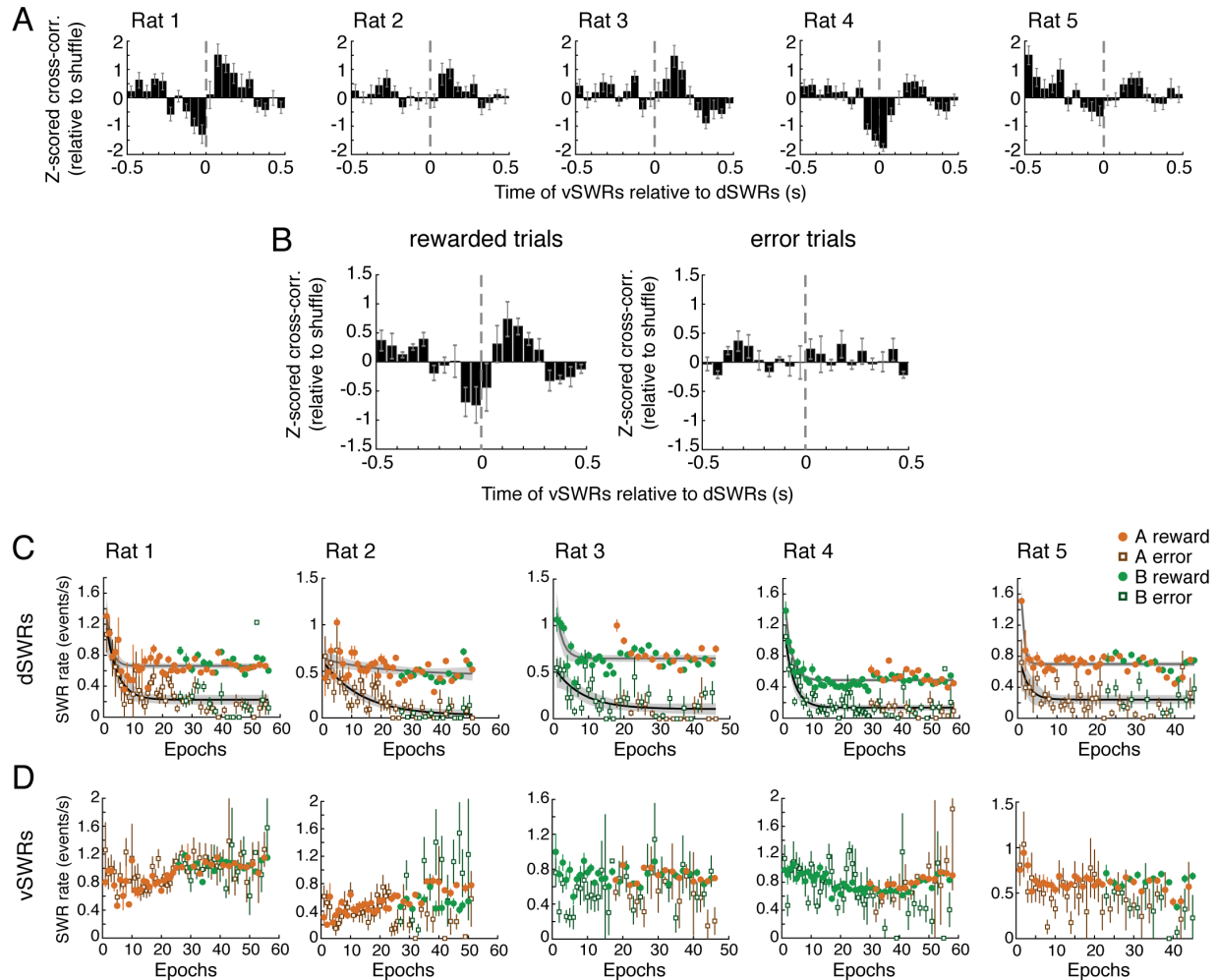
2.5 Supplemental figures
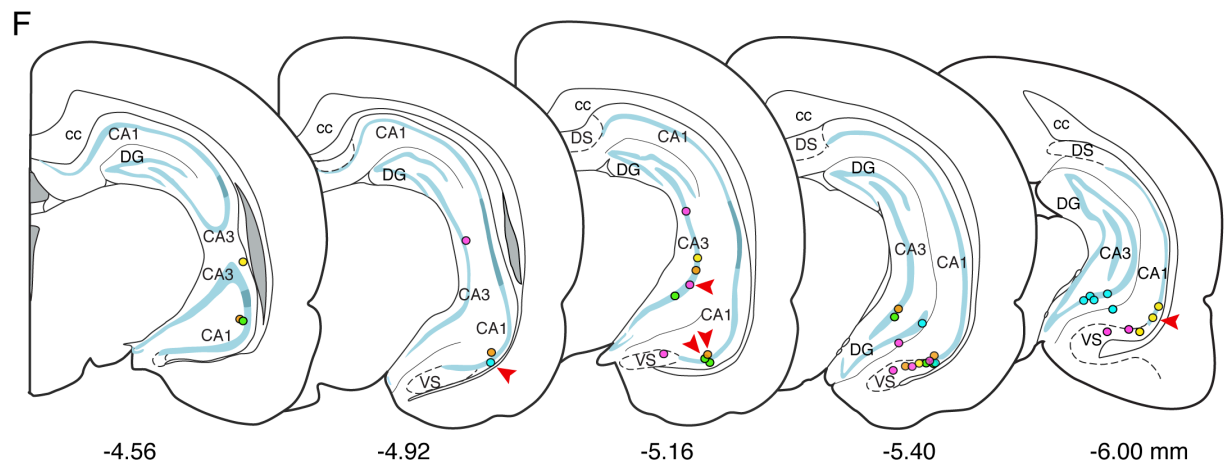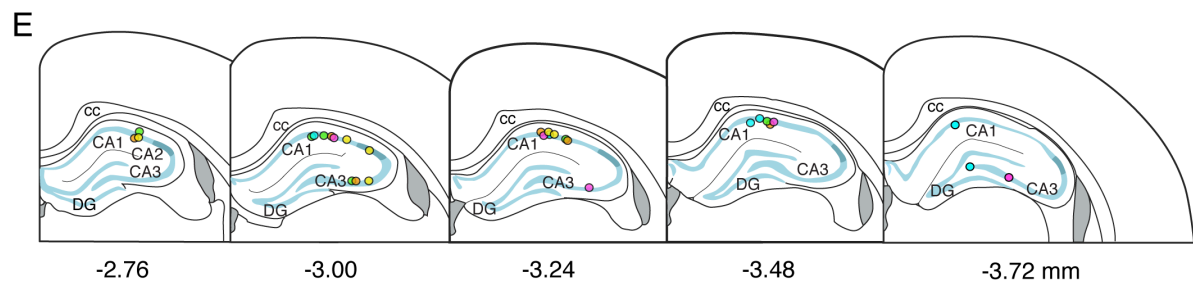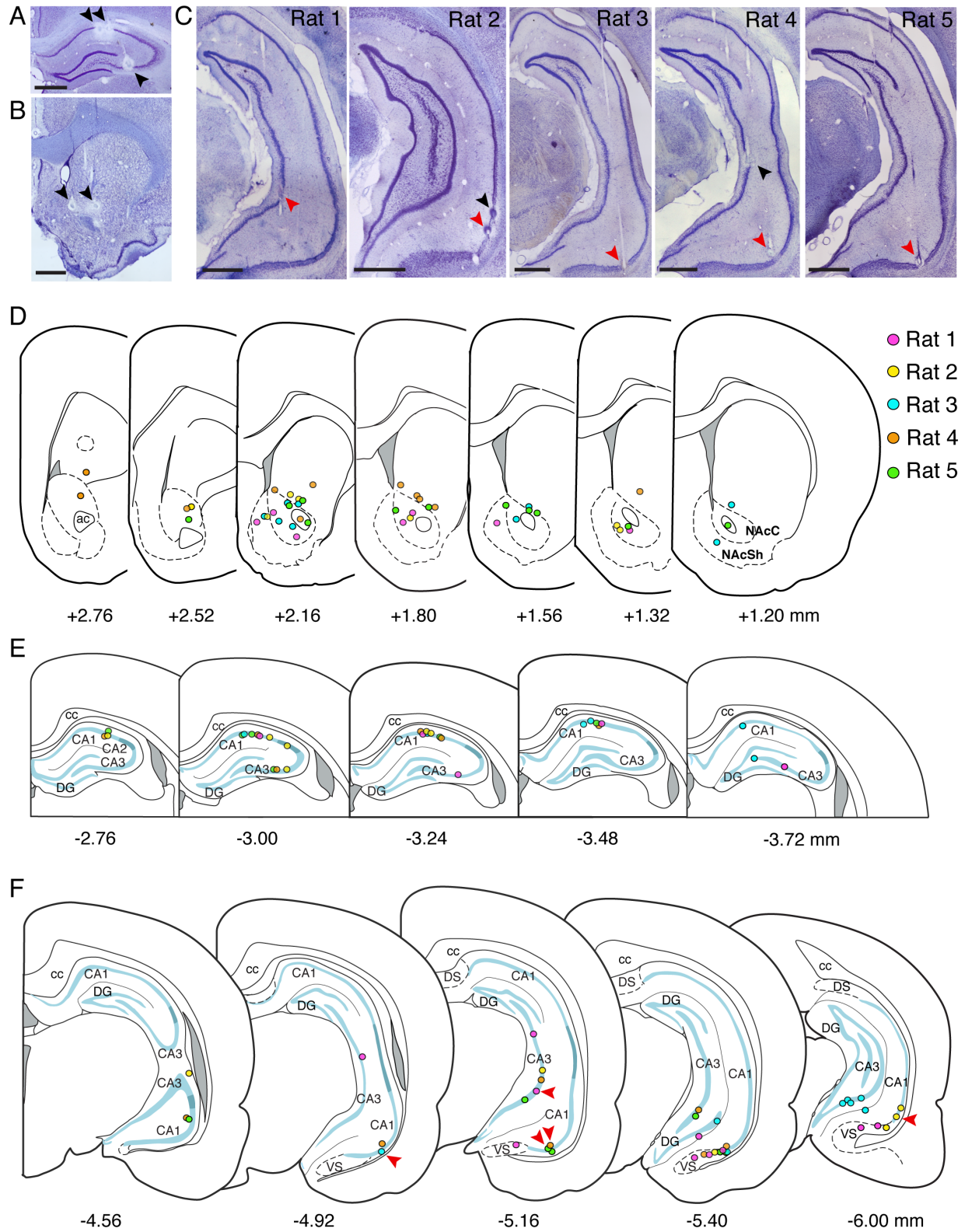
Supplemental Figure 1 (related to Figure 1) | Histological identification of recording sites.
(A and B) Nissl-stained coronal sections showing example tetrode lesions marked by black arrows in (A) dCA1 and dCA3 and (B) NAc, in Rat 5. **(C)** Nissl-stained coronal sections showing example tetrode lesions in vH. Each section includes the tetrode used for vSWR detection in each rat (red arrows). In A-C, scale bars are 1 mm. **(D)** Summary of all NAc recording locations across rats, aligned to the nearest representative section adapted from the Paxinos & Watson Wistar rat brain atlas (2007). Dots mark the last recorded depth of each tetrode at the end of the experiment. Dotted lines indicate approximate borders of NAc core and shell. Grey shaded regions represent ventricles. All distances are in AP coordinates (mm) relative to Bregma and correspond to original plate labels from the atlas; note that theses distances do not correspond exactly to true recording locations in our Long-Evans rats and are for illustration purposes only. For true implant coordinates, see Methods. **(E and F)** Summary of all recording sites in dH (E) and vH (F). Light blue regions represent stratum pyramidale of CA1/CA3 or granule cell layer of dentate gyrus, darker blue regions represent stratum pyramidale of CA2. Grey shaded regions represent ventricles. Red arrows indicate the 5 sites (1 per animal) used for vSWR detection. Abbreviations: ac, anterior commissure; NAcC, nucleus accumbens core; NAcSh, nucleus accumbens shell; cc, corpus callosum; DG, dentate gyrus; DS, dorsal subiculum; VS, ventral subiculum.
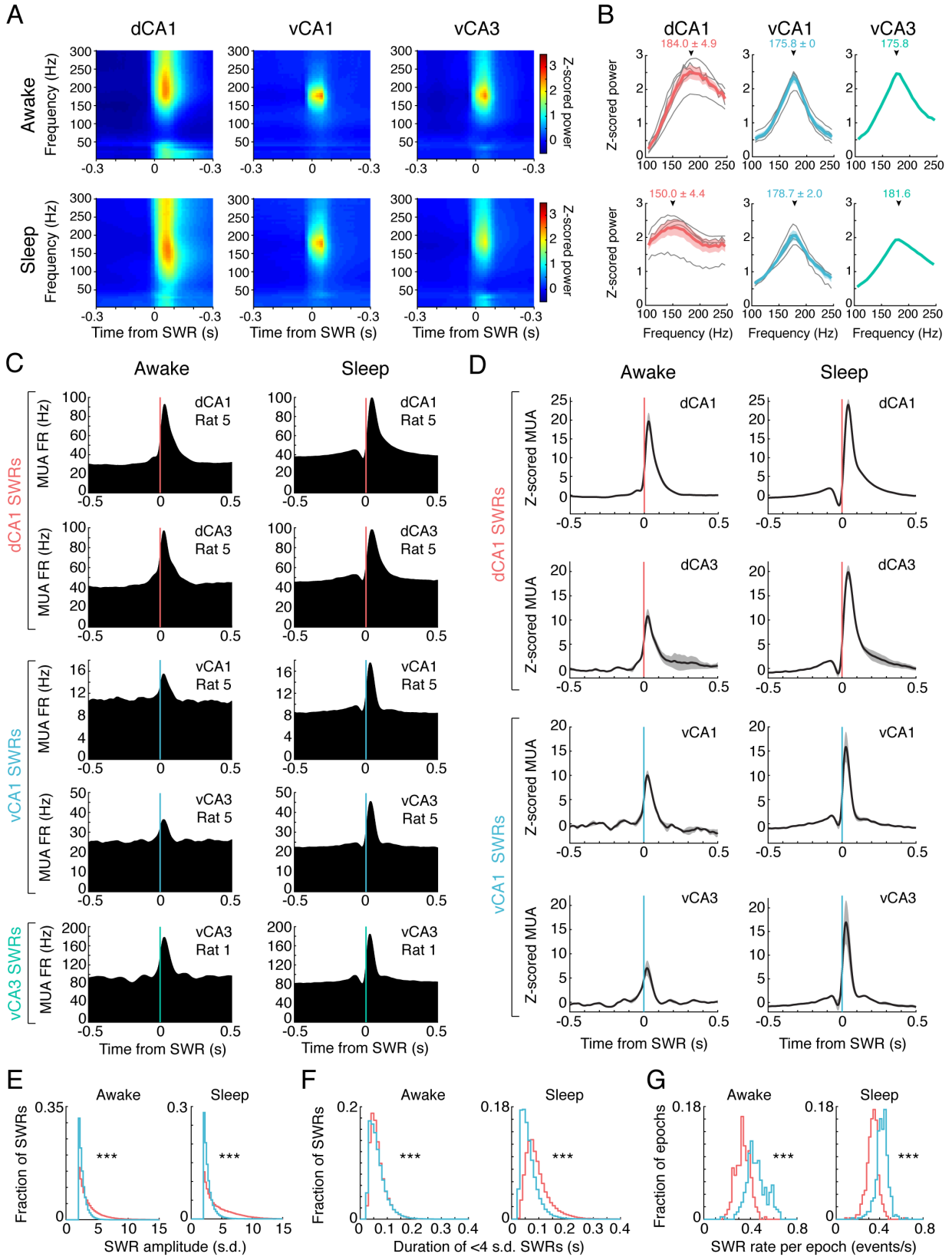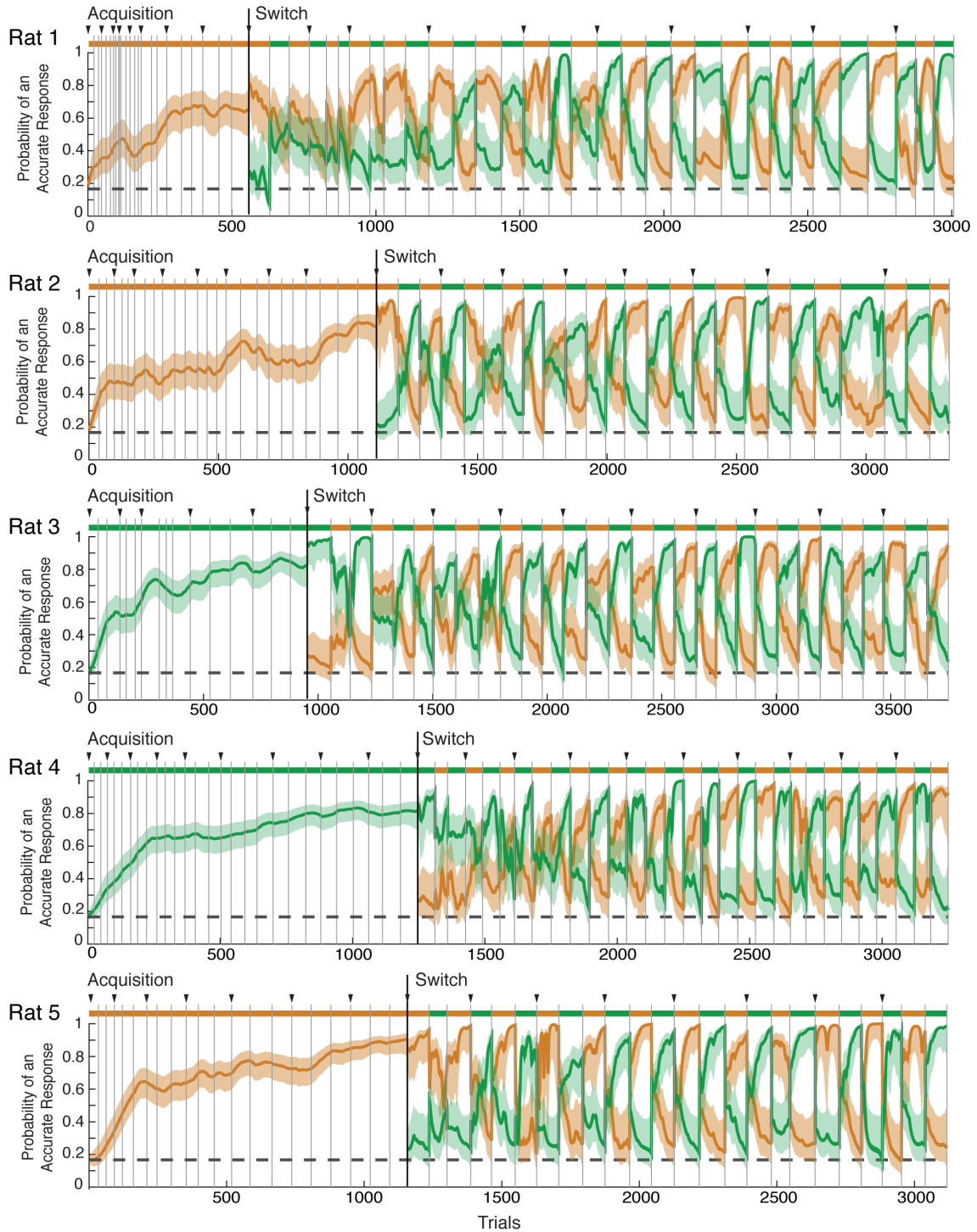
Supplemental Figure 2 (related to Figure 1) | Characterization of dH and vH SWRs.
(A) Examples of mean SWR-onset-triggered spectrograms on one tetrode from each detection region during awake immobility (top) and sleep (bottom). Left: all dCA1 SWRs in Rat 5 (n=9,642 awake, 26,048 sleep); Center: all vCA1 SWRs in Rat 5 (n=9,672 awake, 31,553 sleep); Right: all vCA3 SWRs in Rat 1, the only rat in which vCA3 SWRs were used (n=18,798 awake, 24,536 sleep). All SWRs >2 s.d. are included. Power is z-scored within each epoch and averaged across epochs and days. In (A) and (B) SWRs were detected as described in Methods (3 dCA1 tetrodes and 1 vH tetrode per animal). **(B)** Mean z-scored power (a slice of the SWR-triggered spectrogram) at frequencies between 100-250 Hz, at the time of peak ripple power for each animal during awake immobility (top row) and sleep (bottom row). Grey curves indicate individual animals, colored curves indicate mean ± s.e.m. across animals. Arrows indicate mean ± s.e.m. peak ripple frequency. Left: dCA1 SWRs (n=51,333 awake, 115,158 sleep, 5 rats); Center: vCA1 SWRs (n=47,222 awake, 120,271 sleep, 4 rats); Right: vCA3 SWRs (n=18,798 awake, 24,536 sleep, 1 rat). As vCA1 and vCA3 SWRs occurred at nearly the same frequency, we pooled these ventral SWRs (vSWRs) for the remainder of the study. **(C)** Examples of hippocampal multiunit activity (MUA) in wake and sleep, aligned to the onset of dSWRs (pink lines), vCA1 SWRs (blue lines), or vCA3 SWRs (aqua lines). In the upper right of each panel is the region and rat from which MUA was detected. Firing rate was calculated from the summed spike count from all tetrodes in the region. **(D)** Mean z-scored multiunit firing rate at the time of SWRs. Grey shaded region indicates s.e.m across animals. Top two rows: dCA1 and dCA3 MUA aligned to dCA1 SWRs (n=5 rats). Bottom two rows: vCA1 MUA (n=4 rats) and vCA3 MUA (n=3 rats) aligned to vCA1 SWRs. Z-scores were calculated within animal relative to the pre-SWR period (-500 to 0 ms). Strong similarity in activation timing of vCA3 MUA between vCA1 SWRs and vCA3 SWRs (**C**, bottom) also provided support for the use of vCA3 for SWR detection in Rat 1. **(E)** Distributions of SWR amplitudes across animals. In both wake and sleep, dSWRs (pink) are typically larger amplitude than vSWRs (blue; ***p=0, Wilcoxon rank-sum test). In (E-G), only one dCA1 tetrode per animal was used for SWR detection to allow for direct comparison to vSWRs. In (E) and (G), awake n=54,496 dSWRs, 74,355 vSWRs; sleep n=118,897 dSWRs, 146,995 vSWRs. **(F)** Distributions of SWR durations for <4 s.d. SWRs, across animals. In both wake and sleep, dSWRs (pink) are significantly longer than vSWRs (blue), although this difference is more pronounced in sleep (***$p<10^{-40}$, Wilcoxon rank-sum test; awake n=38,170 dSWRs, 71,029 vSWRs; sleep n=66,382 dSWRs, 135,035 vSWRs). **(G)** Distributions of dSWR (pink) and vSWR (blue) rate per epoch, expressed as the fraction of epochs with each rate (out of 256 awake epochs and 411 sleep epochs across animals). For awake epochs on the maze, rate was calculated per total time spent at <4 cm/s. For sleep epochs, rate was calculated per time spent in NREM sleep (see Methods). In both wake and sleep, the vSWR rate is typically higher than the dSWR rate (***$p<10^{-40}$, Wilcoxon rank-sum test).
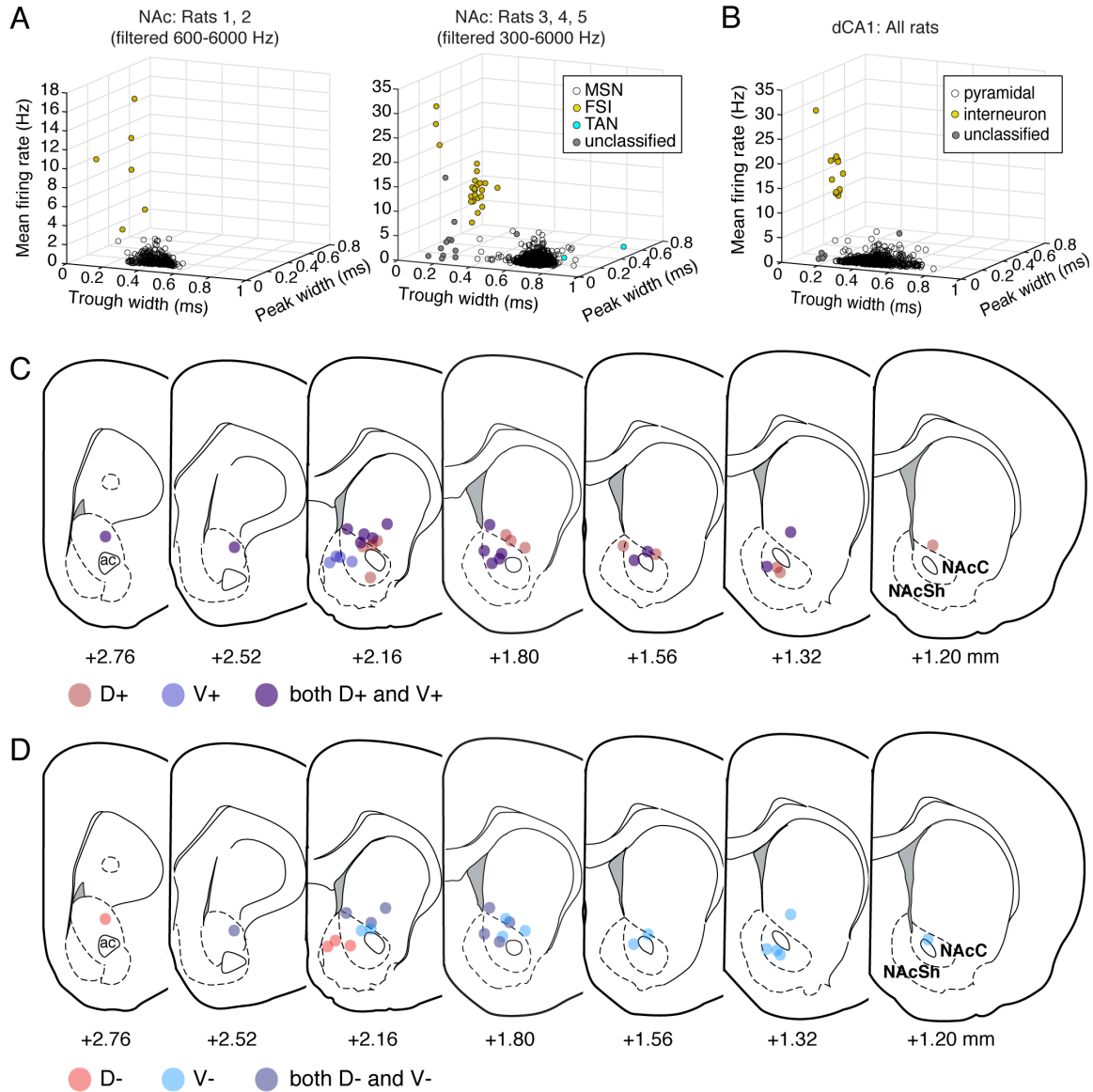
Supplemental Figure 3 (related to Figures 1, 2) | Awake SWR asynchrony and reward modulation.
(A) Cross-correlation histograms (CCH) of awake vSWRs relative to dSWRs within each animal, z-scored relative to shuffle. Note a lack of synchrony at less than 50 ms lag across animals. Error bars indicate s.e.m. across days (n=15-19 days) for each animal. **(B)** Asynchrony between dSWRs and vSWRs is present on both rewarded (left) and error (right) trials. A minimum of 3 s immobility following the time of reward delivery (or expected reward delivery on error trials) was required to include a trial's SWRs (n=5 rats, error bars are s.e.m.). **(C)** Changes in rewarded vs. error dSWR rate over task exposure, as a function of task epochs for each animal. Filled circles indicate mean dSWR rate across rewarded trials within the epoch (± s.e.m.), open squares indicate mean dSWR rate across error trials. Each point is color coded by the rewarded sequence of that epoch (Sequence A: orange; Sequence B: green). Black line indicates an exponential fit ± 95% confidence interval on error dSWR rate, grey line indicates exponential fit on rewarded dSWR rate. **(D)** Changes in rewarded vs. error vSWR rate over task exposure for each animal shown in (C). Note that some error bars extend above the y-axis limit.

Supplemental Figure 4 (related to Figure 2) | Multiple-W behavior.
Behavior from each rat expressed as the probability that the rat is making an accurate choice on each trial according to Sequence A (orange) or B (green) (see Methods). Solid line indicates the mode of the probability distribution, shaded region indicates the 90% confidence interval. Colored bars at the top of each plot indicate the rewarded sequence, grey vertical lines mark epoch boundaries, black triangles mark the start of days, and the horizontal dotted line indicates chance performance: 1/6 (0.167).

135

Supplemental Figure 5 (related to Figure 3) | Cell type classification and mapping of awake SWR-modulated neurons in the NAc.

**(A)** Classification of putative NAc cell types by waveform properties and mean firing rate. Each point represents a single unit. Number of units (wake and sleep included): MSNs: 1799, FSIs: 30, TANs: 2, unclassified: 12. Data from Rats 1 and 2 (left) were classified separately from Rats 3-5 (right) due to narrower bandpass filtering at time of acquisition, as this changes waveform shape. **(B)** Classification of putative hippocampal cell types in dCA1. Number of units (wake and sleep included): pyramidal: 1218, interneuron: 13, unclassified: 18. dCA1 units contribute to Figure S6B,D and Figure 6D. **(C)** Mapping of approximate tetrode locations where at least one D+ (dark red) or one V+ (dark blue) neuron (either MSN or FSI) was detected. All AP coordinates are in mm relative to Bregma and correspond to plate labels from the atlas (see Figure S1). Overlapping colors indicate locations where both D+ and V+ were detected, typically not in the same neuron. Note that borders of core (NAcC) and shell (NAcSh) are approximate, but that D+ modulation is limited largely to the dorsolateral core and its dorsolateral boundary, whereas V+ modulation is seen in the medial shell and also extends into the core. **(D)** Mapping of approximate tetrode locations where at least one D- neuron (light red) or one V- neuron (light blue) was detected, again typically not in the same neuron. Note coincidence of D- sites with V+ sites and V- sites with D+ sites.

136
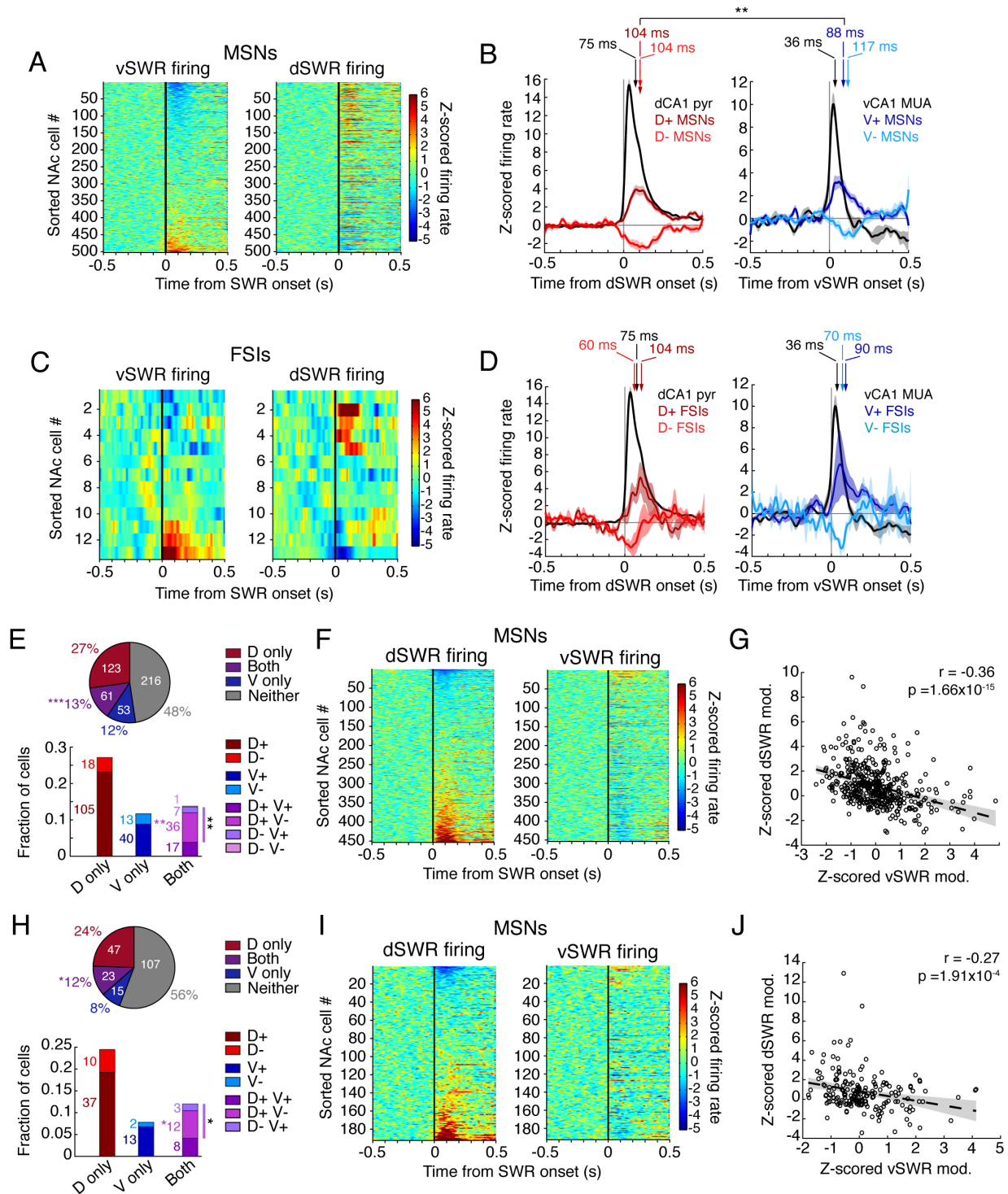
Supplemental Figure 6 (related to Figure 3) | NAc modulation during awake SWRs.
(A) Opposing modulation is not a result of cell ordering. Left: vSWR-aligned z-scored PETHs for each MSN ordered by its modulation amplitude (mean z-scored firing rate in the 200 ms following SWR onset). Right: dSWR-aligned z-scored PETHs for the same ordered MSNs shown on the left. Same MSNs as shown in Figure 3C. **(B)** Timing of significantly modulated MSN ensemble activity, overlaid on dCA1 pyramidal cell firing (n=332 cells) during dSWRs (left) and vCA1 multiunit activity (n=4 rats) during

vSWRs (right). Each curve represents the mean ± s.e.m. z-scored firing rate of the hippocampal (black), D+ (n=49 cells, dark red), V+ (n=16 cells, dark blue), D- (n=13 cells, light red), or V- (n=14 cells, light blue) populations. MSN subpopulations here are restricted to cells that passed the potential duplicate cell control. Arrows indicate the center of mass in the 0-200 ms post-SWR interval of each subpopulation's activity. The D+ center of mass occurs significantly later than the V+ center of mass (**$p<0.01$, permutation test). Timing difference of centers of mass of the D- and V- populations was not significantly different at the $p<0.05$ level. Also note that the centers of mass of the activated NAc ensembles lag the local activation of dH and vH neurons. **(C)** Similar to (A) but for FSIs shown in Figure 3G. **(D)** Timing of significantly modulated FSI ensemble activity during dSWRs (left), and vSWRs (right), overlaid on the same hippocampal activity as shown in (B). Arrows indicate the center of mass in the 0-200 ms post-SWR interval of each population's activity; no significant differences in timing (permutation tests). **(E-G)** Opposing MSN modulation cannot be accounted for by occasional co-occurrence of dSWRs and vSWRs (control for Figure 3B-D). Fraction modulated during Both: ***$p=9.13 \times 10^{-4}$, fraction opposing: **$p=0.0046$, fraction D+V-: **$p=0.0089$ (z-tests for proportions). **(H-J)** Opposing MSN modulation cannot be accounted for by inclusion of potential duplicate cells recorded across days (control for Figure 3B-D). Fraction modulated during Both: *$p=0.016$, fraction opposing: *$p=0.038$, fraction D+V-: *$p=0.046$ (z-tests for proportions).
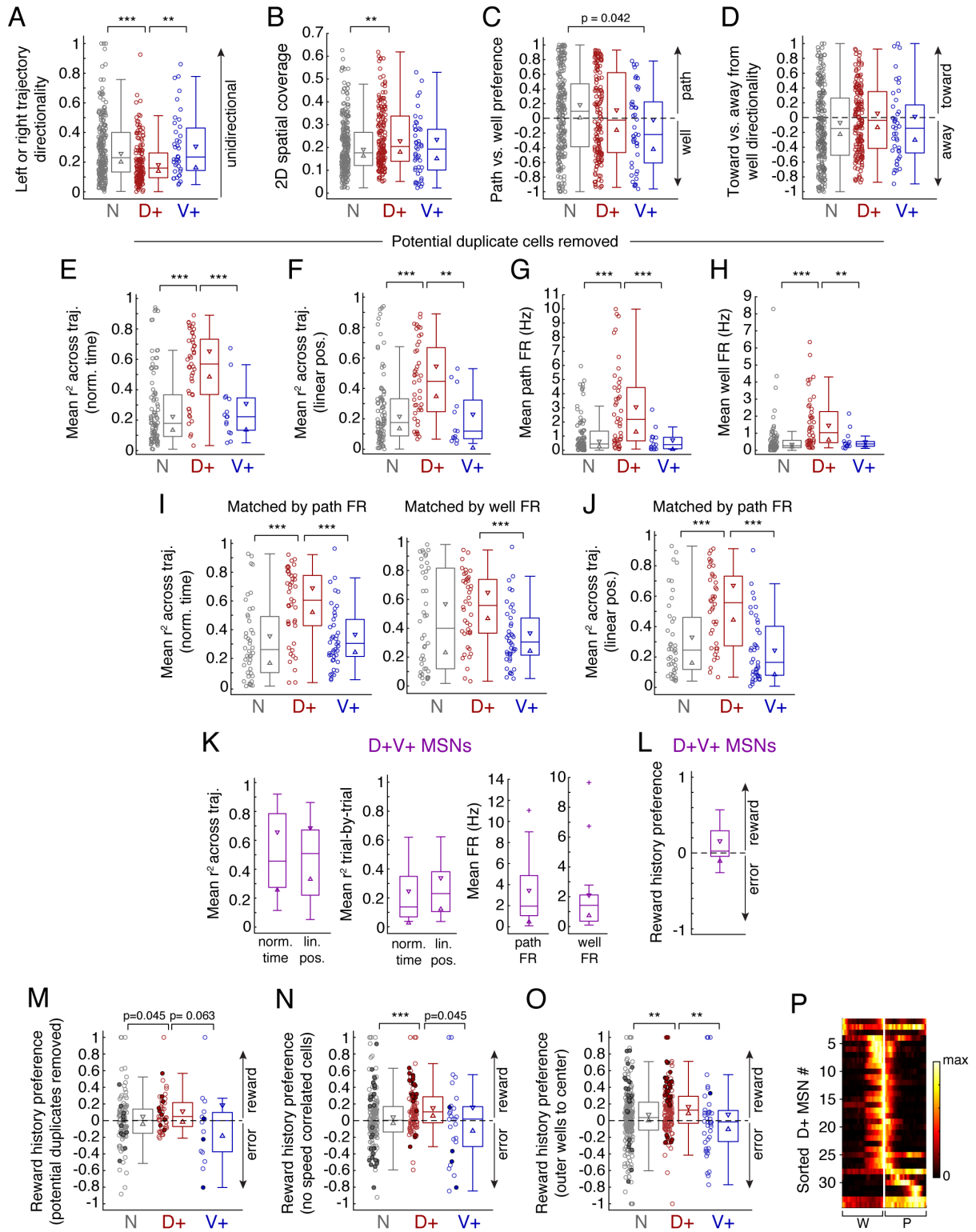
Supplemental Figure 7 (related to Figures 4, 5) | Population task-related firing patterns of D+ and V+ MSNs.

(A) Directionality for either leftward- or rightward-moving trajectories, where 0 indicates bidirectionality and values closer to 1 indicate stronger unidirectionality. N (n=217 cells) vs. D+ (n=152 cells): ***p=9.56x10^{-6}; D+ vs. V+ (n=39 cells); **p=0.0013. All tests between populations in A-J, M-O are Wilcoxon rank-sum tests with Bonferroni correction for multiple comparisons, setting significance level at p<0.017. **(B)** Two-dimensional spatial coverage of the environment, expressed as a fraction of occupied area on which cells fired >10% of their peak rate. N (n=246 cells) vs. D+ (n=161 cells): **p=0.008; D+ vs. V+ (n=45 cells): p=0.067. **(C)** Preference for the path (>0) vs. well (<0) components of all trajectories. While individual cells exhibit strong preferences, the populations do not (N n=226 cells, D+ n=154 cells, V+ n=42 cells). **(D)** Directionality for moving toward (>0) or away (<0) from a reward well (regardless of reward outcome). While individual cells exhibit strong preferences, the populations do not (N n=231 cells, D+ n=160 cells, V+ n=41 cells). **(E-H)** Controls for Figure 4F,G,J,K with potential duplicate cells removed (see Methods). In E, G, H: N n=93 cells, D+ n=45 cells, V+ n=15 cells; in F: N n=89 cells, D+ n=44 cells, V+ n=13 cells. **p<0.01, ***p<0.001. **(I)** D+ MSN firing similarity across trajectories in normalized trial time is maintained when populations are matched for mean firing rate on the path (left: N vs. D+: ***p=1.18x10^{-4}; D+ vs. V+: ***p=1.22x10^{-4}) or well (right: N vs. D+: p=0.34; D+ vs. V+: ***p=4.17x10^{-4}; n=42 cells in each subpopulation). **(J)** D+ MSN firing similarity across trajectories in linearized position is maintained when populations are matched for mean firing rate on the path (N vs. D+: ***p=5.23x10^{-4}; D+ vs. V+: ***p=4.54x10^{-6}; n=40 cells in each subpopulation). **(K)** D+V+ MSNs resemble D+ MSNs in task firing pattern properties (n=16 cells, related to Figure 4F-K). Crosses indicate outliers. **(L)** Reward history preference of all D+V+ MSNs is not significantly greater than zero (n=16 cells, p=0.10, one-tailed signed-rank test). **(M)** Control for Figure 5B with potential duplicate cells removed (N n=100 cells, D+ n=49 cells, V+ n=16 cells). D+ population is still significantly shifted greater than zero (p=0.0041, one-tailed signed-rank test). **(N)** Control for Figure 5B removing cells that are significantly correlated with trial-by-trial changes in mean speed. This aims to control for the possibility that differing speed alone on trials following reward vs. error could account for reward history preference, despite our original control for trial speed (see Methods). D+ population is significantly shifted greater than zero (p=1.95x10^{-7}, one-tailed signed-rank test). N (n=169 cells) vs. D+ (n=107 cells): ***p=8.95x10^{-4}. V+ n=28 cells. **(O)** Control for Figure 5B, examining only paths coming from the outer two wells to the center well of each rewarded sequence. D+ population is significantly shifted greater than zero (p=3.75x10^{-9}, one-tailed signed-rank test). N (n=222 cells) vs. D+ (n=158 cells): **p=0.0035; D+ vs. V+ (n=43 cells): **p=0.0076. **(P)** Ordered firing of D+ MSNs with significantly positive reward history preference on the path, as a function of normalized trial time. Mean well firing is included for illustration purposes only (W = well, P = path). The mean firing rate profile of each cell is calculated from all trials following reward across trajectories and normalized to the cell's maximum firing rate.

2.6 Methods

Animals. All procedures were in accordance with guidelines from the University of California San Francisco Institutional Animal Care and Use Committee and US National Institutes of Health. Long-Evans rats were pair-housed with a 12-hour light/dark cycle (lights on 6 am – 6 pm) and had *ad libitum* access to food until the beginning of food restriction, when they were single-housed. For this study, we used five male rats (500-650 g, 5-8 months old).

Implants and behavior. Animals were food restricted to 85% of their baseline weight and pre-trained to run back and forth on a 1 m long linear track for liquid reward (evaporated milk plus 5% sucrose), delivered automatically from reward wells at the ends of the track. Animals were incrementally introduced to a delay between well entry (nosepoke) and reward delivery of up to 2 seconds. After animals learned to alternate consistently for at least ~30 well visits per 5 min (4-6 days), they were switched back to an *ad libitum* diet and then surgically implanted with microdrive arrays.

Each microdrive housed a maximum of 28 independently movable tetrodes in a custom 3D-printed drive body (PolyJetHD Blue, Stratasys Ltd.) cemented to 3 stainless steel cannulae at fixed relative positions, targeting NAc vertically (8-12 tetrodes) and dH (6-7 tetrodes) and vH (9-13 tetrodes) at a 12° angle from vertical (tilted mediolaterally). NAc and dH tetrodes were made of 12.7 µm-diameter nichrome (Sandvik), while vH tetrodes were made of 12.7 µm nichrome, 12.7 µm tungsten, or 20 µm tungsten (California Fine Wire). Tetrode ends were plated with gold to a final impedance of ~240-350 kOhms. The microdrive was stereotaxically implanted over the right hemisphere such that the center of each cannula was targeted to the following coordinates relative to the animal's Bregma: dH: AP -3.9-4.0 mm, ML +1.7 mm; vH: AP -5.6-5.7 mm, ML +4.0 mm; NAc: AP +1.3-1.4 mm, ML +1.3 mm (Rat 1 vH: AP -5.75, ML +4.1, oval-shaped cannula). The approximate AP/ML spread of tetrodes in each area was defined by the inner radius of each cannula as follows: dH: ±0.49 mm, vH: ±0.87 mm, NAc: ±0.60 mm. A ground screw was inserted in the skull above the right cerebellum as a global reference.

While animals recovered from surgery, tetrodes were manually adjusted over ~2-3 weeks to their target depths relative to brain surface (dCA1: ~2.2-3.3 mm, 12˚ angle; vCA1: ~7.0-8.3 mm, 12˚ angle; NAc: ~5.4-7.5 mm, 0˚ angle), using electrophysiological landmarks such as unit density and SWR amplitude. Each rat was then food restricted again and re-trained on the linear track for 4-6 days with neural recording (not analyzed in this study). Animals were then introduced to the Multiple-W task (Fig. 2.1 [B-C]), a version of which has been described previously (Singer and Frank, 2009). Tetrodes were sometimes advanced a small amount after the conclusion of the day's recording on a case-by-case basis to improve cell yield.

The Multiple-W track consisted of six 76 cm arms spaced ~36 cm apart at their midpoints, with 3 cm high walls, connected to a "back" which extended past the first and sixth arm by 14 cm on each side (to mimic the availability of a right and left turn from these arms), and elevated 76 cm off the ground. On each day, the animal experienced three 20 min "run" (task) epochs on the track flanked by four 20-45 min sleep epochs in a separate high-walled rest box; only in rare cases (2 epochs each for Rats 1-2, 1 epoch each for Rats 3-4) were there four run epochs. The track was separated from the experimenter by an opaque black curtain, and the white walls of the room were marked with black distal cues of various shapes. Each arm contained a visually identical reward well connected to milk tubing, and milk was run through each well at the beginning of the day to create similar olfactory cues in all wells.

In each run epoch, the animal was placed at the back of the center arm of the rewarded sequence and was required by trial-and-error to find the 3 rewarded wells and figure out the alternation sequence between them, Sequence A (SA) or Sequence B (SB). Trials are defined as well visits. A visit to the center well of the sequence (well 3 in SA, well 4 in SB) was rewarded if the animal came from any other well. If a center visit was the first of the epoch or followed an error to a non-sequence arm, the animal could initiate an "outer" well visit to either of the center-adjacent wells to get reward. If a center visit followed a visit to a center-adjacent well, the animal had to then visit the opposite center-adjacent well, requiring hippocampal-dependent memory of the previous trial (Kim and Frank, 2009). For example, a correct series of trials for SA would be 3-2-3-4-3-2; for SB, 2-1-2-3-2-1. Consecutive visits to the same well were counted as errors, such that chance performance was defined as 1 out of 6 (0.167). The nosepoke at each well was detected

by an infrared beam break, which automatically triggered liquid reward delivery (105 µL evaporated milk plus 5% sucrose) via a syringe pump (OEM Systems) after a 2 second delay, and the animal's departure from the well was self-paced.

During the "Acquisition" phase (5-9 days), the same sequence was rewarded on every epoch: 3 animals acquired SA and 2 animals acquired SB. When the animal achieved greater than 80% correct performance on the Acquisition sequence for at least 1 epoch (assessed in real time as an epoch average), the novel sequence was introduced in the second epoch of the first "Switch" day. Only Rat 1 failed to reach 80% correct but was advanced to the Switch phase after achieving >75% correct and one full week of training; this rat was thus excluded from the 70-80% and >80% Acquisition performance bins in Fig. 2.2 (B-C). In the Switch phase, the rewarded sequence was switched on each run epoch, such that the starting sequence of each Switch day was also alternated (8-10 days).

Data collection and processing. Spiking, local field potential (LFP), position video, and reward well digital inputs and outputs were collected using the NSpike data acquisition system (L.M.F and J. MacArthur, Harvard Instrumentation Design Laboratory). For Rats 1-3, LFP data were collected at 1500 Hz sampling rate and digitally filtered online at 1-400 Hz (2-pole Bessel for high- and low-pass). Spikes were sampled at 30 kHz and saved as snippets of each waveform, filtered at 600-6000 Hz for hippocampus and 600-6000 Hz (2 rats) or 300-6000 Hz (1 rat) for NAc. For Rats 4-5, LFP and spikes were collected continuously at 30 kHz and filtered online at 1-6000 Hz, with post-hoc filtering applied in Matlab to extract LFP and spike waveforms using the same parameters as above (300-6000 Hz for NAc spikes). Subsets of spike data were collected as snippets in these animals to verify our post-hoc filtering. Note that negative voltages are displayed upward (e.g. Fig. 2.1 [D]). All LFP and spikes were collected relative to local references lacking spiking activity, which were themselves referenced to cerebellar ground: for dH tetrodes, the reference tetrode was located in corpus callosum (4 rats) or deep cortex with no units (1 rat); for vH, in ventral corpus callosum (1 rat) or in white matter at the ventrolateral edge of the midbrain (internal capsule or optic tract; 4 rats); for NAc, typically in corpus callosum, the lateral ventricle, or anterior commissure.

Overhead video of the track, collected at 30 frames/s, allowed us to track the animal's position via an array of infrared diodes attached to the top of the headstage, a few cm above the rat's head.

Spike sorting was performed using a combination of manual clustering in Matclust (M. Karlsson; Rats 1-3) and automated sorting with manual curation in Mountainsort (Chung et al., 2017) (Flatiron Institute; all data for Rats 4-5, individual days for Rats 1-3). Cells were clustered within epochs but tracked across all run and sleep epochs for which they could be isolated; with Mountainsort, this was done with a drift-tracking extension of the core pipeline and manual merging as needed (Chung et al., 2019). In Matclust, clustering was performed in amplitude and principal component space, and only well-separated units with clear refractory periods in their ISI distributions were accepted. In Mountainsort, we generally accepted clusters with isolation score >0.96, noise overlap <0.03 (median isolation score ~0.995, median noise overlap ~0.002), and clear separation from other clusters in amplitude and principal component space. The similarity of cluster quality between Mountainsort and Matclust was verified manually on a subset of the data and has been extensively verified in previous work (Chung et al., 2017). The same pattern of SWR-modulation of NAc cells was observed within each animal (data not shown), indicating that our results were not due to unit clustering in certain animals.

Histology. At the conclusion of the experiment, animals were anesthetized with isoflurane and small electrolytic lesions were made at the end of each tetrode to mark recording locations (30 µA of positive current for 3 seconds, on 2-4 channels of the tetrode). The animal recovered for 24 hours to allow gliosis and was then euthanized with pentobarbitol and perfused transcardially with PBS followed by 4% paraformaldehyde in 0.1M PB. The brain was post-fixed in 4% paraformaldehyde, 0.1M PB *in situ* for at least 24 hours, followed by removal of the tetrodes and cryoprotection in 30% sucrose in PBS. Brains were embedded in OCT compound and sectioned coronally at 50 µm thickness. Tissue was either Nissl stained using cresyl violet, or for a subset of dH sections, immunostained for RGS14, a marker of CA2, using previously described methods (Kay et al., 2016).

To reconstruct recording sites (Fig. S1), evenly spaced plates from the Paxinos and Watson Rat Atlas (2007), which is based on Wistar rats, were stretched and modified to align to representative sections from each brain region, using landmarks such as the ventricles, corpus callosum, and hippocampal pyramidal layers as guides. These modified plates were then treated as atlases to align the remaining sections and recording sites across animals.

Data analysis. All analyses were performed using custom code written in Matlab (Mathworks).

Behavioral analysis. The animals' task performance was analyzed using a state space algorithm (Smith et al., 2004) which estimates the probability that the animal is performing accurately according to Sequence A or B on each trial. This algorithm provides 90% confidence intervals which reveal when the animal is performing one sequence significantly better than the other. All trials in the Acquisition phase were analyzed together and background probability was set at chance (0.167), so that behavior of all animals could be compared from a similar starting point. During the Switch phase, each epoch was estimated independently with an unspecified background probability to get the most accurate representation of the animals' behavior; this means that occasionally the behavioral state could "jump" at an epoch boundary. The mode of the probability distribution was used to assign trials into performance stages for the SWR rate analysis in Fig. 2.2 (B-C), which yielded a different number of trials per stage from each animal.

SWR detection. SWRs were detected in dCA1 and vCA1 in 4 rats (Rats 2-5), and dCA1 and ventral CA3 in 1 rat (Rat 1), using methods described previously (Kay et al., 2016). Briefly, each tetrode's LFP was filtered to the ripple band at 150-250 Hz, the ripple amplitude was squared, summed across tetrodes (3 per animal in dH, only 1 per animal in vH, as this was the minimum number present in all animals), and smoothed with a 4 ms s.d., 32 ms wide Gaussian kernel. We then took the square root of this trace as the power envelope to detect excursions greater than 2 s.d. of the mean power within an epoch, lasting at least 15 ms. Tetrodes for detection were chosen based on ripple band power and proximity to the center of the

pyramidal layer. The SWR start time (when the envelope first crosses the threshold) was used as the event detection time. For spiking, characterization, and cross-correlation analyses, we excluded SWRs that occurred within 0.5 s of a previous SWR (i.e. chained SWRs). SWRs were only included for all analyses if detected at head speeds <4 cm/s.

As a control, we also detected "noise ripples," events in the 150-250 Hz band that exceeded a 2 s.d. threshold on our reference tetrodes for dH and vH (which were not in the hippocampus). These events are highly unlikely to be SWRs, but instead may reflect muscle artifacts or other high-frequency noise. For all analyses of SWRs other than NAc spiking (to include the maximum number of NAc spikes), we excluded SWRs with start times occurring within 100 ms of a "noise ripple" on the local reference.

Behavioral state definitions. During run epochs, periods of "immobility" were defined as times with a head movement speed <4 cm/s calculated as the derivative of the smoothed position data from the headstage-mounted diodes. We defined "sleep" as periods of immobility in sleep epochs that occurred >60 s after any movement at >4 cm/s. To calculate overall sleep SWR rate in Fig. S2, NREM sleep periods were defined by exclusion of REM sleep as defined previously (Kay et al., 2016). Specifically, REM periods were detected as times when the ratio of Hilbert amplitudes of theta (5–11 Hz) to delta (1–4 Hz), referenced to cerebellar ground, exceeded a per-animal threshold of 1.4-1.7 for at least 10 s.

Characterization of SWR properties. To characterize the spectral properties of dSWRs and vSWRs, multi-tapered spectrograms of the raw LFP triggered on SWR start times were generated using the Chronux toolbox (mtspecgramtrigc, sliding 100 ms window with 10 ms overlap, bandwidth 2-300 Hz), and z-scored to the mean power in each epoch before averaging across epochs and days. To approximate the peak ripple frequency, a slice of this spectrogram was taken at the time of peak ripple power per animal. For the remaining properties described in Fig. S2: we defined SWR amplitude as the minimum threshold in s.d. that would be required to detect the event (see above). SWR duration is the time between first threshold

crossing and return of the envelope to the mean. Mean epoch SWR rate was calculated for all immobility periods in run epochs and all NREM sleep periods during sleep epochs.

SWR cross-correlation. Cross-correlations between vSWRs and dSWRs were performed within day, using dSWRs as the reference, in 50 ms bins up to 0.5 s lag, and were normalized to the number of dSWRs in each day before averaging across days and animals. To create a z-scored version of the cross-correlation histogram, vSWR event times were circularly shuffled 1000 times within immobility periods (by a random amount up to ±half the mean immobility period length) to create 1000 shuffled histograms. The real cross-correlation values were z-scored relative to the distribution of shuffled values within each bin, such that a z-score of 0 indicates that the real data is no different than the mean of the shuffles.

SWR rate relative to reward and novelty. In Fig. 2.2 (B-C), we calculated the rate of SWR events per time spent immobile after reward delivery time on individual rewarded or error trials, and then averaged those rates across trials in each learning stage from each animal. Trials with less than 1 s spent immobile were excluded. In Fig. S3 (C-D), this rate was averaged across trials within each run epoch for each animal. In Fig. 2.2 (D-E), we calculated SWR rate in 200 ms bins from 0 to 5 s after nosepoke. We subsampled rewarded and error trials based on speed by excluding any trial where the animal spent more than 5 position samples (150 ms) moving faster than 4 cm/s (allowing for some jitter of head position), from 1.5 s after nosepoke to the end of the 5 s window. As the animal's retreat from the reward well is self-paced, this greatly reduced the number of included error trials and focused exclusively on error trials when the animal waited at the well beyond the expected reward delivery time. We also excluded any bins that were not below the speed threshold, as SWRs could not be detected in these bins according to our criteria. SWR rate per bin was then calculated per the number of included bins in each animal, and we required at least 2 s total of data per bin (10 accepted bins) to calculate a rate across animals.

Unit inclusion. Only units firing at least 100 spikes in a given epoch were included in the current study (865 total NAc units in run, 1678 units in sleep, from all five rats across days). Additional inclusion criteria were applied per analysis.

Putative cell type classification. NAc single units were classified similar to methods described previously (Atallah et al., 2014; Berke, 2008), using mean firing rate, mean waveform peak width at half-maximum, mean waveform trough width at half-minimum, and ISI distribution. These values were averaged across epochs when a cell was present in multiple epochs within a day. When plotted, mean firing rate and waveform features generated distinguishable clusters (Fig. S5 [A]), the boundaries of which were defined as follows: fast-spiking interneurons (FSIs): firing rate >3 Hz, peak width <0.2 ms, and a ratio of trough width to peak width (TPR) <2.7 (TPR was estimated by k-means clustering and was more reliable than exact trough width for FSIs); tonically-active neurons (TANs): <5% of ISIs less than 10 ms, a median ISI >100 ms, and peak width and trough width above the 95th percentile for the remainder of the units; unclassified units had low TPR and/or narrow trough widths (<0.2 or 0.3 ms) but firing rates <2 Hz; all other units were considered putative medium-sized spiny neurons (MSNs). Only MSNs and FSIs are included in the current study.

Hippocampal units were also classified according to mean firing rate and peak and trough width. Putative interneurons were defined as having firing rates >5 Hz, peak width <0.2 ms and trough width <0.3 ms. All other non-unclassified units were considered putative pyramidal cells.

SWR-triggered spiking activity. For all analyses of SWR-aligned spiking, we created SWR-onset-triggered rasters (1 ms bins) in a 1 s peri-SWR window. From this raster, the mean firing rate was smoothed with a 10 ms s.d., 80 ms wide Gaussian kernel to generate a peri-event time histogram (PETH). For analyses based on z-scored firing rates (e.g. Fig. 2.3 [C,G]), the raster was padded with a 100x repetition of its start and end values, smoothed, unpadded, and z-scored to the pre-SWR period -500 to 0 ms.

For multiunit activity (MUA) analysis in dH and vH, we thresholded all spike events at 40 µV on tetrodes with clear multiunit firing in the pyramidal layer. In Rats 4 and 5, MUA was extracted by post-hoc thresholding of the 600-6000 Hz filtered LFP. SWR-triggered MUA spike counts were summed across tetrodes and then divided by the total time per bin to calculate a mean firing rate per animal.

To detect significant SWR-modulation of NAc cells, we followed a procedure described previously (Jadhav et al., 2016). Briefly, for each cell, we circularly shuffled each SWR-triggered spike train by a random amount up to ±0.5 s to generate 5000 shuffled PETHs. We then calculated the summed squared difference of the real PETH relative to the mean of the shuffles in a 0-200 ms window post SWR-onset, and compared it to the same value for each shuffle relative to the mean of the shuffles. Significance at $p<0.05$ indicates that the real modulation exceeded 95% of the shuffles. The direction of modulation was defined from a modulation index, calculated as the mean firing rate in the 0-200 ms window minus the mean baseline firing rate from -500 to -100 ms, divided by the mean baseline firing rate. This sign of this index was used to assign cells as significantly positively or negatively SWR-modulated.

To categorize cells according to both dSWRs and vSWRs, we only included cells that fired at least 50 spikes in the peri-event rasters for both types of SWRs. Cells were subsequently categorized according to their significance and direction as unmodulated (Neither, N), dSWR-significant only (D only), vSWR-significant only (V only), significant during both (Both), dSWR-activated (D+), dSWR-suppressed (D-), vSWR-activated (V+), vSWR-suppressed (V-), or combinations of these: D+V+, D+V-, D-V+, or D-V-. In both wake and sleep, we observed more dSWR- and vSWR-modulated cells than the chance level of 5%. To assess the significance of the "both" modulation categories, we compared each fraction to the chance overlap of our empirical fractions of dSWR- and vSWR-modulated cells using a nonparametric z-test for proportions. We defined "modulation amplitude" as the mean z-scored firing rate of each cell (relative to the pre-SWR period -500 to 0 ms) in the 0-200 ms window following SWR onset.

Potential duplicate cell control. To control for the possibility that cells stably recorded on the same tetrode across days could have been counted more than once and could influence any of our results, we excluded

potential duplicate cells based on waveform similarity (Schmitzer-Torbert and Redish, 2004). We first established a waveform correlation threshold based on cells recorded on different tetrodes on the same day, which are different cells by definition. For each pair of cells, we aligned their mean waveforms at the peak (on the maximum channel) of one of the cells and calculated a Pearson's correlation coefficient on each channel (channel 1 of cell A was compared to channel 1 of cell B, and so on). In cases where the waveform snippets were different lengths (due to different spike extraction in Matclust as compared to Mountainsort), we aligned the snippets at their peaks and padded the edges with zeroes as needed. The resulting r values for each channel were then averaged to establish a mean r for that pair. The 95th percentile of r values in this different-cell distribution, 0.979 for wake and 0.980 for sleep, was taken as the threshold for waveform correlation. Next, if a tetrode was moved ≥78 μm across days (Berke, 2008), we considered the newly acquired cells to be "unique." If a tetrode was moved less than 78 μm between days, we computed the mean r for all pairs of cells on that tetrode across all previous days of similar depth. This could exclude cells that disappeared and "came back" across multiple days, even though this scenario would seem to be unlikely. Cell pairs with a mean r greater than the threshold were tagged as potential duplicates. We first kept cells from the day with the most cells on that tetrode (randomly selected if multiple days tied for maximum cell count). If a given potential duplicate cell had not yet been kept, one instance of that cell was randomly selected to keep. Cells present in both wake and sleep were classified as potential duplicates based on their r in wake. We note that this system will result in some false positive exclusions and false negative inclusions; different MSNs can have highly similar waveforms even though they are different cells (false positive), and waveforms can change dramatically from day to day even for the same cell due to changes in cell health or relative position of the tetrode (false negative). However, applying this conservative control did not change any of our main results.

NAc neuron task firing. We analyzed trajectory firing patterns using two methods: normalized trial time and linearized position. In the normalized trial time method, each trial was split into normalized progression of time spent at the well (from nosepoke to when the animal turns around; "well") and time spent moving

along the path between wells (from turnaround to next nosepoke; "path"). The turnaround time was detected by a >4 cm movement in the x-direction, a change in head direction of >0.25 radians (~14˚), and a speed of >2 cm/s. Additionally, we required that the animal had moved away from the well in the y-direction one second in the future, otherwise the turnaround time was incremented. Path and well time were divided into bins of 0.5% of the total completion time. Firing rate was calculated by dividing the number of spikes in each bin by the bin width in seconds on that particular trial (excluding spikes during either dSWRs or vSWRs), smoothing the rate with a 5 bin (2.5%) s.d., 40 bin (20%) wide Gaussian kernel, and then averaging across trials of the same trajectory type (defined by start and end well). We further attempted to control for variation in the animal's behavior on individual trials in three ways: by only calculating mean trajectory rates when there were at least 3 trials on that trajectory; by performing a pairwise speed profile correlation across trials and only accepting trials that fell at or above the 25th percentile of speed similarity values; and by only accepting trials with a duration at or below the 75th percentile of the trial length distribution. These methods excluded trials that were long, slow, or had many stops.

In the linearized position method, we projected the animal's 2D position to a line connecting each junction and endpoint of the maze, generating a linearized position relative to the start of each trajectory defined by start and end well. Each trajectory thus contained a specific set of maze segments, and we again controlled for behavioral variation by only accepting trials where the animal deviated ≤12 linear cm onto segments not included in the current trajectory (this allowed for small "head swings" onto neighboring segments). Only data during movement >4 cm/s were included. From the set of included trials on each trajectory, we calculated a firing rate per time spent moving (occupancy) in each linear position bin of 2 cm, smoothed it with a 4 cm s.d., 20 cm wide Gaussian kernel, and calculated the mean rate on that trajectory within day. Bins with <100 ms total occupancy were excluded. Trajectories missing more than 5 bins (as a result of diode occlusion or low time occupancy) were excluded from firing similarity analysis (5 or fewer missing bins were interpolated), and linearized distance was normalized before pairwise correlation across trajectories (below).

To assess the firing similarity of a given cell across trajectories that differ in spatial location and direction, we focused on the 6 rewarded trajectories (across SA and SB) depicted in Fig. 2.4 (A). We calculated the coefficient of determination between the mean firing profiles of each pair of trajectories (as a function of normalized trial time or linearized position), and then took the mean r^2 across pairs. We controlled for the effect of firing rate by matching cells in the V+ population to D+ and N cells with the closest firing rates, generating subsampled D+ and N populations. Note that the variety of behavioral controls applied to both methods excluded slightly different numbers of cells, depending on whether the cells were active on enough trials that passed our criteria to compute an r^2.

Trial-by-trial correlation was performed with the same controls for behavioral variability as described above. Specifically, we correlated successive pairs of individual trials (minimum 10 traversals per included trajectory) to get a mean r^2 for each trajectory, and then took the mean r^2 across trajectories. In the linearized position version, this was done with firing rate in 4 cm bins, smoothed with a 4 cm s.d., 20 cm wide Gaussian. A larger bin size was used to account for lower time occupancy in any given bin on a single trial, and we excluded bins with <30 ms occupancy (~1 position sample).

To ask whether NAc neurons were more or less engaged on the task than in the sleep box, we computed a task vs. box index as (mean task FR – mean box FR)/(mean task FR + mean box FR), such that values >0 indicated higher firing rate on the task, and values <0 indicate higher firing rate in the box. Mean firing rates were computed for all movement times of speed >4 cm/s, and for all immobility times <4 cm/s on the task and <4 cm/s within 7 s of a movement >4 cm/s in the sleep box, outside of SWRs (Kay et al., 2016).

We explored a variety of additional task-related firing parameters to characterize NAc MSNs. Left/right trajectory directionality was calculated as the absolute area between leftward and rightward trajectory firing rate curves on the same maze segments in linearized position, divided by their sum (values closer to 1 indicate a stronger preference in one direction, either left or right). Toward vs. away from well directionality was calculated from the linearized position firing rate curves on the same vertical segment in opposite directions (difference between the two curves divided by their sum). For two-dimensional (2D)

spatial coverage, we first generated an occupancy-normalized firing rate map of each cell in each task epoch, in 1 cm^2 bins smoothed with a symmetric 2D Gaussian (4 cm s.d.). Coverage was defined as the fraction of the area with >5% of non-zero occupancy where the cell fired >10% of its peak spatial firing rate; coverage was then averaged per cell across epochs. Path vs. well preference was calculated from each cell's mean path and well firing rates (excluding SWR times) across trajectories in normalized trial time, as (path – well)/(path + well), such that values greater than zero indicate path preference and values less than zero indicate well preference.

NAc neuron reward and reward history firing. To examine reward history preference, we calculated firing rate on the path in normalized trial time, using the same methods as above (but smoothed with a 1.5% s.d., 12% wide Gaussian kernel), now comparing all paths (regardless of trajectory) following a rewarded well visit or an error well visit. We required a minimum of 2 s (the delay between nosepoke and reward delivery) to be spent at the well for a trial to be included, as this is the minimum time at which the animal would know if the trial was rewarded. We only included cells for which at least 3 rewarded and 3 error trials passed our speed profile and trial length controls. The reward history preference was calculated from the mean firing rate curves as (post-reward – post-error)/(post-reward + post-error). Significance of reward preference (>0) vs. error preference (<0) was calculated with a permutation test from the set of rewarded and error trials.

To calculate reward vs. error preference at the wells (based on current reward or error), we used two methods. In the first method (Fig. 2.5 [C-D]), we calculated firing rate on rewarded and error well visits as a function of normalized time at the wells, excluding SWR spikes, again requiring a minimum dwell time of 2 s. Specifically, we separately normalized the time from nosepoke to reward delivery (2 s) and from delivery to turnaround in 1% bins each, such that expected delivery time would be aligned across rewarded and error trials. The mean firing rate curve for the whole well period was then smoothed with a 3 bin s.d., 24 bin wide Gaussian. We additionally applied a pairwise speed profile correlation to only include trials that fell at or above the 25th percentile of speed similarity values, and only included cells for which at

least 3 rewarded and 3 error trials met the above criteria. We then calculated a reward vs. error index per cell from the mean firing rate curves as (reward – error)/(reward + error), exclusively in time bins for which the mean speed on both rewarded and error trials was <2 cm/s. Significance of reward preference (>0) or error preference (<0) was calculated with a permutation test.

In the second method for reward preference at the wells (Fig. 2.5 [E-F]), we calculated rewarded and error firing rates as a function of true time from nosepoke (0 to 4 s, 100 ms bins; smoothed with a 100 ms s.d., 800 ms wide Gaussian). We then computed a reward vs. error index from the mean firing rate curves post-reward-delivery (2 to 4 s, excluding SWR spikes) as (reward – error)/(reward + error). We again controlled for speed by excluding any trial where the animal spent more than 5 position samples (150 ms) moving faster than 4 cm/s, and required at least 5 included trials of both types to compute an index. Significance was again assessed with a permutation test in the 2-4 s window.

Spike cross-correlations. Spike cross-correlations between pairs of cells were calculated in 10 ms bins at up to 0.5 s lag. Each CCH was first normalized by the square root of the product of the number of spikes from each cell. To z-score the CCH of each cell pair, one of the spike trains was circularly shuffled 1000 times (by a random amount up to ±half the mean immobility period length) to create 1000 shuffled CCHs. Each real and shuffled CCH was smoothed with a 20 ms s.d., 160 ms wide Gaussian. The real cross-correlation values were then z-scored relative to the distribution of shuffled values within each bin. We averaged the cross-correlation z-score ±10 ms around 0 to get an approximate "0 lag" value.

SWR coactivity. Coactivity z-scores between pairs of cells were calculated as previously described (Cheng and Frank, 2008; Singer and Frank, 2009). Briefly, we counted the number of spikes each cell fired during awake dSWRs (for D+/D+ and D+/dCA1 pairs) or vSWRs (for V+/V+ pairs) within a day, where the boundaries of each SWR were defined by the 2 s.d. threshold (see above). From this set of events, the observed coincidence of spiking was calculated as a z-score:

$$z = \frac{n_{AB} - \frac{n_A n_B}{N}}{\sqrt{n_A n_B (N - n_A)(N - n_B)/(N^2(N-1))}}$$

where N is the total number of SWR events, n_A is the number of events in which cell A spiked, n_B is the number of events in which cell B spiked, and n_{AB} is the number of events in which both cells spiked.

Quantification and statistical analysis. No statistical methods were used to predetermine sample size. The minimum number of required animals was established beforehand as four or more, in line with similar studies in which this number yields data with sufficient statistical power. All statistical tests were non-parametric and two-sided unless otherwise specified.

2.7 References

Adhikari, A., Topiwala, M.A., and Gordon, J.A. (2011). Single units in the medial prefrontal cortex with anxiety-related firing patterns are preferentially influenced by ventral hippocampal activity. Neuron *71*, 898-910.

Ambrose, R.E., Pfeiffer, B.E., and Foster, D.J. (2016). Reverse Replay of Hippocampal Place Cells Is Uniquely Modulated by Changing Reward. Neuron *91*, 1124-1136.

Atallah, H.E., McCool, A.D., Howe, M.W., and Graybiel, A.M. (2014). Neurons in the ventral striatum exhibit cell-type-specific representations of outcome during learning. Neuron *82*, 1145-1156.

Bannerman, D.M., Rawlins, J.N., McHugh, S.B., Deacon, R.M., Yee, B.K., Bast, T., Zhang, W.N., Pothuizen, H.H., and Feldon, J. (2004). Regional dissociations within the hippocampus--memory and anxiety. Neurosci Biobehav Rev *28*, 273-283.

Berke, J.D. (2008). Uncoordinated firing rate changes of striatal fast-spiking interneurons during behavioral task performance. J Neurosci *28*, 10075-10080.

Berke, J.D., Breck, J.T., and Eichenbaum, H. (2009). Striatal versus hippocampal representations during win-stay maze performance. J Neurophysiol *101*, 1575-1587.

Berke, J.D., Okatan, M., Skurski, J., and Eichenbaum, H.B. (2004). Oscillatory entrainment of striatal neurons in freely moving rats. Neuron *43*, 883-896.

Britt, J.P., Benaliouad, F., McDevitt, R.A., Stuber, G.D., Wise, R.A., and Bonci, A. (2012). Synaptic and behavioral profile of multiple glutamatergic inputs to the nucleus accumbens. Neuron *76*, 790-803.

Brog, J.S., Salyapongse, A., Deutch, A.Y., and Zahm, D.S. (1993). The patterns of afferent innervation of the core and shell in the "accumbens" part of the rat ventral striatum: immunohistochemical detection of retrogradely transported fluoro-gold. J Comp Neurol *338*, 255-278.

Buzsaki, G. (2015). Hippocampal sharp wave-ripple: A cognitive biomarker for episodic memory and planning. Hippocampus *25*, 1073-1188.

Buzsaki, G., and Moser, E.I. (2013). Memory, navigation and theta rhythm in the hippocampal-entorhinal system. Nat Neurosci *16*, 130-138.

Carelli, R.M. (2002). The nucleus accumbens and reward: neurophysiological investigations in behaving animals. Behav Cogn Neurosci Rev *1*, 281-296.

Castro, D.C., and Bruchas, M.R. (2019). A Motivational and Neuropeptidergic Hub: Anatomical and Functional Diversity within the Nucleus Accumbens Shell. Neuron *102*, 529-552.

Cheng, S., and Frank, L.M. (2008). New experiences enhance coordinated neural activity in the hippocampus. Neuron *57*, 303-313.

Chersi, F., and Burgess, N. (2015). The Cognitive Architecture of Spatial Navigation: Hippocampal and Striatal Contributions. Neuron *88*, 64-77.

Chung, J.E., Joo, H.R., Fan, J.L., Liu, D.F., Barnett, A.H., Chen, S., Geaghan-Breiner, C., Karlsson, M.P., Karlsson, M., Lee, K.Y.*, et al.* (2019). High-Density, Long-Lasting, and Multi-region Electrophysiological Recordings Using Polymer Electrode Arrays. Neuron *101*, 21-31.e25.

Chung, J.E., Magland, J.F., Barnett, A.H., Tolosa, V.M., Tooker, A.C., Lee, K.Y., Shah, K.G., Felix, S.H., Frank, L.M., and Greengard, L.F. (2017). A Fully Automated Approach to Spike Sorting. Neuron *95*, 1381-1394.e1386.

Ciocchi, S., Passecker, J., Malagon-Vina, H., Mikus, N., and Klausberger, T. (2015). Brain computation. Selective information routing by ventral hippocampal CA1 projection neurons. Science *348*, 560-563.

de Hoz, L., and Martin, S.J. (2014). Double dissociation between the contributions of the septal and temporal hippocampus to spatial learning: the role of prior experience. Hippocampus *24*, 990-1005.

Diba, K., and Buzsaki, G. (2007). Forward and reverse hippocampal place-cell sequences during ripples. Nat Neurosci *10*, 1241-1242.

Eichenbaum, H. (2017). On the Integration of Space, Time, and Memory. Neuron *95*, 1007-1018.

Fanselow, M.S., and Dong, H.W. (2010). Are the dorsal and ventral hippocampus functionally distinct structures? Neuron *65*, 7-19.

Floresco, S.B., Seamans, J.K., and Phillips, A.G. (1997). Selective roles for hippocampal, prefrontal cortical, and ventral striatal circuits in radial-arm maze tasks with or without a delay. J Neurosci *17*, 1880-1890.

Foster, D.J., and Wilson, M.A. (2006). Reverse replay of behavioural sequences in hippocampal place cells during the awake state. Nature *440*, 680-683.

Frank, L.M., Brown, E.N., and Wilson, M.A. (2000). Trajectory encoding in the hippocampus and entorhinal cortex. Neuron *27*, 169-178.

Girardeau, G., Inema, I., and Buzsaki, G. (2017). Reactivations of emotional memory in the hippocampus-amygdala system during sleep. Nat Neurosci *20*, 1634-1642.

Gomperts, S.N., Kloosterman, F., and Wilson, M.A. (2015). VTA neurons coordinate with the hippocampal reactivation of spatial experience. eLife *4*.

Goto, Y., and Grace, A.A. (2005). Dopaminergic modulation of limbic and cortical drive of nucleus accumbens in goal-directed behavior. Nat Neurosci *8*, 805-812.

Groenewegen, H.J., Vermeulen-Van der Zee, E., te Kortschot, A., and Witter, M.P. (1987). Organization of the projections from the subiculum to the ventral striatum in the rat. A study using anterograde transport of Phaseolus vulgaris leucoagglutinin. Neuroscience *23*, 103-120.

Humphries, M.D., and Prescott, T.J. (2010). The ventral basal ganglia, a selection mechanism at the crossroads of space, strategy, and reward. Prog Neurobiol *90*, 385-417.

Ito, R., Robbins, T.W., Pennartz, C.M., and Everitt, B.J. (2008). Functional interaction between the hippocampus and nucleus accumbens shell is necessary for the acquisition of appetitive spatial context conditioning. J Neurosci *28*, 6950-6959.

Jadhav, S.P., Rothschild, G., Roumis, D.K., and Frank, L.M. (2016). Coordinated Excitation and Inhibition of Prefrontal Ensembles during Awake Hippocampal Sharp-Wave Ripple Events. Neuron *90*, 113-127.

Ji, D., and Wilson, M.A. (2007). Coordinated memory replay in the visual cortex and hippocampus during sleep. Nat Neurosci *10*, 100-107.

Jimenez, J.C., Su, K., Goldberg, A.R., Luna, V.M., Biane, J.S., Ordek, G., Zhou, P., Ong, S.K., Wright, M.A., Zweifel, L.*, et al.* (2018). Anxiety Cells in a Hippocampal-Hypothalamic Circuit. Neuron *97*, 670-683.

Joo, H.R., and Frank, L.M. (2018). The hippocampal sharp wave-ripple in memory retrieval for immediate use and consolidation. Nat Rev Neurosci *19*, 744-757.

Karlsson, M.P., and Frank, L.M. (2009). Awake replay of remote experiences in the hippocampus. Nat Neurosci *12*, 913-918.

Kay, K., Sosa, M., Chung, J.E., Karlsson, M.P., Larkin, M.C., and Frank, L.M. (2016). A hippocampal network for spatial coding during immobility and sleep. Nature *531*, 185-190.

Keinath, A.T., Wang, M.E., Wann, E.G., Yuan, R.K., Dudman, J.T., and Muzzio, I.A. (2014). Precise spatial coding is preserved along the longitudinal hippocampal axis. Hippocampus *24*, 1533-1548.

Kheirbek, M.A., Drew, L.J., Burghardt, N.S., Costantini, D.O., Tannenholz, L., Ahmari, S.E., Zeng, H., Fenton, A.A., and Hen, R. (2013). Differential control of learning and anxiety along the dorsoventral axis of the dentate gyrus. Neuron *77*, 955-968.

Kim, S.M., and Frank, L.M. (2009). Hippocampal lesions impair rapid learning of a continuous spatial alternation task. PLoS ONE *4*, e5494.

Kjelstrup, K.B., Solstad, T., Brun, V.H., Hafting, T., Leutgeb, S., Witter, M.P., Moser, E.I., and Moser, M.B. (2008). Finite scale of spatial representation in the hippocampus. Science *321*, 140-143.

Kjelstrup, K.G., Tuvnes, F.A., Steffenach, H.A., Murison, R., Moser, E.I., and Moser, M.B. (2002). Reduced fear expression after lesions of the ventral hippocampus. Proc Natl Acad Sci *99*, 10825-10830.

Komorowski, R.W., Garcia, C.G., Wilson, A., Hattori, S., Howard, M.W., and Eichenbaum, H. (2013). Ventral hippocampal neurons are shaped by experience to represent behaviorally relevant contexts. J Neurosci *33*, 8079-8087.

Lansink, C.S., Goltstein, P.M., Lankelma, J.V., Joosten, R.N., McNaughton, B.L., and Pennartz, C.M. (2008). Preferential reactivation of motivationally relevant information in the ventral striatum. J Neurosci *28*, 6372-6382.

Lansink, C.S., Goltstein, P.M., Lankelma, J.V., McNaughton, B.L., and Pennartz, C.M. (2009). Hippocampus leads ventral striatum in replay of place-reward information. PLoS Biol *7*, e1000173.

Lansink, C.S., Jackson, J.C., Lankelma, J.V., Ito, R., Robbins, T.W., Everitt, B.J., and Pennartz, C.M. (2012). Reward cues in space: commonalities and differences in neural coding by hippocampal and ventral striatal ensembles. J Neurosci *32*, 12444-12459.

Lansink, C.S., Meijer, G.T., Lankelma, J.V., Vinck, M.A., Jackson, J.C., and Pennartz, C.M. (2016). Reward Expectancy Strengthens CA1 Theta and Beta Band Synchronization and Hippocampal-Ventral Striatal Coupling. J Neurosci *36*, 10598-10610.

Lavoie, A.M., and Mizumori, S.J. (1994). Spatial, movement- and reward-sensitive discharge by medial ventral striatum neurons of rats. Brain Res *638*, 157-168.

LeGates, T.A., Kvarta, M.D., Tooley, J.R., Francis, T.C., Lobo, M.K., Creed, M.C., and Thompson, S.M. (2018). Reward behaviour is regulated by the strength of hippocampus-nucleus accumbens synapses. Nature *564*, 258-262.

Li, Z., Chen, Z., Fan, G., Li, A., Yuan, J., and Xu, T. (2018). Cell-Type-Specific Afferent Innervation of the Nucleus Accumbens Core and Shell. Front Neuroanat *12*, 84.

Mohebi, A., Pettibone, J.R., Hamid, A.A., Wong, J.T., Vinson, L.T., Patriarchi, T., Tian, L., Kennedy, R.T., and Berke, J.D. (2019). Dissociable dopamine dynamics for learning and motivation. Nature *570*, 65-70.

Moser, M.B., and Moser, E.I. (1998). Functional differentiation in the hippocampus. Hippocampus *8*, 608-619.

Mulder, A.B., Tabuchi, E., and Wiener, S.I. (2004). Neurons in hippocampal afferent zones of rat striatum parse routes into multi-pace segments during maze navigation. Eur J Neurosci *19*, 1923-1932.

O'Neill, J., Senior, T., and Csicsvari, J. (2006). Place-selective firing of CA1 pyramidal cells during sharp wave/ripple network patterns in exploratory behavior. Neuron *49*, 143-155.

O'Neill, J., Senior, T.J., Allen, K., Huxter, J.R., and Csicsvari, J. (2008). Reactivation of experience-dependent cell assembly patterns in the hippocampus. Nat Neurosci *11*, 209-215.

Padilla-Coreano, N., Bolkan, S.S., Pierce, G.M., Blackman, D.R., Hardin, W.D., Garcia-Garcia, A.L., Spellman, T.J., and Gordon, J.A. (2016). Direct Ventral Hippocampal-Prefrontal Input Is Required for Anxiety-Related Neural Activity and Behavior. Neuron *89*, 857-866.

Parfitt, G.M., Nguyen, R., Bang, J.Y., Aqrabawi, A.J., Tran, M.M., Seo, D.K., Richards, B.A., and Kim, J.C. (2017). Bidirectional Control of Anxiety-Related Behaviors in Mice: Role of Inputs Arising from the Ventral Hippocampus to the Lateral Septum and Medial Prefrontal Cortex. Neuropsychopharmacology *42*, 1715-1728.

Patel, J., Fujisawa, S., Berenyi, A., Royer, S., and Buzsaki, G. (2012). Traveling theta waves along the entire septotemporal axis of the hippocampus. Neuron *75*, 410-417.

Patel, J., Schomburg, E.W., Berenyi, A., Fujisawa, S., and Buzsaki, G. (2013). Local generation and propagation of ripples along the septotemporal axis of the hippocampus. J Neurosci *33*, 17029-17041.

Pennartz, C.M., Berke, J.D., Graybiel, A.M., Ito, R., Lansink, C.S., van der, M.M., Redish, A.D., Smith, K.S., and Voorn, P. (2009). Corticostriatal Interactions during Learning, Memory Processing, and Decision Making. Journal of Neuroscience *29*, 12831-12838.

Pennartz, C.M., Groenewegen, H.J., and Lopes da Silva, F.H. (1994). The nucleus accumbens as a complex of functionally distinct neuronal ensembles: an integration of behavioural, electrophysiological and anatomical data. Prog Neurobiol *42*, 719-761.

Pennartz, C.M., Ito, R., Verschure, P.F., Battaglia, F.P., and Robbins, T.W. (2011). The hippocampal-striatal axis in learning, prediction and goal-directed behavior. Trends Neurosci *34*, 548-559.

Pennartz, C.M., Lee, E., Verheul, J., Lipa, P., Barnes, C.A., and McNaughton, B.L. (2004). The ventral striatum in off-line processing: ensemble reactivation during sleep and modulation by hippocampal ripples. J Neurosci *24*, 6446-6456.

Riaz, S., Schumacher, A., Sivagurunathan, S., Van Der Meer, M., and Ito, R. (2017). Ventral, but not dorsal, hippocampus inactivation impairs reward memory expression and retrieval in contexts defined by proximal cues. Hippocampus *27*, 822-836.

Rothschild, G., Eban, E., and Frank, L.M. (2017). A cortical-hippocampal-cortical loop of information processing during memory consolidation. Nat Neurosci *20*, 251-259.

Royer, S., Sirota, A., Patel, J., and Buzsaki, G. (2010). Distinct representations and theta dynamics in dorsal and ventral hippocampus. J Neurosci *30*, 1777-1787.

Schmitzer-Torbert, N., and Redish, A.D. (2004). Neuronal activity in the rodent dorsal striatum in sequential navigation: separation of spatial and reward responses on the multiple T task. J Neurophysiol *91*, 2259-2272.

Singer, A.C., Carr, M.F., Karlsson, M.P., and Frank, L.M. (2013). Hippocampal SWR Activity Predicts Correct Decisions during the Initial Learning of an Alternation Task. Neuron *77*, 1163-1173.

Singer, A.C., and Frank, L.M. (2009). Rewarded outcomes enhance reactivation of experience in the hippocampus. Neuron *64*, 910-921.

Singer, A.C., Karlsson, M.P., Nathe, A.R., Carr, M.F., and Frank, L.M. (2010). Experience-dependent development of coordinated hippocampal spatial activity representing the similarity of related locations. J Neurosci *30*, 11586-11604.

Sjulson, L., Peyrache, A., Cumpelik, A., Cassataro, D., and Buzsaki, G. (2018). Cocaine Place Conditioning Strengthens Location-Specific Hippocampal Coupling to the Nucleus Accumbens. Neuron *98*, 926-934.

Smith, A.C., Frank, L.M., Wirth, S., Yanike, M., Hu, D., Kubota, Y., Graybiel, A.M., Suzuki, W.A., and Brown, E.N. (2004). Dynamic analysis of learning in behavioral experiments. J Neurosci *24*, 447-461.

Sosa, M., Gillespie, A.K., and Frank, L.M. (2016). Neural Activity Patterns Underlying Spatial Coding in the Hippocampus. Curr Top Behav Neurosci *37*, 43-100.

Strange, B.A., Witter, M.P., Lein, E.S., and Moser, E.I. (2014). Functional organization of the hippocampal longitudinal axis. Nat Rev Neurosci *15*, 655-669.

Tabuchi, E.T., Mulder, A.B., and Wiener, S.I. (2000). Position and behavioral modulation of synchronization of hippocampal and accumbens neuronal discharges in freely moving rats. Hippocampus *10*, 717-728.

Tang, W., Shin, J.D., Frank, L.M., and Jadhav, S.P. (2017). Hippocampal-Prefrontal Reactivation during Learning Is Stronger in Awake Compared with Sleep States. J Neurosci *37*, 11789-11805.

Tepper, J.M., Koos, T., Ibanez-Sandoval, O., Tecuapetla, F., Faust, T.W., and Assous, M. (2018). Heterogeneity and Diversity of Striatal GABAergic Interneurons: Update 2018. Front Neuroanat *12*, 91.

Trouche, S., Koren, V., Doig, N.M., Ellender, T.J., El-Gaby, M., Lopes-Dos-Santos, V., Reeve, H.M., Perestenko, P.V., Garas, F.N., Magill, P.J.*, et al.* (2019). A Hippocampus-Accumbens Tripartite Neuronal Motif Guides Appetitive Memory in Space. Cell *176*, 1393-1406.

van der Meer, M.A., Johnson, A., Schmitzer-Torbert, N.C., and Redish, A.D. (2010). Triple dissociation of information processing in dorsal striatum, ventral striatum, and hippocampus on a learned spatial decision task. Neuron *67*, 25-32.

van der Meer, M.A., and Redish, A.D. (2011). Theta phase precession in rat ventral striatum links place and reward information. J Neurosci *31*, 2843-2854.

van Strien, N.M., Cappaert, N.L., and Witter, M.P. (2009). The anatomy of memory: an interactive overview of the parahippocampal-hippocampal network. Nat Rev Neurosci *10*, 272-282.

Wilson, M.A., and McNaughton, B.L. (1994). Reactivation of hippocampal ensemble memories during sleep. Science *265*, 676-679.

Witter, M.P. (2007). Intrinsic and extrinsic wiring of CA3: indications for connectional heterogeneity. Learn Mem *14*, 705-713.

Yoshida, K., Drew, M.R., Mimura, M., and Tanaka, K.F. (2019). Serotonin-mediated inhibition of ventral hippocampus is required for sustained goal-directed behavior. Nat Neurosci *22*, 770-777.

Yu, J.Y., Kay, K., Liu, D.F., Grossrubatscher, I., Loback, A., Sosa, M., Chung, J.E., Karlsson, M.P., Larkin, M.C., and Frank, L.M. (2017). Distinct hippocampal-cortical memory representations for experiences associated with movement versus immobility. eLife *6*.

Yu, J.Y., Liu, D.F., Loback, A., Grossrubatscher, I., and Frank, L.M. (2018). Specific hippocampal representations are linked to generalized cortical representations in memory. Nat Commun *9*, 2209.

2.8 Acknowledgments

CHAPTER 3

Conclusions and implications

3.1 Significance

In this work, we have described a potential neural substrate for the brain's ability to separately store and retrieve different aspects of experience. Specifically, we showed for the first time that the dorsal and ventral subdivisions of the hippocampus coordinate largely distinct neuronal networks in the nucleus accumbens (NAc), and that these networks are coordinated in opposing ways. Previous work had separately implicated either dorsal hippocampal or ventral hippocampal input to the NAc in linking spatial information to reward during learning and memory recall. Many of these studies relied on artificial stimulation or inactivation of these circuits. As such, it was unknown whether dorsal hippocampus (dH), ventral hippocampus (vH), or both engaged representations related to space or reward in the nucleus accumbens under normal conditions. Our study is the first to examine all three regions simultaneously using *in vivo* neural recordings to ask how these circuits interact. We used sharp-wave ripples (SWRs), neural events that support memory encoding and retrieval, to identify times of inter-regional information processing. We demonstrate that only the NAc network associated with the dH encodes information relevant to reward outcomes and the traversal of spatial paths in an appetitive task. This finding is contrary to previous hypotheses in the field: that vH would be primarily involved in associations of space and valence given its patterns of anatomical connectivity. Instead, we suggest that dH and vH and their associated downstream neuronal networks support distinct cognitive functions, with the dH primarily involved in spatial-reward learning. The opposition we observe between these networks during SWRs could fundamentally support the encoding and recall of distinct aspects of experience at different times. Our results have broad implications for how task-relevant information could be compartmentalized in a specific communication channel in the brain.

3.2 Distinct task engagement of dorsal and ventral hippocampus

The differences we observed between dorsal and ventral hippocampal sharp-wave ripples (dSWRs and vSWRs) are consistent with largely distinct roles for dH and vH during spatial task learning and performance. We showed that in addition to being asynchronous, dSWRs and vSWRs show distinct

patterns of modulation in response to novelty and reward. While dSWRs are enhanced by novelty and reward, vSWRs are unaffected, occurring at a consistent rate across learning and in both rewarded and unrewarded conditions. This finding strongly suggests that dSWRs and vSWRs are differentially involved in spatial learning and memory and may convey different types of information to downstream circuits, as reflected by the distinct task firing patterns of dSWR- and vSWR-activated neurons in the NAc.

It is important to note that this divergence of function could be task-specific. Both dH and vH can be sufficient for spatial learning depending on the structure of the experiment (de Hoz et al., 2003; Ferbinteanu et al., 2003; Loureiro et al., 2012), and vH has been shown to be particularly involved in dissociating broad spatial contexts (de Hoz and Martin, 2014; Komorowski et al., 2013), a process not involved in the Multiple-W task.

These previous studies provide some hints as to what vSWRs could be "doing" in our task. For instance, it is possible that the steady SWR rate observed in vH over the course of our experiment could correspond to the unchanging contextual information present in our task. In addition, vH has been implicated in the transfer of learned spatial search strategies to new contexts (de Hoz and Martin, 2014). Another possibility, therefore, is that the sustained SWR rate could reflect prolonged engagement of vH as the animal must adaptively switch between rewarded alternation sequences (e.g. a type of context). In this scenario, vSWRs could be broadcasting a representation of which sequence context the animal currently occupies to downstream brain regions (though likely not to the NAc, as we saw no evidence for this representation). Further work will be required to understand the content of vSWR replay events; this work will likely need to include advancement in recording techniques and/or optical imaging, as tetrodes are not well suited for single unit isolation in the vH.

By contrast, based on our results and the work of many others (Buzsaki, 2015), dSWRs are likely broadcasting precise spatial representations of paths in the task for both memory storage and the evaluation of available choices. Importantly, these functions need not be mutually exclusive (Joo and Frank, 2018). For example, when a reward is delivered, the retrieval of the previously traversed route at the time of reward consumption can help the animal decide which route to take next while simultaneously storing the

association between that route and reward. Thus, replay during dSWRs could both facilitate the association of information represented across brain regions (i.e. spatial paths and reward) and retrieve those associations to update them (Foster and Wilson, 2006; Mattar and Daw, 2018).

The asynchrony between dSWRs and vSWRs provides further support for disparate functions, as the ability of downstream regions to access unique outputs from dSWRs and vSWRs would be facilitated by their offset timing. This unique parsing of outputs seems to be reflected in the unique task firing patterns of dSWR- and vSWR-activated NAc neurons. Moreover, these distinct networks in the NAc could only be revealed by the temporal asynchrony between dSWRs and vSWRs, as synchronous SWRs would occlude the different firing rate changes of NAc cells in response to dSWRs versus vSWRs.

3.3 Considerations for the absence of reward information in the vH-NAc network

Perhaps the most surprisingly result of this work is the lack of cohesive reward representation in NAc neurons modulated by the vH (V+ neurons). Prior evidence had implicated the vH as the hippocampal subdivision specialized for emotional and valence representations. Crucially, however, this hypothesis was largely based on anatomical and manipulation studies. First, unlike dH, vH sends dense, direct anatomical outputs from both ventral CA1 and subiculum to numerous brain regions involved in reward processing and food consumption, including the NAc, basolateral amygdala, lateral hypothalamus, and medial prefrontal cortex (Fanselow and Dong, 2010; Moser and Moser, 1998; Strange et al., 2014). Second, inactivation of the vH and its connections to these regions lead to deficits in reward-seeking behavior (Floresco et al., 1997) and spatial reward memory (LeGates et al., 2018; Riaz et al., 2017). Stimulation of the vH can even lead to changes in dopaminergic activity in the ventral tegmental area and NAc (Blaha et al., 1997; Lisman and Grace, 2005). Finally, vH pyramidal cell activity can be particularly modulated near goal locations (Ciocchi et al., 2015; Royer et al., 2010). Together, these findings had led to the assumption that the vH would coordinate neural representations of reward downstream. Despite these previous suggestions, our findings yielded no evidence of specialization for reward processing in vSWRs or vSWR-activated NAc neurons.

170

As discussed in Chapter 2, the discrepancy between our work and previous studies can likely be explained by the contrast between broadly manipulating a circuit and studying fine-time-scale physiological patterns of activity. Additionally, however, the nature of the "space" in the spatial-reward association may be important. In our study, reward associations relied on discrete spatial paths marked primarily by distal spatial cues. In non-linear environments such as conditioned place preference chambers (e.g. LeGates et al., 2018), the reward-paired space is defined by local contextual cues such as odors, textures, and proximal wall markings. These different types of cues have been proposed to differentially involve dH and vH (Riaz et al., 2017). As such, our task may have preferentially engaged more dorsal hippocampal reference frames for finding reward.

It is also possible that vH activity may engage representations of reward elsewhere in the brain. Ventral CA1 pyramidal neurons have been shown to arborize to multiple downstream regions (Dougherty et al., 2012), and increasing evidence suggests projection-specific functional specialization of the vH (Chen et al., 2019; Jimenez et al., 2018; Xu et al., 2016). Different projection targets are correlated with distinct vH activity patterns (Ciocchi et al., 2015), with only some vH cells showing modulation near goal locations (Ciocchi et al., 2015; Royer et al., 2010). This raises the possibility that the V+ MSNs we observed receive vH inputs that do not correspond to reward. The projection-defined heterogeneity of the vH could also contribute to the overall higher rate of vSWRs compared to dSWRs, as a higher gain on SWR output may be required to reach a greater number of downstream targets.

An intriguing possibility is that the vH-NAc network might be preferentially quiet during reward-seeking behavior. A recent study reported that vH is overall suppressed during goal-directed behavior, particularly when reward receipt requires sustained effort (Yoshida et al., 2019). Similarly, our Multiple-W task requires substantial physical effort and is a sustained goal-directed task. The low activity levels of V+ neurons, especially during movement, indeed imply that excitatory output from vH may be minimal in our task.

Finally, the nucleus accumbens is remarkably heterogeneous, with different functions, anatomical connectivity, and neuromodulators occupying subregions within the core and shell (Carelli, 2002; Castro

and Bruchas, 2019). While we recorded from both core and shell, we cannot exclude the possibility that more extensive sampling of the medial and ventral shell, where vH input is most dense, could have revealed vSWR-activated neurons encoding space and/or reward.

3.4 Speculative role of the vH-NAc network

An obvious question remains: what do the V+ NAc cells do? I conducted an extensive set of analyses not reported here to look for features of the task that the V+ neurons encoded. Based on the properties I examined, with respect to dSWR-activated (D+) and unmodulated cells, the V+ cells apparently do *not*: have unique speed tuning, predict whether the next trial is correct or incorrect, cover a larger fraction of the environment, encode specific arms or trajectories, encode a specific direction of movement, encode a specific task sequence (e.g. Sequence A or B), encode errors at non-sequence wells, encode surprising rewards or errors on sequence switches, encode a relative arm of the sequence, remap more between sequences, fire more during stops on the track away from the well, correlate with trials on which the animal was confused, correlate more with sequence performance, change more over the course of an epoch or day, or encode nosepoke or delay to reward. Given that the V+ neurons are indeed engaged during awake vSWRs on the task, it remains possible that they encode something present in the task that we could not measure with our current techniques (such as fluctuations in attentional state).

An alternative possibility that the V+ population is more heterogenous in its representations than the D+ population. Individual V+ neurons showed interesting behavioral correlates, such as tuning to the turnarounds from the wells or a preference for movement times on the arms of the rewarded sequence (see Chapter 2, Fig. 4C, Cell 3). As a population however, no feature was commonly expressed enough to be significant with respect to the D+ or unmodulated populations. Perhaps a diverse representation in V+ NAc neurons is consistent with a role for the vH in encoding broad representations of entire contexts or experiences.

We speculate that the vH-NAc network could also be specialized for associations not engaged in our task such as those between overall context and negative valence. An increasing number of studies have

172

implicated vH and its projection targets in aversive learning and the regulation of anxiety-related behavior (Adhikari et al., 2010, 2011; Bannerman et al., 2004; Chen et al., 2019; Ciocchi et al., 2015; Jimenez et al., 2018; Keinath et al., 2014; Kheirbek et al., 2013; Kjelstrup et al., 2002; Padilla-Coreano et al., 2016; Parfitt et al., 2017). In our task, the rats were highly accustomed to being on an elevated track and did not display overt anxiety-related behaviors. Interestingly, however, negative outcomes (errors) were associated with an overall higher rate of vSWRs than dSWRs, particularly at later stages of learning. This suggests that vSWRs may equally signal both rewards and errors. In addition, the V+ population showed elevated activity on the task relative to awake times in the sleep box, consistent with modestly elevated anxiety or arousal on the task. Future work could test the role of vH-modulated NAc neurons in aversive spatial tasks, such as those requiring the animal to exit part of the environment to avoid a noxious stimulus.

3.5 Future directions for understanding the dH-NAc network

A central finding of this work is that NAc neurons activated during dSWRs (D+) encode generalizable components of spatial paths to reward. It remains unclear exactly how this information is coordinated with hippocampal replay events (i.e. the actual sequence of hippocampal spiking within SWRs). While I observed cases of preserved spiking order between dH and NAc cells from movement to SWR reactivation (data not shown), the dynamics of this inter-regional replay remain to be explored further. A thorough investigation may require a dataset with greater sampling of hippocampal neurons, in order to observe full spatial trajectories and classify replay events as forward or reverse (Diba and Buzsaki, 2007).

We have largely discussed the coordinated SWR reactivation of dH and NAc cells as a candidate mechanism of association between them. Alternatively, this reactivation could reflect an association that has already formed during preceding movement. In particular, the hippocampal theta rhythm (discussed in Chapter 1) is known to organize both dH and NAc spiking (Lansink et al., 2016; Sjulson et al., 2018; Tabuchi et al., 2000; van der Meer and Redish, 2011). This theta rhythmicity maintains the spiking of dH cells and theta-modulated NAc cells in close, consistent temporal proximity during movement, which could facilitate information transfer between regions. More specifically, both hippocampal cells (O'Keefe and

Recce, 1993) and certain NAc cells (van der Meer and Redish, 2011) phase precess relative to theta. Individual theta cycles therefore contain compressed sequences of both hippocampal and NAc spiking, such that a complete representation of each component of the path and its relationship to reward may be present on a time scale conducive to neural plasticity. Intriguingly, individual theta cycles may also offer representations of specific alternative choices (Kay et al., 2019). Part of our on-going work is to further characterize the theta coordination of dH-NAc spiking and its relationship to reward-guided decision-making.

3.6 Conclusion

Understanding how the hippocampus coordinates representations of experience in downstream brain circuits is critical to our knowledge of how memories are formed and utilized. Here we have described how physiologically dissociable networks in the nucleus accumbens are oppositely engaged by the dorsal and ventral hippocampus – regions that are thought to have unique contributions to memory processing. This study lays the groundwork for future functional dissection of these circuits to understand their role in memory-guided behaviors.

3.7 References

Adhikari, A., Topiwala, M.A., and Gordon, J.A. (2010). Synchronized activity between the ventral hippocampus and the medial prefrontal cortex during anxiety. Neuron 65, 257-269.

Adhikari, A., Topiwala, M.A., and Gordon, J.A. (2011). Single units in the medial prefrontal cortex with anxiety-related firing patterns are preferentially influenced by ventral hippocampal activity. Neuron 71, 898-910.

Bannerman, D.M., Rawlins, J.N., McHugh, S.B., Deacon, R.M., Yee, B.K., Bast, T., Zhang, W.N., Pothuizen, H.H., and Feldon, J. (2004). Regional dissociations within the hippocampus--memory and anxiety. Neurosci Biobehav Rev 28, 273-283.

Blaha, C.D., Yang, C.R., Floresco, S.B., Barr, A.M., and Phillips, A.G. (1997). Stimulation of the ventral subiculum of the hippocampus evokes glutamate receptor-mediated changes in dopamine efflux in the rat nucleus accumbens. Eur J Neurosci 9, 902-911.

Buzsaki, G. (2015). Hippocampal sharp wave-ripple: A cognitive biomarker for episodic memory and planning. Hippocampus.

Carelli, R.M. (2002). The nucleus accumbens and reward: neurophysiological investigations in behaving animals. Behav Cogn Neurosci Rev 1, 281-296.

Castro, D.C., and Bruchas, M.R. (2019). A Motivational and Neuropeptidergic Hub: Anatomical and Functional Diversity within the Nucleus Accumbens Shell. Neuron 102, 529-552.

Chen, B.K., Murawski, N.J., Cincotta, C., McKissick, O., Finkelstein, A., Hamidi, A.B., Merfeld, E., Doucette, E., Grella, S.L., Shpokayte, M., et al. (2019). Artificially Enhancing and Suppressing Hippocampus-Mediated Memories. Curr Biol 29, 1885-1894 e1884.

Ciocchi, S., Passecker, J., Malagon-Vina, H., Mikus, N., and Klausberger, T. (2015). Brain computation. Selective information routing by ventral hippocampal CA1 projection neurons. Science 348, 560-563.

de Hoz, L., Knox, J., and Morris, R.G. (2003). Longitudinal axis of the hippocampus: both septal and temporal poles of the hippocampus support water maze spatial learning depending on the training protocol. Hippocampus 13, 587-603.

de Hoz, L., and Martin, S.J. (2014). Double dissociation between the contributions of the septal and temporal hippocampus to spatial learning: the role of prior experience. Hippocampus 24, 990-1005.

Diba, K., and Buzsaki, G. (2007). Forward and reverse hippocampal place-cell sequences during ripples. Nature Neurosci 10, 1241-1242.

Dougherty, K.A., Islam, T., and Johnston, D. (2012). Intrinsic excitability of CA1 pyramidal neurones from the rat dorsal and ventral hippocampus. J Physiol 590, 5707-5722.

Fanselow, M.S., and Dong, H.W. (2010). Are the dorsal and ventral hippocampus functionally distinct structures? Neuron 65, 7-19.

Ferbinteanu, J., Ray, C., and McDonald, R.J. (2003). Both dorsal and ventral hippocampus contribute to spatial learning in Long-Evans rats. NeurosciLett 345, 131-135.

Floresco, S.B., Seamans, J.K., and Phillips, A.G. (1997). Selective roles for hippocampal, prefrontal cortical, and ventral striatal circuits in radial-arm maze tasks with or without a delay. J Neurosci 17, 1880-1890.

Foster, D.J., and Wilson, M.A. (2006). Reverse replay of behavioural sequences in hippocampal place cells during the awake state. Nature 440, 680-683.

Jimenez, J.C., Su, K., Goldberg, A.R., Luna, V.M., Biane, J.S., Ordek, G., Zhou, P., Ong, S.K., Wright, M.A., Zweifel, L., et al. (2018). Anxiety Cells in a Hippocampal-Hypothalamic Circuit. Neuron 97, 670-683.

Joo, H.R., and Frank, L.M. (2018). The hippocampal sharp wave-ripple in memory retrieval for immediate use and consolidation. Nat Rev Neurosci 19, 744-757.

Kay, K., Chung, J.E., Sosa, M., Schor, J.S., Karlsson, M.P., Larkin, M.C., Liu, D.F., and Frank, L.M. (2019). Constant sub-second cycling between representations of possible futures in the hippocampus. bioRxiv 528976.

Keinath, A.T., Wang, M.E., Wann, E.G., Yuan, R.K., Dudman, J.T., and Muzzio, I.A. (2014). Precise spatial coding is preserved along the longitudinal hippocampal axis. Hippocampus 24, 1533-1548.

Kheirbek, M.A., Drew, L.J., Burghardt, N.S., Costantini, D.O., Tannenholz, L., Ahmari, S.E., Zeng, H., Fenton, A.A., and Hen, R. (2013). Differential control of learning and anxiety along the dorsoventral axis of the dentate gyrus. Neuron 77, 955-968.

Kjelstrup, K.G., Tuvnes, F.A., Steffenach, H.A., Murison, R., Moser, E.I., and Moser, M.B. (2002). Reduced fear expression after lesions of the ventral hippocampus. Proc Natl Acad Sci U S A 99, 10825-10830.

Komorowski, R.W., Garcia, C.G., Wilson, A., Hattori, S., Howard, M.W., and Eichenbaum, H. (2013). Ventral hippocampal neurons are shaped by experience to represent behaviorally relevant contexts. J Neurosci 33, 8079-8087.

Lansink, C.S., Meijer, G.T., Lankelma, J.V., Vinck, M.A., Jackson, J.C., and Pennartz, C.M. (2016). Reward Expectancy Strengthens CA1 Theta and Beta Band Synchronization and Hippocampal-Ventral Striatal Coupling. J Neurosci 36, 10598-10610.

LeGates, T.A., Kvarta, M.D., Tooley, J.R., Francis, T.C., Lobo, M.K., Creed, M.C., and Thompson, S.M. (2018). Reward behaviour is regulated by the strength of hippocampus-nucleus accumbens synapses. Nature 564, 258-262.

Lisman, J.E., and Grace, A.A. (2005). The hippocampal-VTA loop: Controlling the entry of information into long-term memory. Neuron 46, 703-713.

Loureiro, M., Lecourtier, L., Engeln, M., Lopez, J., Cosquer, B., Geiger, K., Kelche, C., Cassel, J.C., and Pereira de Vasconcelos, A. (2012). The ventral hippocampus is necessary for expressing a spatial memory. Brain Struct Funct 217, 93-106.

Mattar, M.G., and Daw, N.D. (2018). Prioritized memory access explains planning and hippocampal replay. Nat Neurosci 21, 1609-1617.

Moser, M.B., and Moser, E.I. (1998). Functional differentiation in the hippocampus. Hippocampus 8, 608-619.

O'Keefe, J., and Recce, M.L. (1993). Phase relationship between hippocampal place units and the EEG theta rhythm. Hippocampus 3, 317-330.

Padilla-Coreano, N., Bolkan, S.S., Pierce, G.M., Blackman, D.R., Hardin, W.D., Garcia-Garcia, A.L., Spellman, T.J., and Gordon, J.A. (2016). Direct Ventral Hippocampal-Prefrontal Input Is Required for Anxiety-Related Neural Activity and Behavior. Neuron 89, 857-866.

Parfitt, G.M., Nguyen, R., Bang, J.Y., Aqrabawi, A.J., Tran, M.M., Seo, D.K., Richards, B.A., and Kim, J.C. (2017). Bidirectional Control of Anxiety-Related Behaviors in Mice: Role of Inputs Arising from the Ventral Hippocampus to the Lateral Septum and Medial Prefrontal Cortex. Neuropsychopharmacology 42, 1715-1728.

Riaz, S., Schumacher, A., Sivagurunathan, S., Van Der Meer, M., and Ito, R. (2017). Ventral, but not dorsal, hippocampus inactivation impairs reward memory expression and retrieval in contexts defined by proximal cues. Hippocampus 27, 822-836.

Royer, S., Sirota, A., Patel, J., and Buzsaki, G. (2010). Distinct representations and theta dynamics in dorsal and ventral hippocampus. J Neurosci 30, 1777-1787.

Sjulson, L., Peyrache, A., Cumpelik, A., Cassataro, D., and Buzsaki, G. (2018). Cocaine Place Conditioning Strengthens Location-Specific Hippocampal Coupling to the Nucleus Accumbens. Neuron 98, 926-934.

Strange, B.A., Witter, M.P., Lein, E.S., and Moser, E.I. (2014). Functional organization of the hippocampal longitudinal axis. Nat Rev Neurosci 15, 655-669.

Tabuchi, E.T., Mulder, A.B., and Wiener, S.I. (2000). Position and behavioral modulation of synchronization of hippocampal and accumbens neuronal discharges in freely moving rats. Hippocampus 10, 717-728.

van der Meer, M.A., and Redish, A.D. (2011). Theta phase precession in rat ventral striatum links place and reward information. J Neurosci 31, 2843-2854.

Xu, C., Krabbe, S., Grundemann, J., Botta, P., Fadok, J.P., Osakada, F., Saur, D., Grewe, B.F., Schnitzer, M.J., Callaway, E.M., et al. (2016). Distinct Hippocampal Pathways Mediate Dissociable Roles of Context in Memory Retrieval. Cell 167, 961-972 e916.
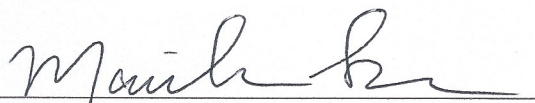
Yoshida, K., Drew, M.R., Mimura, M., and Tanaka, K.F. (2019). Serotonin-mediated inhibition of ventral hippocampus is required for sustained goal-directed behavior. Nat Neurosci 22, 770-777.
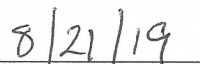
Publishing Agreement

It is the policy of the University to encourage the distribution of all theses, dissertations, and manuscripts. Copies of all UCSF theses, dissertations, and manuscripts will be routed to the library via the Graduate Division. The library will make all theses, dissertations, and manuscripts accessible to the public and will preserve these to the best of their abilities, in perpetuity.

Please sign the following statement:

I hereby grant permission to the Graduate Division of the University of California, San Francisco to release copies of my thesis, dissertation, or manuscript to the Campus Library to provide access and preservation, in whole or in part, in perpetuity.

_____
Author Signature

_8/21/19_
Date